Production of a probe tip compensation method for reverse engineering free-form features

Stephen O'Grady

A thesis submitted in partial fulfilment of the requirements of Sheffield Hallam University for the degree of Doctor of Philosophy

June 2024

I hereby declare that:

1. I have not been enrolled for another award of the University, or other academic or professional organisation, whilst undertaking my research degree.

2. None of the material contained in the thesis has been used in any other submission for an academic award.

3. I am aware of and understand the University's policy on plagiarism and certify that this thesis is my own work. The use of all published or other sources of material consulted have been properly and fully acknowledged.

4. The work undertaken towards the thesis has been conducted in accordance with the SHU Principles of Integrity in Research and the SHU Research Ethics Policy.

5. The word count of the thesis is 35,560 approx.

Name	Stephen O'Grady
Award	PhD
Date of Submission	June 2024
Research Institute	Materials & Engineering Research Institute (MERI)
Director(s) of Studies	Dr David J Tipper Dr Lyuba Alboul

Signed….S.O'Grady

Abstract

Reverse engineering is now a part of the modern engineering framework. It is used in the main to remanufacture products where documentation of the original design form is lost.

Arm mounted Laser scanning instruments can collect large amounts of data rapidly at rates of 600K points per second, but at the expense of accuracy. Static coordinate measuring machines (CMM) can deliver more accurate measurements, but the process is slower with touch trigger probing data acquisition of the order of 25 points per minute. Prismatic objects that can be defined by equations (planar faces, cylinders etc.), are relatively easy to measure as their topology is well understood. Objects to be reverse engineered may be more difficult, for example castings formed from handmade patterns or forgings made from worn dies.

An investigation has been carried out to determine the accuracy of an articulated arm mounted laser scanner measuring a diffuse and reflective reference planar target. Tactile probed data was gained from the targets to form a planar best fit reference. Laser scan data was taken of the targets at various angles and stand-off to their surface normals. Planar primitives were best fitted to this laser scan data. Scanner error was taken as the offset between the best fitted laser scanned plane and the tactile probed best fitted reference planes. The scanner systematic error was found to be most greatly influenced by scanner stand-off.

Scanner systematic errors have been observed between ±0.070 mm. If surface microstructure produces speckle reflection, scan error becomes influenced not by this systematic error, but by the least squares residuals standard deviation of the planar feature best fit routine. Speckle reflection causes saturation of the CCD and laser scattering from the target microstructure causes high volumes of outliers.

Two techniques have been developed to allow probe tip correction to be carried out on freeform features. Both techniques use laser scan data to represent the free form surface. This virtual representation allows the surface directly below a contact probe to be estimated and a compensation calculated in the probe approach direction. The second method uses the laser scan data representation of the target surface to determine the probe contact position with the target surface.

Both methods were tested on virtual and actual scanned data for a 150.032 mm hemispherical form. The probe compensation in the probe approach direction gave adequate diameter errors of 0.018 mm for a 2 mm diameter probes, but 6 mm diameter probes gave diameter accuracies of 0.085 mm.

Compensation in the surface contact normal direction produced results on a par with those expected from a static CMM probing prismatic parts for both the virtual and actual hemispherical form, producing diameter errors of 0.002 mm and 0.003 mm for 2 mm and 6 mm diameter probes respectively.

Scan data density has proved a factor in the success of both compensation methods. It has been shown that sparse data reduces the accuracy of both methods. Prob tip correction establishing the probe contact point proved the most accurate and robust technique. This method was further validated with virtual data generated from a Bezier curve driven surface. Compensation errors from the compensated point to the virtual surface of 0.0015 mm were achieved. A value less than the CMM maximum permissible error (MPE) (0.0017 mm). Compensation accuracy was clearly seen to decrease with increasing probe diameter due to the basic trigonometry of the compensation method.

Of the various data gathering techniques available, gaining laser scan data as a polygonal mesh in real time proved the most accurate and convenient as data cleaning of mesh data is a relatively straight forward process.

Acknowledgements

I would like to thank my Ph.D. supervisors Dr David Tipper and Dr Lyuba Alboul for their hard work in guiding and supporting this thesis. I would also like to thank the Metrology and workshop technicians at Sheffield Hallam University; Jamie Boulding and Robin Sykes for their help and advice throughout the project.

I would also like to give great thanks to Professor Andrew Longstaff of Huddersfield university the advice and guidance he gave to a complete stranger. This advice proved invaluable.

I would like to dedicate this report to Jean and Malcolm O'Grady. If I had worked a little harder and progressed a little quicker, they may have been around to see the thesis completed.

Table of contents

Table of figures

Table of Tables

Table of equations

Table of Acronyms / terminology

Close coupled device: -	'CCD'.
Computer aided design: -	'CAD'.
Computer aided manufacture: -	'CAM'.
Coordinate measuring machine: -	'CMM'.
Machine coordinate system: -	Coordinate system based on the CMM undertaking the measurement process.
Minimum permissible error	MPE
Non-uniform rational basis spline: -	'NURBS'.
Prismatic part: -	'PP'
Scan Plane: -	The notional plane defined by the probe axis and its direction of travel
Work piece coordinate: -	Coordinate system based on the features of the object being measured

Chapter 1. Introduction

Accurate measuring techniques are used widely in engineering and throughout manufacturing processes. They are used extensively to confirm that intended sizes and tolerances have been achieved for the process being undertaken or to check goods inwards.

More latterly these mainstream measuring techniques have been adopted by practitioners of reverse engineering: a process that starts from an existing product to 'capture' the initial design form such that the product can be reproduced or developed further. The design lead time and risk can be reduced by starting the design process with a known product . Reverse engineering is used in situations where the original designs are lost, to form a record of historic artefacts or reform patterns and moulds for castings and forgings or the likes of.

Reverse engineering in its modern incarnation is a rapidly expanding technology being pushed by improvements in scanning equipment and cheaper computing power and being pulled by a design and manufacturing industry that wishes to reduce lead times and development costs . The process consists of multiple stages which build one upon another, all capable of inputting inaccuracies into the final product.

Accurate measurement is a vital part of the manufacturing process. It is essential to both validate the designed form, ensuring correct product functionality but also to investigate past designs by reverse engineering existing products. Highly accurate measurement (µm level) is time consuming and usually requires relatively expensive equipment. Arm mounted laser scanning is less accurate than touch trigger / tactile scanning and static CMM laser mounted scanning, but it is relatively quick and can record in the order of 600K data point per second.

To measure accurately using contact probing, it is essential that the intended contact point of the probe and surface and the actual contact point are one and the same. If this is not the case an adjustment

must be applied to the contact probe reading. This is called probe compensation. This compensation can be applied in the direction of probe travel or can be used to determine the actual contact point of the probe and the surface. Both compensations are being considered in this thesis.

Little or no research has been undertaken into the accuracy of arm mounted scanning systems and the use of laser scan data to reduce probe compensation error.

Prismatic objects such as spheres, conics and planar objects are relatively easy to measure accurately when prior knowledge of the surface shape is available. Objects to be reverse engineered, such as pump impellors and plastic injection mould tooling are also straightforward to measure if there is prior knowledge of surface topology in the form of a digital model, although errors may still occur with the alignment of the digital model and actual component..

Objects such as die tooling where the drawings are no longer available can be difficult to measure accurately and quickly. The original design form of a prismatic feature may have been lost by the product being damaged. Manufacturing processes such as open die forging and casting may have required very large tolerances, or the part may be badly worn. A more comprehensive list of situations where reverse engineering is used is detailed .

Portable arm CMM units equipped with touch trigger probes are commonplace in many manufacturing industries where they are used both in the metrology labs and on the shop floor. Laser attachments are less common but are used in automotive and aerospace design / manufacturing facilities. The marginal cost of adding a laser scanner to an existing touch trigger arm has become more affordable and so their use is becoming more widespread.

If arm mounted laser scanning error can be characterised and the process better understood, the quickly obtained scan data could be used for the formation of more accurate digital models as part of the reverse engineering process.

If the advantageous speed of data acquisition provided by a portable arm scanner can be combined with the accuracy of static CMM tactile probing to measure objects where surface prior knowledge does not exist, then measurement accuracy levels only thought possible for known prismatic objects would be achievable.

Measurement techniques to used to reverse engineer an existing product is time consuming and expensive requiring highly skilled labour and can cause a bottleneck to the design process. If the digital representation is to be used in a forward engineering process such as digitising a clay mock-up of a car body, this may affect lead times and cause accuracy issues that can potentially cause problems and expense downstream when metal tooling is being formed.

Modern machining techniques have evolved to allow designers to specify highly complex forms with a high degree of accuracy, but the manufacturing of these forms is being constrained by the lack of "*measurement confidence and suitable measurement traceability*" , .

Modern metrology equipment such as probing systems are evolving, such as the development of 5 axis systems (probe head has 2 rotational axes), but these systems are relatively expensive and not always backward compatible with existing hardware and software. The technique developed in this thesis has the potential to counter some of these issues when used on objects where there is no prior knowledge of their surface form. This could reduce the need to replace perfectly serviceable and accurate metrology equipment by extending its life.

This thesis will examine the accuracy of arm mounted laser line scanning equipment. This will include the position of the scanner relative to target object and the objects surface finish. This work will use arm mounted laser line scan data to develop a system to increase the accuracy of static CMMs equipped with three-dimensional touch trigger probe / tactile scanning probe to more accurately measure objects where no prior knowledge of surface topology exists. That is to take probe 'centre point' data and add probe tip compensation informed by arm mounted laser scan data to give more

accurate measurement of surfaces. The 3D probe senses when contact is made with the target in either the 'X', 'Y', or 'Z' direction. Once the contact has been sensed, the CMM records the position.. Different probe types are discussed in section 2.9. 'Probe types'.

1.1. Aims and Objectives

The main aims and objectives of this thesis are as follows: -

Thesis aims: -

To produce a probe tip compensation method that will raise the level of freeform surface measurement to that achievable on a static CMM measuring prismatic features. The method will produce probe tip correction in the absence of surface prior knowledge.

Thesis objectives: -

- Determine the error associated with an articulated arm mounted laser line scanner, such that systematic error estimates can be used to inform and validate the probe tip correction method.
- Understand the issues involved with tactile probed compensation when dealing with surface topology where no prior knowledge is available such that a robust compensation method is realized and can be performed on both prismatic and freeform surfaces.
- Develop probe tip compensation method(s) using the laser scanner error estimates and newly gained understanding of probe tip correction.
- Validate the probe tip correction method(s) developed. Producing accurate artifacts that can be used as reference models is challenging as the machining process can add error which may be associated with the probe compensation process. So, validation may need to use prismatic or virtual parts.

- Provide a good indication of future work that could enhance the already robust procedure for probe tip compensation developed here.

1.2. Contribution of the work

The probe tip correction method developed in this thesis will allow existing static CMM and articulated arm scanners to have greater functionality. The compensation method developed allows freeform objects that are not accompanied by prior surface knowledge to be measured with an accuracy associated with a static CMM measuring prismatic parts. No other system has been seen that can deliver this level of single micron accuracy associated with measuring freeform objects. Future work has been suggested that could improve accuracy and productivity levels even more by gaining the data for probe tip correction from a single CMM / coordinate system.

It is considered that the developed compensation system could be used for measuring a variety of engineering objects, but in the main it would be used where there is no prior knowledge of the surface / feature. This provides a great opportunity when reverse engineering products to capture surface detail with an accuracy not seen before. The probe tip compensation method developed in this thesis allows the designer to have more confidence in the accuracy of the form measurements taken and so to have more confidence in the forward engineering process. The new / modified designs need to be based on accurate form knowledge. The probe tip compensation method developed her will do that. It is anticipated that the use of this methodology will extend the functionality of older metrology equipment.

1.3. Chapter outlines

Chapter 2 will examine the current situation with reverse engineering to gain an understanding of the various workflows associated with the process. Accuracy levels associated with tactile and laser scanning systems will be investigated and metrology software functionality examined.

Chapter 3 will characterise the systematic error associated with articulated arm laser line scanning. Error will be examined with respect to laser scanner angle to the work piece and stand-off. Surface reflectivity can have an impact on the accuracy of the laser scanning process, so both a diffuse and reflective target will be used.

Chapter 4 develops a rational for a hybrid approach to probe tip compensation. The rational introduces the use of scan data received from an articulated arm mounted laser line scanner being used as a substitute / for prior surface knowledge. The discussions are concerned with issues involved with using relatively inaccurate laser scanner data (± 0.070mm) and its inherent issues with outlying data and gaps in data. Two probe tip method have been suggested and a broad outline of their working principles noted

One method will give probe tip correction in the probe approach direction and the second method will determine the actual probe / target surface contact point. This chapter is setting out the hybrid background needed for the realisation of the compensation methods.

Chapter 5 realizes the probe compensation outlines proposed in Chapter 4 and develops them into functional robust probe tip compensation methods. The compensation methods are optimized and validated using virtual data.

Chapter 6 validates the compensation methods using an actual component. Data density requirements are investigated to ensure probe compensation methods are robust. The most accurate probe tip compensation method is further validated by measuring a pseudo freeform Bezier curve driven surface. Chapter 7 is concerned with discussion of results.

Chapter 8 is concerned with the dissertation conclusions and a discussion of future work.

Chapter 2. Background Research

This chapter sets out to investigate the various workflows for the reverse engineering process. Initially these workflows will be discussed along with associated data capture and data manipulation methods. Additional to this investigation, the methodology will be discussed.

2.1. Reverse engineering

Reverse engineering started with the use of pantographs, primarily used by sculptors for scaling full size editions from maquette's, with hydraulic copy lathes and millers being the modern industrial equivalent. This copying process leaves the user with no permanent record of the objects shape, whereas modern techniques aim to provide a digital model of the original . Initially measuring was carried out using rulers, micrometres and callipers. From the 1970's onwards manually operated CMMs, and more latterly semi-automated (software driven) versions of the same equipment have been available. The gathering of coordinate data in this manner can be time consuming and problematic when dealing with non-prismatic components. Once the point data has been obtained, it can be manually entered into a CAD package. Although a highly accurate method with positional accuracy of 3 – 5 µm , CMMs have mainly been restricted to quality assurance inspection and digitising sculpted objects such as clay 'mock-ups' of car bodies for the manufacture of press or mould tooling. A major issue with CMMs is that the majority require physical contact with the object being measured, making it unsuitable for deformable, flexible, or irreplaceable objects such as historic statuary. The process is relatively slow especially when applied to parts with complex free-form surfaces so current research is concerned with automatic path generation / optimisation and more latterly path generation of free-form targets using 5 axis tactile scanning , . This equipment combines the 3 linear axes of a static CMM plus 2 rotational axes of the probe head to maintain a sweep style continuous contact between probe and target work piece. develop a method where laser scan data is used to analyse the

complexity of the surface such that touch trigger probe points can be optimised to enable best fitting of B-Spline curves to the surface where the author reported accuracies of 15 µm.

Contactless laser line scanning can replace tactile probing to speed up data acquisition and allow the relatively easy measurement of free-form products, but this may be at the expense of measurement accuracy. The laser scanning process accuracy can be dependent on both surface finish, scanner relative orientation to target object, laser stand-off and surface structure. Crystalline structures such as those present in marble statuary , can cause the laser line to reflect / scatter from below the object's surface (sub surface scattering) and highly reflective surfaces can cause error in the received cloud point data through specular reflection.

An alternative for measurement of large objects that will not fit on a static CMM, is an arm mounted tactile probe system which commonly has 7 axes of rotation, with encoders at each arm joint. This system is also capable of having a laser line scanner attached to it as seen in Fig. 2.1b.

The use of reverse engineering to create a digital twin or to characterise a component at one specific point in time seems to miss the power of the process. Reverse engineering may capture the original designer's intent in the form of measurements and surface finish. It may be the case that the part now is outdated or never worked as well as intended or more modern manufacturing techniques are now available using more modern materials. It seems appropriate that reverse engineering is seen as the starting point of a 'forward' engineering process and not seen as an end point. Reverse engineering allows engineers and designers to reduce the risk of developing new products, as they can look back on the functionality, performance and longevity of the product being reverse engineered, to give guidance in the development of the new product.

2.2. CMM measuring equipment

Any equipment that returns the 'X', 'Y' and 'Z' position of a target surface can be considered a coordinate measuring machine (CMM). A more formal definition describes a CMM as:

> *"a measuring system with the means to move a probing system and the capability to determine spatial coordinates on the surface of the part being measured."*

They can be manufactured in a number of forms ranging from static machine with three linear orthogonal axes ('X', 'Y','Z'), which may be augmented with additional one or two axes in the form of a rotating probe head; to six or seven axis portable arms Fig. 2.1a and b.

(a). 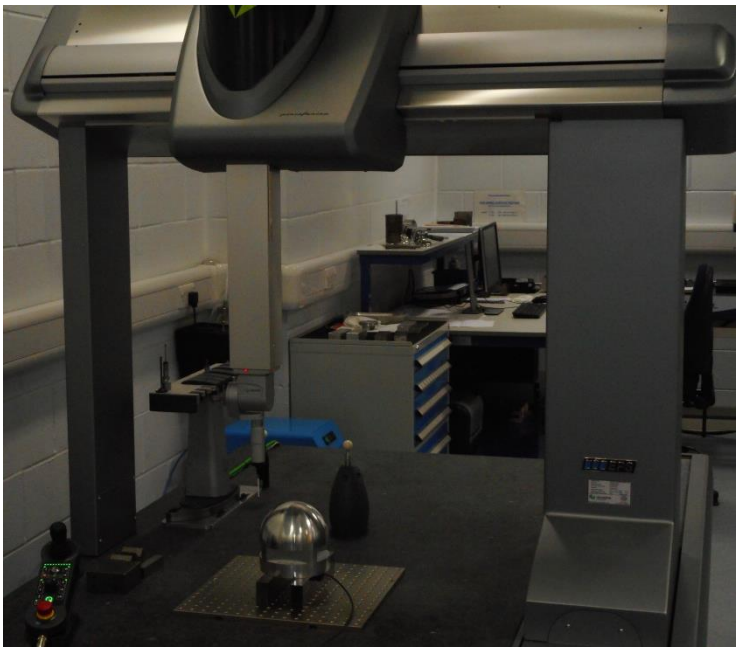 (b). 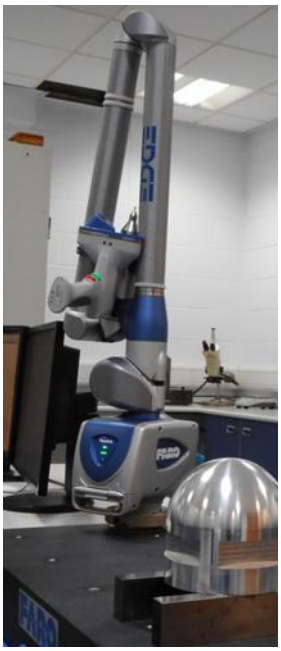

Fig. 2.1. Modern coordinate measuring machines found in a typical metrology laboratory, (a). Moving bridge type. (b). Seven axis articulated arm CMM.

One and two axis rotating heads may be mounted to a static CMMs. CMMs can also be fitted with a laser scanner head, but they require additional space such that they can be articulated to gain line of sight of the target object from all directions and can scan a target objects face in the normal direction. They may not be able to be accommodated on smaller static CMMs. They also require relatively powerful computers to run modern metrology software which involves the processing of large datasets containing tens of millions of cloud point data points.

Static CMM contact measuring has been reported as having accuracies "*many tens of micrometres different from optical based measurement*" .

The use of tactile probes may require human intervention to record a surface point (hard probe) as shown in Fig. 2.1b, where the articulated arm mounted system is equipped with both laser scanner and contact probe head. To obtain a contact reading, the trigger must be applied by the operator. In general, the physical contact of probe with surface is sufficient to record a data point. Scanning probes have the facility to maintain continuous contact with the surface taking discrete data points as the probe traverses a pre-defined path over the work piece. A now no longer produced CMM, the Renishaw Cyclone was a continuous-contact digitizer, capable of scanning speeds of up to 3 m per minute and scanning rate of 400 points per second. Although data gathering was rapid, repeatability was 5 µm. .

The geometric product specification, acceptance and reverification tests for coordinate measuring machines is covered in the ISO 10360 series of standards, with the maximum permissible error (MPE) calculation detailed in . This will give an indication of the accuracy levels achieved from the proposed tip compensation methods.

Optical probes can use a variety of techniques to record surface topology such as 'time of flight' and 'triangulation'. This laser scanner used in this investigation will be of the triangulation type where a laser beam is projected onto the target surface which is reflected onto a charge-coupled device (CCD). Through triangulation of the scent and reflected beam the target position is determined Fig. 2.2**.**

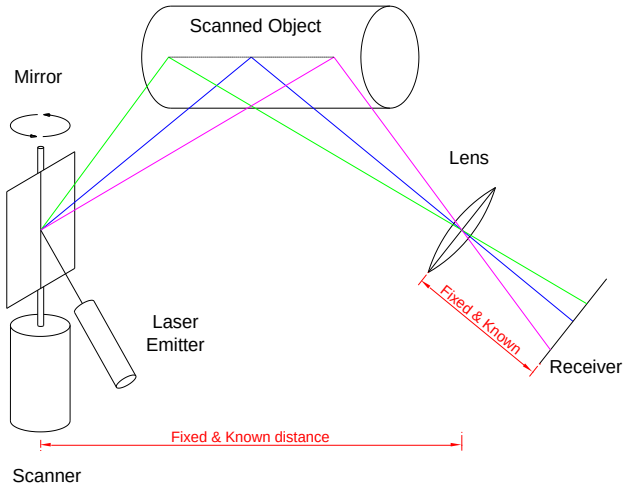

Fig. 2.2. A schematic representation of 3D laser line scanning using triangulation.

In this dissertation a static coordinate measuring machine which can be equipped with a touch trigger probe, tactile scanning probe or a laser scanner will be referred to as a static CMM. Although a portable seven axis articulated arm system is by definition a CMM, for clarity it will be referred to as an articulated arm or articulated arm CMM.

2.3. Reverse engineering data capture and processing

The measuring techniques discussed in this section can apply to the measurement of most objects found in a general engineering / manufacturing environment. This investigation is concerned with the measurement of objects by both tactile probing using a static CMM and an articulated arm mounted laser scanner. This requires the objects to be rigid (does not deform when being contact probed) and to have surface characteristics (surface finish and non-occluded features) that are capable of being laser scanned. These requirements will be discussed in section 4.2. “Considerations used in forming hybrid probe compensation”.

The measurement methods and data processing techniques employed during the reverse engineering process are highly dependent on the surface form and component size. Features to be measured fall into two main geometric types, prismatic and free-form.

> *"Prismatic parts (PPs) are an important group of mechanical parts frequently used in industry, PPs are consisted from the basic geometric features such as plane, cylinder and cone From the metrological aspect, this group also implies free-form surfaces whose inspection is not strictly required and they are present mainly due to esthetical or some related reason"*

> *"Artefacts measured on CMMs fall into two categories:*
> *purely prismatic components, examples of which include engine blocks, brake components and bearings; and*
> *free-form components, examples of which include car doors, body panels, mobile phone covers and IT peripherals.*
> *Prismatic components can be broken down into easily defined elements, for example planes, circles, cylinders, cones and spheres. A measurement will consist of breaking down the component into these geometries and then looking at their interrelationships, for example the distance between two holes or the diameter of a pitch circle.*
> *Free-form components cannot be broken down as with prismatic components. Generally, the surface is contacted at a large number of points and a surface approximated to the data".*

> *"A surface, the shape of which, cannot be described by a simple mathematical Expression".*

If an object is sufficiently large that it cannot be measured in a single orientation, the surface may need to be scanned in several positions. Each scan must have sufficient overlap with the next such that a registration process can be used to combine the individual data sets into a single file within a single coordinate system. discuss the registration of multiple data sets for a military tyre. The paper reports a 1% to 1.5% registration error in a tyre with a nominal diameter of 1.5 m diameter. Registration can be aided by the addition of temporary fiducial features (small ball bearings) or fixturing may be able to give the required overlap.

The discussions below assume measurements can be obtained in a single orientation and no registration of multiple position scan sets is required, but the methods developed in this thesis would apply to data sets formed by the registration of scans taken from multiple positions.

Some common workflows for the Reverse Engineering process used across a number of manufacturing industries are detailed in Fig. 2.3. and are discussed below. These various workflows are not seen as exhaustive but do cover the main processes available when using 'commonly available' metrology equipment and reverse engineering software. defines reverse engineering as

> *"The process of obtaining geometric CAD model from 3D points acquired by scanning / digitizing the existing products"*

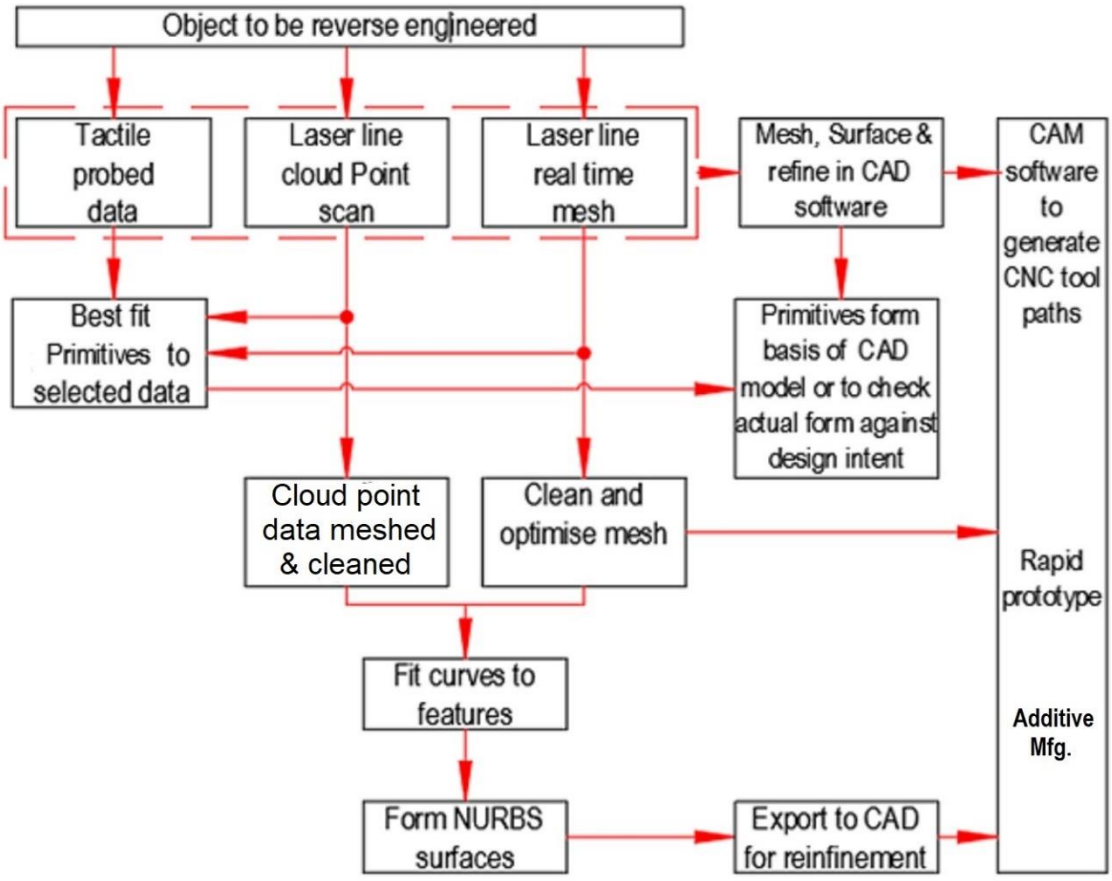

Fig. 2.3. Common Reverse engineering workflows.

Contact probed data gained from an articulated arm or CMM usually results in fewer data points than when measuring is undertaken using a laser line scanner. The 'on-board' CMM software is used to best fit appropriate prismatic features to the data, which requires prior knowledge of the target surface form so that the correct best fit algorithm can be used i.e., plane, cylinder, sphere etc. The position of

these features can be used directly to check a target object against an existing reference (drawing / CAD model), or the features can be transferred to a CAD package to construct a reverse engineered model. This method works well where easily identifiable features are present but is not appropriate for non-prismatic objects.

Laser scan cloud point data is usually obtained in large volumes, with the use of reverse engineering / metrology software allowing the removal of unwanted data and best fitting of individual scans to each other; optimising overlaps before finally forming a polygonal mesh. A polygonal mesh can be formed in real time with data being best fitted and optimized as laser line scanning progresses. Real time meshing has the advantage of removing outliers and making data clean-up of spurious triangles a more streamline process. Once a polygonal mesh is formed, both these techniques follow the same methodology, with extraneous data being removed, holes filled and edges and fine detail refined, reformed or removed as required. Non-uniform rational basis splines (NURBS) are added to the meshed model, defining features and areas of the mesh with similar curvature. NURBS patches are fitted to the curve network and are optimised as required to either match the target surface faithfully with issues at patch boundaries or produce a high-quality surface that may be less faithful to the data, but more appropriate for a downstream manufacturing or analytical process. This data manipulation process is well documented in the reverse engineering / metrology software help section of for example Geometric Polyworks .

Little or no prior knowledge of the surface topology is required for this form of reverse engineering. Changes in curvature can be identified from changes in mesh size and colour maps provided by the reverse engineering software, which makes this an ideal process for reverse engineering of free-form objects. If required; cloud point or meshed data can be selected and prismatic features fitted directly to the data as previously discussed with tactile scanned data.

There are variants on these procedures such as a 'Hybrid technique suggested by where a combination of surface fitted NURBS curves and freehand sketched curves are used to satisfy the correct combination of aesthetics and faithfulness to the surface form, although aesthetic considerations may have been prioritised by the use of manual techniques.

Three-dimensional modelling software manufactures such as SolidWorks have inbuilt reverse engineering tools. 'Scan to 3D' converts cloud point data directly into surface models within the SolidWorks CAD package, although the ability to manage and repair mesh data and control the surface generation process at this moment in time does not match that provided by dedicated reverse engineering / metrology software.

Fig. 2.3**.** shows the reverse engineering process feeding the finalised / refined CAD models into a computer aided manufacturing (CAM) package, to remanufacture the reverse engineered products. This may not necessarily be the case. The CAD model could be produced simply to provide a permanent record of a product's geometry, a measure of a product's wear / state of decay; or the models could be refined / modified and rapid prototyped as part of a 'forward engineering' process.

If the aim of the reverse engineering process is to remanufacture by computer numerically controlled (CNC) machining, it can be seen from Fig. 2.3, that error free, watertight polygonal models can be exported directly as an STL file into a tool path generation software, This eliminates much of the reverse engineering process. The disadvantage of this 'shortcut' is that the STL file cannot be easily modified. If a change of material to enhance the products performance is beneficial, size changes may be required, or more modern manufacturing techniques not available when the product was originally produced, may require a different shrinkage allowance or surface form. This lack of flexibility makes this route less attractive. It is highly likely that the reverse engineered product is going to feed into a 'Forward engineering process' where outdated design form and original design issues can be rectified.

The STL file also gives little control over the tool path generation process and the final surface quality of the machined surface. It may be required to cap a hole or remove / modify a feature that cannot be produced by the CMM package.

Data volumes for laser scanning are larger than those seen in tactile measuring by virtue of the large speed at which cloud point data is being collected. The number of data points gathered in the 5 passes over the test targets measured in Chapter 3 is approximately 330K points. The number of points collected depends on the scanner resolution setting and the size of the object being scanned. For larger objects needing multiple scanner position and overlap between scans such that they can be aligned will generate larger data sets. Components with little change in curvature and little fine detail will require smaller numbers of triangles than an object of the same size, but with a great deal of curvature and detail, so file size is influenced by scan resolution, component size and surface features.

2.4. Reverse engineering and metrology software

It can be seen in Fig. 2.3. that when reverse engineering an object, surfaces can be represented by cloud point data or by a polygonal mesh.

The cloud point data is 'raw' laser scan data with each data point representing a position in three-dimensional space that the laser beam reflected from the target object, such that the cloud point data set is simply a series of unrelated points in space each possessing an 'X', 'Y', 'Z' coordinate. Whereas a polygonal mesh possesses both vertices (the cloud data points) and triangle facets connecting the vertices. These triangular meshes incorporate surface normal information.

It is highly unlikely that an object could be fully laser scanned, gaining all its surface detail in one pass of the scanner. The laser beam has a limited width and depth of field and opposing faces and features

require scanning from different directions. It is the norm that multiple scan passes will be required to cover the whole object Fig. 2.4.

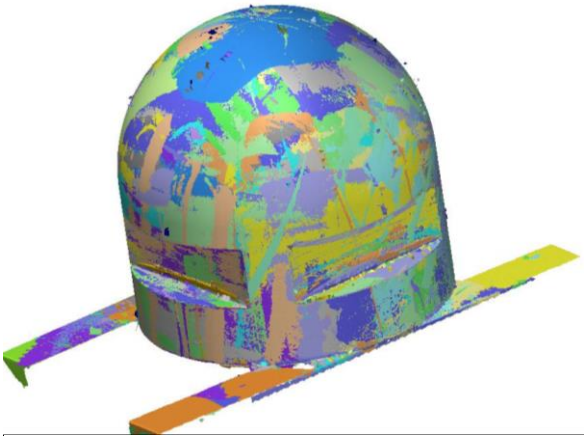

Fig. 2.4. Multiple scans required to give full surface representation. Each scan pass is represented by a different colour.

The requirement to scan the whole surface without gaps will result in overlapping scan data. The inaccuracies within the laser scanning process, scan noise and spurious data from specular reflection ensure there are positional differences between individual scans representing the same parts of the surface. The polygonal meshing process best fits these individual overlapping cloud point scans (section '2.3. Reverse engineering data capture and processing'), removing overlapping cloud point data and forming a mesh from that data. The process parameters can be set to remove 'outliers'; that is cloud point data points that are an excessive distance away from their direct neighbours. Modern reverse engineering software has taken advantage of more powerful readily available computers to be able to mesh scan data in real time as the scanning process is being undertaken. That is, the same process as detailed above for the conversion of cloud point data to a polygonal mesh, but instead of it being completed as a separate process after the scan data has been obtained, it is completed in real time as each scan is obtained.

As stated previously, the polygonal mesh represents the surface by holding additional surface normal direction data that the 'raw' cloud point data does not. This extra complexity can introduce topological errors into the mesh. These are discussed below and shown Fig. 2.5.

- Degenerate triangles where all three vertices of the triangle are collinear Fig 2.5a.
- Duplicate triangles where one triangle lays on top of another Fig 2.5b.
- Degenerate triangular edges which occur when more than two triangles share an edge which results in a triangle emerging from a manifold surface Fig 2.5c.
- Inconsistent edges occur when adjacent triangles (joined by an edge) have a surface normal pointing in opposing direction to its direct neighbour Fig 2.5d.

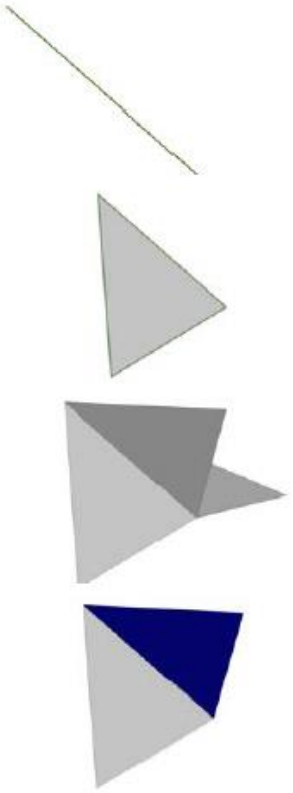

Fig. 2.5. Polygonal topological errors (a). top image to (d). bottom image. Taken directly from .

Cloud point and polygonal mesh data of the same object are shown Fig. 2.6. The data shown Fig. 2.6a has relatively few scan points and so the individual data points are visible. If a polygonal mesh is being considered Fig. 2.6b. the image can be viewed as a smooth continuous surface to speed up image manipulation in the graphical user interface. This plain polygonal mesh surface representation can be overlaid with a wire frame representation of the mesh Fig. 2.6c but this is at the expense of image manipulation speed.

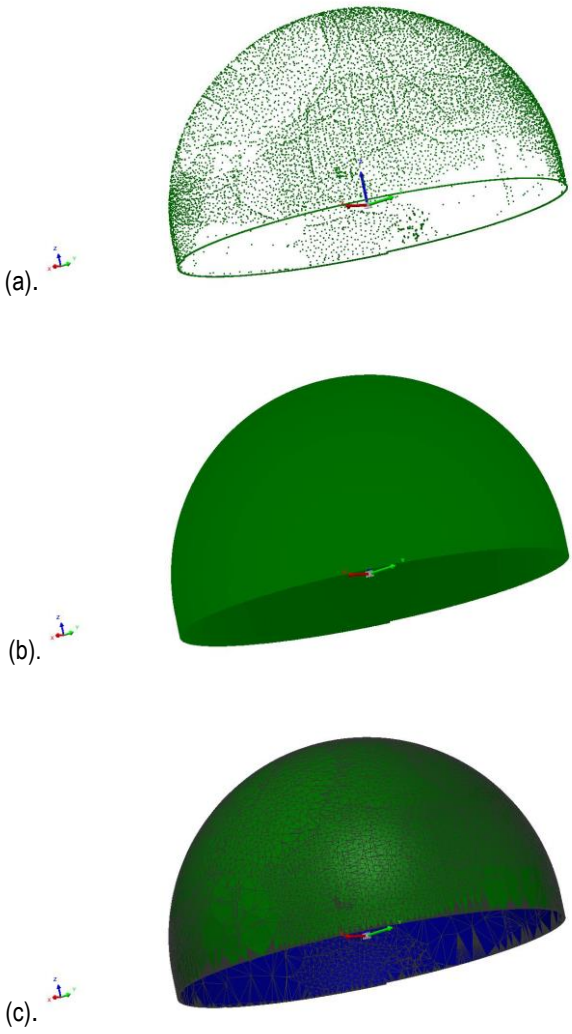

Fig. 2.6. Images of a surface digital data representation produced in Polyworks metrology software. (a). cloud point data shown as individual points. (b). Polygonal mesh shown as a smooth continuous surface. (c). The polygonal mesh is detailed with a wire frame image of the mesh over laying the smooth surface.

The removal of erroneous data (outliers) can be a time consuming and a subjective task when dealing with cloud point data as individual points are not connected to their neighbours. Whereas a polygonal mesh relates individual points with connecting triangles. Selection of outlying data not connected to the required mesh body Fig. 2.7b or topological errors in the mesh (as discussed in section '2.3. Reverse engineering data capture and processing') can be removed using the reverse engineering software selection tools Fig. 2.7c, with unwanted data simply being deleted Fig. 2.7d.

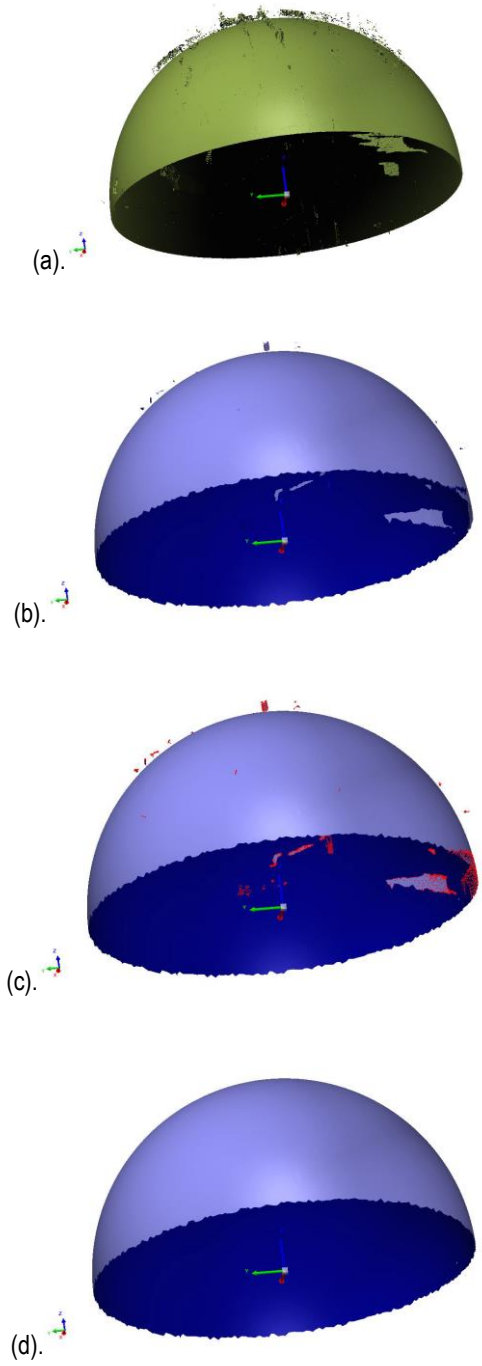

Fig. 2.7. Cloud point and polygonal mesh models in a raw and cleaned state. (a). Raw cloud point data with noise and spurious points. (b). Raw polygonal mesh with spurious triangles. (c). Outlier data not connected to the main body selected. (d). Spurious, floating mesh data deleted.

Reverse engineering software can accommodate accurate data collection by rejecting outliers. This can be achieved in several ways: -

- Specifying a maximum ‘point to point’ distance there may be between two neighbouring points, with the data points beyond this distance being rejected.
- Clusters of outliers can be rejected on the size of the bounding box enclosing them. This allows outliers that fall within the maximum ‘point to point’ distance detailed above to still be rejected because the group is considered undesirable.

Although not part of this investigation as it relies on feature prior knowledge. Prismatic feature best fitting algorithms can incorporate outlier filtering: -

- Data points are fitted to the prismatic feature selected, minimising the least square residuals. Any data points deemed too far from he fitted feature are then excluded and a second data fit cycle is undertaken without outliers.
- Outliers that lie furthest from the average of the data points used to fit the prismatic feature can be rejected on their standard deviation value after a preliminary fitting is made. The data is then recalculated without outliers.
- A prismatic feature is preliminary fitted to the data points, then a percentage of the data points that lie furthest from the average distance are rejected and the prismatic feature refitted.

Further to rejecting outliers, during scanning high noise levels can be identified automatically and scan passes rejected, or the local areas of high data point deviation highlighted for later manual intervention.

2.5. Working coordinate systems and alignment of coordinate systems

When working with CMMs it is highly unlikely that the salient features of the component being measured will align directly with the measuring machine’s orthogonal axes and origin. More importantly it could be unproductive to attempt such an alignment physically prior to starting the measurement process. The machine coordinate systems are shown for moving bridge and articulated arm CMMs Fig. 2.8.

The coordinate systems follow the 'Right hand rule' where the thumb represents '+X', forefinger (index finger) +Y' and middle finger 'Z'. A similar rule applies for the direction / rotation of rotary axis machines.

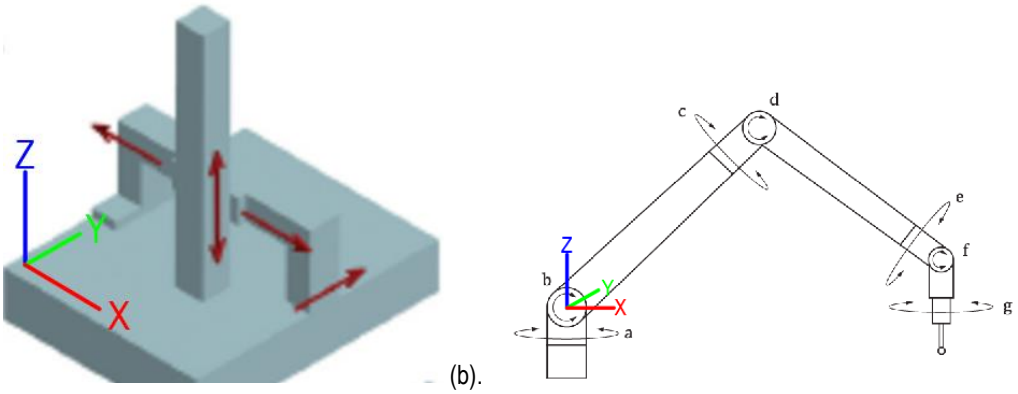

Fig. 2.8 (a). Moving bridge type CMM with its coordinate system to the front left of the table with X positive from left to right across the table, Y increasing from front to back of the table and z increasing vertically upwards . (b). The seven axis articulated arm has its origin at its base where it is attached .

These arbitrary machine coordinate systems may prove inconvenient or ineffective depending on the purpose the measurements are to be put. So, the on-board CMM or third-party metrology software can be used to transform data gained in the machine coordinate system onto important functional or datum features of the work piece. This process requires the object to have prismatic features that can have planes, axes, or points extracted from the measured data points. These features such as planes and cylinders may be formed directly from best fits to data points, or indirectly by generating lines from the intersection of planes or the axis of a cylinder.

A physical object has six degrees of freedom and so: -

> *"To define a datum (co-ordinate) system for a rectangular part with flat surfaces that has its origin in one corner would require six contact points Fig. 2.9. Three points are required to define a flat surface or plane (the XY plane – primary datum A), a further two points are required to define a line which lies on the YZ plane (secondary datum B) and a final point in the XZ plane (tertiary datum C)" Note that the three planes are created to be mutually perpendicular and the point of intersection of these three planes is the origin of the system x = 0, y = 0 and z = 0".*

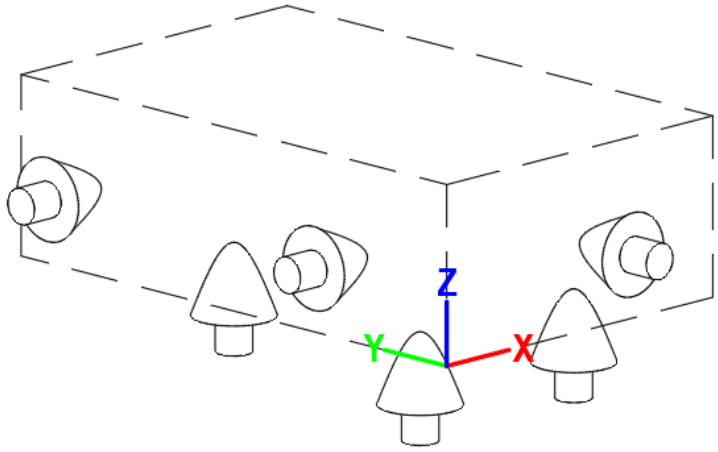

Fig. 2.9. Three, two, one alignment based on ,

This same principle applies when locating probed and laser scan data onto a pre-existing CAD model to compare measured data of a manufactured object with the designers requirements, or in this thesis data from one CMM being aligned and superimposed onto data of the same object derived from another CMM. The alignment can use planes, lines or points. A line can be formed from the axis of a cylinder, the intersection of two planes and points can be formed from the intersection of lines or the intersection of lines and planes. Planes, lines, points formed by fitting features to measured data points are then matched to the equivalent futures on the CAD model or features formed from the 'X', 'Y', 'Z' planes and origin of a work piece coordinate system. This alignment system which translates and rotates data sets from one coordinate system to another is undertaken within the metrology software. Metrology software has other alignment tools such as matching point pair best fit algorithms that translate one data set onto another by matching the local points selected.

Accuracy of data set registration has not been considered in this investigation, but it is discussed in section "8.2 Future work" where a system is proposed that could eliminate the need for scan transformations onto different coordinate systems.

As discussed above, measurement techniques can be split into two categories, one where the measuring equipment contacts the component being measured and one where it does not. This

investigation is concerned with typical equipment associated with CMM contact probing and laser scanning based on triangulation. Each method has its strengths and weaknesses, which are discussed here.

2.6. Laser scanning error measurement

The use of arm mounted laser line scanners for measurement of free-form objects which may not be able to be physically probed makes it difficult to assess the systems measurement accuracy. The limited line width of the scan beam requires an object scan data set to be made up of multiple individual scans combined by means of a 'best fit' system to bring individual scans together. If the object is too large to be scanned from one position, co-registration of scan sets gained from multiple coordinate systems must be undertaken, combining these multiple data sets into a single coordinate system. The use of such equipment may be seen as a form of Black box technology , where users may focus more on the number of scans per second obtained, rather than the system accuracy and data noise, and gaps.

Although limited; CMM mounted laser line scanner accuracy has been investigated, but no research can be found for the accuracy of arm mounted systems. A variety of target forms including spheres, steps, edges and a combination of planes and spheres have been used to investigate static CMM mounted laser scanner accuracy . As previous research has shown , , scanner accuracy is influenced by the stand-off distance between the scanner head and the target object, as well as the scanner's relative orientation to the target object's surface normal.

Previous work , , has highlighted surface finish as having an effect on scan data accuracy. Highly polished reflective surfaces can prove difficult to scan and produce specular reflections which can cause misleading results, as opposed to the case of matte surfaces that produce diffuse reflections

which are relatively straightforward to scan. This is evident when the scanner beam is oriented normal to the target surface producing a situation where the scan noise is at its greatest. Highly reflective metallic surfaces are typical of what could be found in an engineering metrology environment.

2.7. Tactile probing / analogue scanning error measurement

A touch trigger probe / CMM records a single data point when it contacts the work piece, it then needs to move away and it contacts again to record the next point whereas an analogue / scanning probe remains in contact with the work. The system records the position at preset intervals as the probe follows the contour of the work piece. It must be remembered that the probe triggers with work piece contact, but it is the CMM that records the position.

Contact probing systems can suffer from probe tip compensation error. CMMs equipped with tactile probes determine the probe ball centre , . suggests there are several methods for tip radius correction that estimate the contact point.

Probe radius compensation is not required if the probe approach direction and probe 'push-off' is normal to the surface. If this is not the case, compensation must be applied to determine the point on the surface contacted by the probe. repot the accuracy of measuring free-form surfaces on a bridge type CMM as ±<5 µm although this is seen as dependant on the CMM and the environmental conditions the measurements were taken. If a target surface is well understood, that is prior knowledge of is form exists through visual inspection or in the form of a CAD model, the probe can approach the work normal to the surface such that the intended and actual contact points are the same or probe compensation can be applied in the correct direction. For prismatic parts constructed from basic geometric features described as planes, cylinders and cones , where the relationship between the actual contact point of

the probe and the theoretical contact point is well understood, probe tip compensation is straight forward to apply Fig. 2.10 where probe error is:-

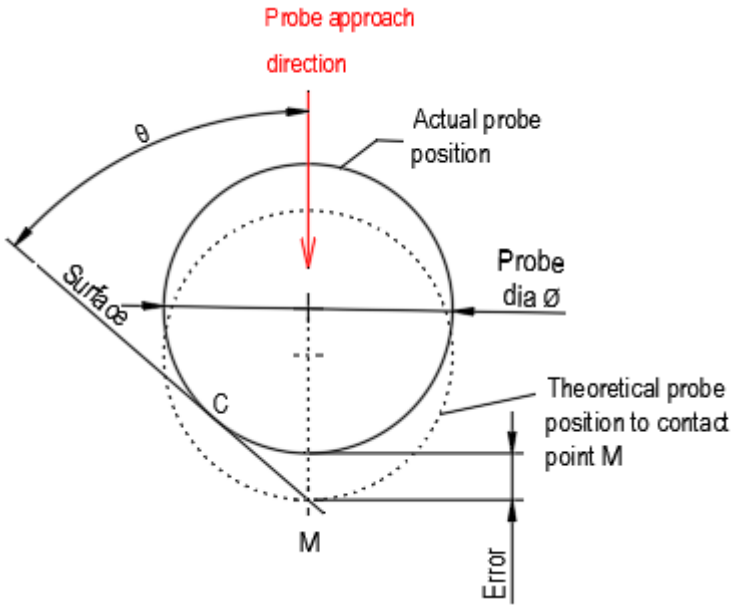

Fig. 2.10. Probe error on a planar inclined surface which is well understood with a known relationship between point M and point C.

$$Error = \left(\frac{\frac{\emptyset}{2}}{\sin\theta}\right) - \frac{\emptyset}{2} \quad (2.1)$$

Ø is the probe diameter and θ is the angle formed between the probe approach direction and the surface to be measured.

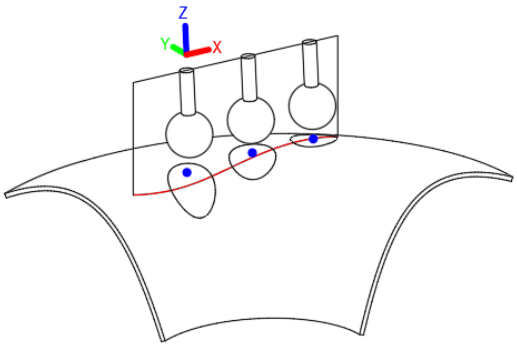

Fig. 2.11. Probe axis is constrained to the scan plane with the analogue scan path (area of the surface being measured) shown as a red curve. The probe is contacting the surface on the blue dots, off of the scan plane. The actual and intended measured points are different.

Fig. 2.11 shows an analogue (continuous) tactile scan moving from left to right, taking 3 discrete measurements. There may be a misconception that the path described by the intersection of the probe 'scan plane' and target surface (red line) is the component of the surface that is being measured. On a free-form surface this is not likely to be the case. The probe can contact the surface at any point under the probe (shown as a vertically projected black envelope below each probe position). In Fig. 2.11, two of the probe 'Z' direction measurements have been influenced by the surface contacting the rear flank of the probe (blue dots), with the right most measurement being influenced by an area close to the intended path. Without prior knowledge of this surface the exact contact position cannot be determined. Fig. 2.12 shows this issue where there is no 'known' direct relationship between the actual contact point 'C' and the theoretical measured point 'M'.

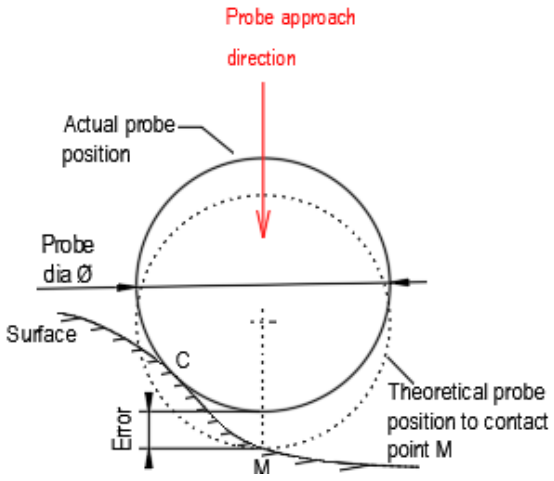

Fig. 2.12. Ball probe error on a free-form surface where the surface is not well understood and there is no known relationship between point M and C.'

To reduce probe compensation error, probe approach direction should be as perpendicular to the surface as possible . To facilitate this requirement modern metrology software used to drive / control the motion of a computer numerically controlled CMM can incorporate learning algorithms that modify the probe approach direction to be perpendicular to a line formed between the last two probed points when contact probing along a scan plane as seen in Fig. 2.13. If tactile probing is undertaken such that the probe does not break contact with the surface, the probe approach direction cannot be modified. In this case the algorithm adds probe compensation to the probe centre point moving the measured probe centre point along the surface contact point normal direction by a distance equal to the probe radius. If this learning technique is not used, the probe centre can be taken as the measured point.

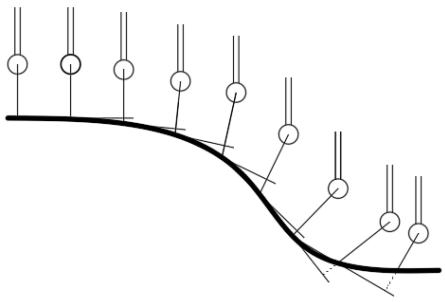

Fig. 2.13. Probe learning along a free-form surface where previous probed points determine the approach direction of future points based on

A more complex learning process suggested by uses multiple scans passes in an iterative process to minimise probe compensation errors, refining the surface normal to develop accurate surface cross sections which are then surface patched with estimations of Bezier curves. This estimation yielded accuracy levels of 0.045 mm for a free-form surface. Both the software learning algorithm and this iterative process ignore the issue with probe flank contact as probe compensation is developed in the scan plane only.

Free-form objects have always been a part of the engineering / manufacturing landscape, for example pump impellors, car bodies, moulds for injection moulded products and the like. What has changed is the ability to optimise product performance at the design stage. Modern analytical CAD software allows this optimisation to be undertaken on pre-production virtual models far more effectively and accurately than previously; demanding more accurate measuring techniques to validate actual form against the designers more stringent design requirements. Modern CMMs and their on-board software may be able to accommodate these requirements when there is prior surface knowledge in the form of a digital model. The CMMs coordinate system is aligned to the components CAD model, the surface normals of the digital model are then used to define the correct probe approach direction ensuring the probe contacts the surface where it is intended, such that no probe compensation is required. The accuracy of this technique is based on there being prismatic features to align the different coordinate systems and the accuracy of the ‘best fit’ registration of the different coordinate systems.

To ensure reverse engineering techniques can deliver the same order of accuracy on free-form surfaces where there is no prior surface knowledge, a more accurate / comprehensive probe compensation method needs to be developed that counters probe flank contact issue.

2.8. Probe tips

There are several important considerations when selecting the probe tip. Initially material selection is important to ensure there is not excessive wear of the tip during the probing process and that there is not material transfer from the target object to the probe tip. It is also required that no damage is done to the target object by the probing process. The most used tips are ruby spheres. These may be unsuitable for probing Aluminium target objects as there may be transfer of target material to the probe tip, 'adhesive wear' .

Probe tip diameter must be related to the size of feature being measured and its surface finish / roughness. If geometric features being measured such as holes or cavities are smaller than the probe tip size, then they cannot be measured. On free-form surfaces or surfaces where geometric features are combined with concave blends, the surface can only be measured if the target surface has a smaller curvature than the probe tip curvature. That is the probe tip will fit into the target surface concavities.

If probe tip radius is similar to the target surface finish / roughness, there may be issues with deciphering what is being measured. When measuring surface form using a CMM, it is likely that surface finish information is not required. If surface finish is of interest, then measurement by other means, for example a Talysurf machine may be more appropriate .

If the ball is sufficiently small, it may record surface finish detail. This may require special filters to

control / modify the flow of information travelling between the probe and the metrology software discusses the capabilities of 4 such filters.

Probe tip diameter can be used as a mechanical filter, with the smaller curvature of a large probe describing the highpoints of the surface. This is shown in detail by for both depth and diameter dimensions taken on a sintered product and a general discussion is provided by .

2.9. Probe types

There are a number of different probes that can be attached to a CMM, below is a brief description of some of the probe types available: -

- A Hard probe is controlled by the operator of the CMM. The probe is advanced to give contact at the required position on the target object. The machine is allowed to settle prior to the operator activating the system to record the contact point. This is the type of probe fitted to an articulated arm CMM.
- A 2D probe senses when it hits the target in the 'X' and 'Y' direction. On sensing a contact, the CMM records the position of the probe centre point.
- A 3D probe triggers when it hits the target in either the 'X', 'Y' or 'Z' direction. On sensing a contact, the CMM records the position of the probe centre point.
- A 5 axis probe head has 2 axes of rotation which when added to the CMMs 3 axis of movement gives the 5 axes. The probe head can scan from side to side and up and down.

2.10. Thesis Methodology

The flow diagram detailed in Fig. 2.14 shows the workflow of this thesis. Background research was undertaken to reveal the current understanding of CMM measuring techniques for both static and arm

mounted equipment when measuring prismatic and free-form features. Gaining sufficient information to have a good understanding of tactile probing as well as arm mounted laser scanner data acquisition was also essential.

Laboratory work was carried out to determine the influence of factors including laser stand-off, scanner orientation to the target surface along with surface reflectivity on accuracy levels obtainable. A good appreciation of laser scanner accuracy will be taken forward to inform the development of hybrid probe tip compensation methods.

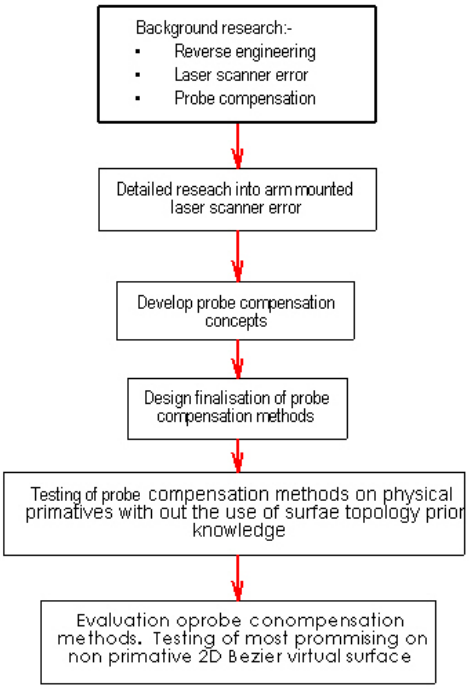

Fig. 2.14. Flow diagram shows this thesis workflow.

With a sound understanding of probe tip compensation associated with prismatic objects gained, two different approaches were used to develop a 'hybrid' technique combining laser scan data of an object to improve probe tip correction when tactile probing by a static CMM.

Two methods for probe tip correction were developed; one using laser scan data to estimate the surface below the probe tip to calculate the probe intended contact point in the probes approach direction and one using the scan data to determine the probe tips actual contact point with the target surface.

Testing of the two developed techniques on theoretical and actual data was undertaken on a hemispherical (prismatic) test piece. Of the two techniques developed, the most promising was further tested using theoretical data to represent a non-prismatic, free-form object of the like found in an injection moulding tool or car body panel.

2.11 Summary

The background research has set the scene for an understanding of the reverse engineering process. Objects where there is no knowledge of the design form must be recreated from remaining items that may be worn, damaged, perhaps products produced from processes that hide or distort the original design features, such as those formed by hand process like pattern making and open die forging. It is this area of work that could benefit from additional techniques to improve measuring accuracy.

The research undertaken gives a good understanding of the elements influencing laser line scanning accuracy. Chapter 3 “Investigation of arm mounted laser line scanning” has been directed by the research undertaken on static CMM laser mounted devices. Probe compensation research has provided the starting point for Chapter 4 “Development of probe compensation methods”.

Chapter 3. Accuracy investigation of arm mounted laser line scanning

Before a probe compensation system can be developed, an understanding of arm mounted laser scan accuracy is necessary. Much work has been undertaken on static CMM mounted laser scanner accuracy, but little has been undertaken on arm mounted systems and little accuracy determination has been determined using graphical metrology software. Chapter 3 attempts to fill this gap by investigating the accuracy of a Faro arm mounted laser line probe system.

3.1. Experimental rationale

As has been discussed in Chapter 2.6. 'Laser scanning error measurement'; a variety of target forms including spheres, steps, edges and a combination of planes and spheres have been used to investigate laser scanner accuracy. Previous research discussed in Chapter 2 has shown that scanner accuracy is influenced by the stand-off distance between the scanner head and the target object, as well as the scanner's relative orientation to the target object's surface normal.

Commercially available metrology / reverse engineering software, such as Polyworks as used in this investigation, uses a Gaussian least squares method to best-fit planes to scan data. The relative position of these fitted planes, compared to an arm mounted touch probed generated planes was used to calculate the accuracy of the scanned data.

Previous work , highlighted surface finish as influencing scan accuracy. Highly polished reflective surfaces can produce specular reflections which can cause misleading results, as opposed to matte surfaces that produce diffuse reflections which are relatively straightforward to scan. Highly reflective polished metallic surfaces are typical of what could be found in an engineering metrology environment and can produce inaccurate data points. and suggest surfaces with uniform colour and diffuse reflection are preferred.

To make the investigation match what could be seen in a typical metrology lab' this work examined scan errors from a reflective ground planar parallel (Sa 0.0689 µm and flatness 0.004 mm), and a matte white scanner compensation plate (Sa 1.8725 µm and flatness 0.018 mm).

Surface finish was measured on a Taylor Hobson - Form Talysurf PGI 1500E Accuracy details are detailed in.

Flatness was measured on an IMS (International Metrology Systems) - IMPACT 600 CMM. The maximum permissible error of the CMM is calculated as being: - $0.0014mm + 0.003\left(\frac{L}{1000}\right)mm.$ For a 200 mm long, parallel this equates to 0.002 mm

The two forms were also selected to challenge the laser scanner's ability to deal with diffuse and speckle reflection. A reflective target can be difficult to scan and can produce erroneous points. Speckle reflection will be discussed later in section 3.4. 'Discussion of experimental laser line scan error measurement'.

3.2. Experimental measurement of scanner error

The experimental setup is shown in Fig. 3.1 The targets investigated were a matte white laser compensation plate and a highly reflective steel parallel.

The compensation plate is the artifact used to calibrate the articulated arm laser scanner prior to use. It is a Lambertian (diffuse) rough surfaces which reflects the laser beam uniformly in all directions.

The reflective steel parallel (specular) is a flat surface which reflects the laser beam in a combination of ways varying from mirror like reflection to Lambertian reflection.

These objects were placed side by side, with their top surfaces nominally coincident so that the scanner stand-off was the same for both surfaces, allowing direct comparison of the data sets and calculated errors.

Scanner error is defined as the difference in 'the Z' direction between the planes best fitted to the tactile probed reflective and Matte targets, to their respective planes, best fitted to their laser scanned data.

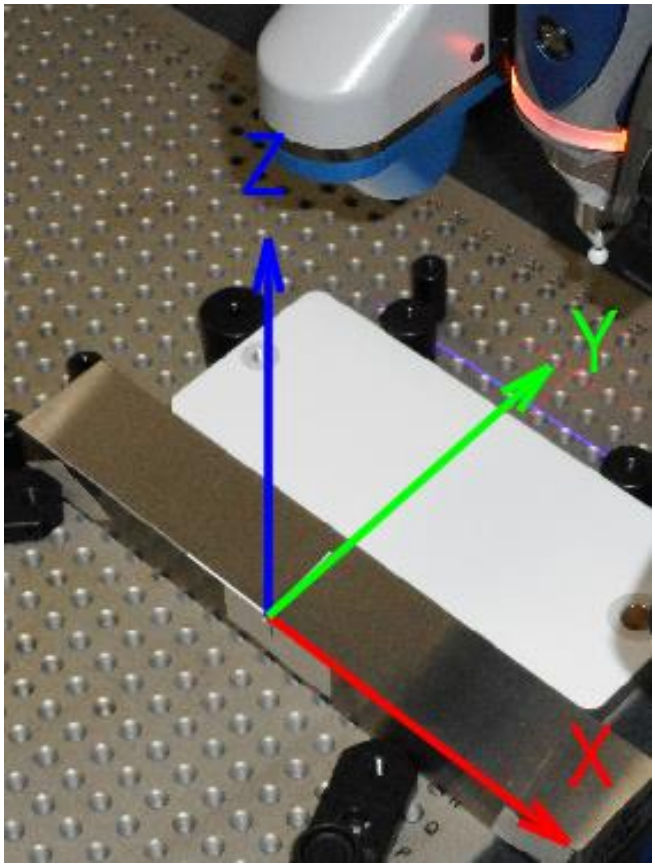

Fig. 3.1. Arm mounted laser scanner experimental setup.

A Faro Laser line probe V6 HD mounted on a Faro Edge seven axis arm (2.7 meter) with combined touch probe was used to scan the target objects. The laser line probe was attached to a manually controlled manipulator. The manipulator consisted of a Cast Iron support with the ability to orientate the in-plane and out-of-plane angle to within 0.5 degree repeatability and stand-off relative to target to within 0.5 mm repeatability. Gauges were used to aid the setting of laser head stand-off.

The manipulator was aligned with the experimental coordinate system allowing orthogonal adjustment in the 'X' and 'Z' directions with free linear movement to scan target objects in the Y direction and rotary adjustment about the X and Y axis Fig. 3.1. The manipulator enabled the accurate control of the in-plane and out-of-plane angle of the laser beam and the stand-of distance from the work surface. The definition of these movements is the same as has been given in previous research and is detailed in Fig. 3.2.

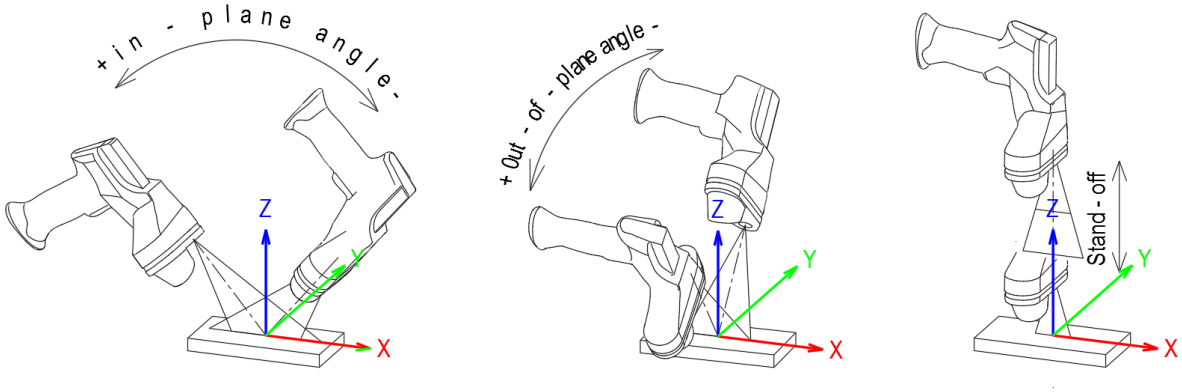

Fig. 3.2. Definition of in-plane, out-of-plane and stand-off relative to target work piece and scanner direction of travel.

A series of scans were undertaken changing one variable at a time as per the methodology of previous work undertaken on static CMMs , , . Laser line scanner stand-off was varied from 115 mm at the near range to 215 mm at the far range in 25 mm increments. Both in-plane and out-of-plane angles were varied independently in 10° increments. The in-plane range was varied from +40° to -30° (while maintaining out-of-plane scan angle at 0°) and the out-of-plane range varied from +40° to -50°, (while maintaining in-plane scan angle at 0°) requiring 85 separate positional setups.

For each positional setup, 5 separate scan passes were taken and amalgamated to reduce experimental variation.

The digitising arm was set up with adjacent arm sections having joint angles as close to right angles as possible with the laser scanner set at angles in-plane 0° and the out-of-plane 0°. This setup was consistent throughout the investigation, with joint position changing only to accommodate the scanning process and the experimental positional changes.

The Faro V6 HD Laser line head is equipped with 2 red orthogonal 'range finder' laser beams which bisect the main laser line beam. Using the on-board range finder laser, each scan pass was set such that the centre of the laser line beam was centred on X = 0 of the targets Fig. 3.1.

Prior to laser line scanning, the arm mounted touch probe was used to determine the position of the top surface of each of the two target pieces (X – Y plane).

Laser line scan measurements were obtained by translating the scanner across the work pieces in the Y direction, with the manipulator keeping the stand-off, in-plane and out-of-plane beam angles constant. To reduce the risk of vibration compromising the measurement accuracy, the scanner was activated and scanning travel initiated and terminated off the target objects, such that any disturbed scan data could be discarded during processing. Cloud point data was cleaned and separated for each target, such that no extraneous points from the surrounding geometry or target edges were included, only points from the top surface of each target object were considered. This was accomplished by a window selection technique within the graphical user interface of the Polyworks software. The files for the Matte white target and the reflective parallel were saved separately with appropriate names detailing the angle, range and target material.

The initial scans were obtained in the scanners coordinate system, rather than the experimental coordinate system detailed in Fig. 3.1. Within the Polyworks software the tactile probed (hard probed) planes were used to translate and rotate all the scanned cloud points onto the experimental coordinate system. This not only allowed individual scan plane position error (as detailed in section '3.1

Experimental rationale') to be determined directly in the Z direction and scan beam width data to be determined in the X direction, but it also aided visual analysis of the data.

None of the scans or touch probed points were moved relative to each other during this process. To facilitate the processing of large volumes of data, ensure consistency and reduce the chance of error, macro scripts were employed within the software environment to perform error calculations.

An initial trial was undertaken to identify a suitable scanning speed. Using the method described above several scans were acquired at varied scanner stand-offs (190 mm, 165 mm and 140 mm) and various out-of-plane angles from +30˚ to -30˚ (10˚ increments), with the in-plane angle maintained at 0˚. Scans were taken at nominal speeds of 200 mm/s, 100 mm/s and 50 mm/s using the white matte scanner compensation plate as a target. The largest difference in absolute error (difference in 'Z' between the tactile probed reference plane and the planes fitted to the data from the various scan passes) associated with speed change for each stand-off was 0.0036 mm. This showed scan error is not sensitive to the scan speeds investigated. The scanning process was undertaken at a nominal speed of 100 mm/sec. This low speed related error showed that exact scan speed was not considered to be an issue.

Initially trials were undertaken with all scanner settings as default, which resulted in inconsistent data. The automatic default exposure setting caused repeatability issues; the scanner could not react in time to the different reflectivity properties of the adjacent reflective and matte target surfaces. This was resolved by setting the exposure level to 4ms for the whole investigation.

All data gathering scans (85 sets) were undertaken 6 times and the average value used to promote experimental consistency. Fig. 3.3 shows the average error with experimental variance indicated by standard deviation error bars for 190 mm stand-off scan. Data points have been joined for clarity purposes only. Results from the white matte target showed a maximum standard deviation of less than 0.0097 mm with the in-plane reflective target having a greatest standard deviation of 0.016 mm at -30˚.

The reflective out-of-plane standard deviation of 0.043 mm at 0° was not representative of the target's other angles. For this target, the average standard deviation was 0.011 mm. These results showed that consistent results were obtained with the reflective target suffering from random noise in one particular scanner orientation. The experimental setup was considered to be consistent.

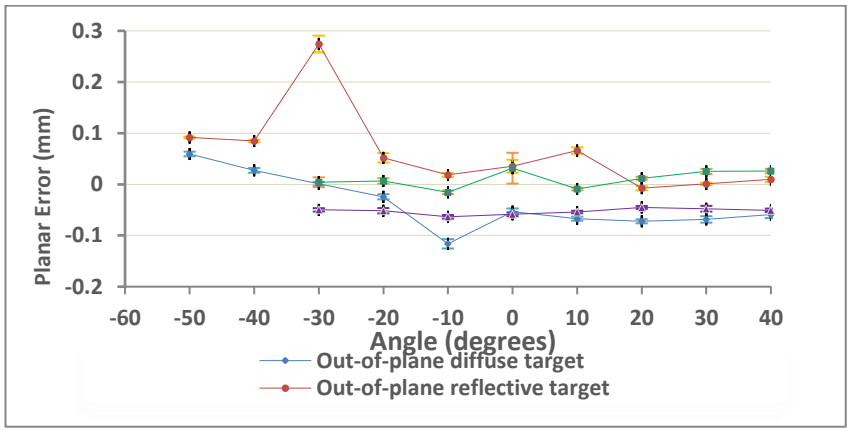

Fig. 3.3. Mean of experimental planar error from 6 scan sessions with standard deviation error bars, (data points joined for clarity).

3.3 Results of experimental laser line scan error measurement

The planar error (differences in planar scan distances from the mechanically probed planes) are shown in Fig. 3.4.

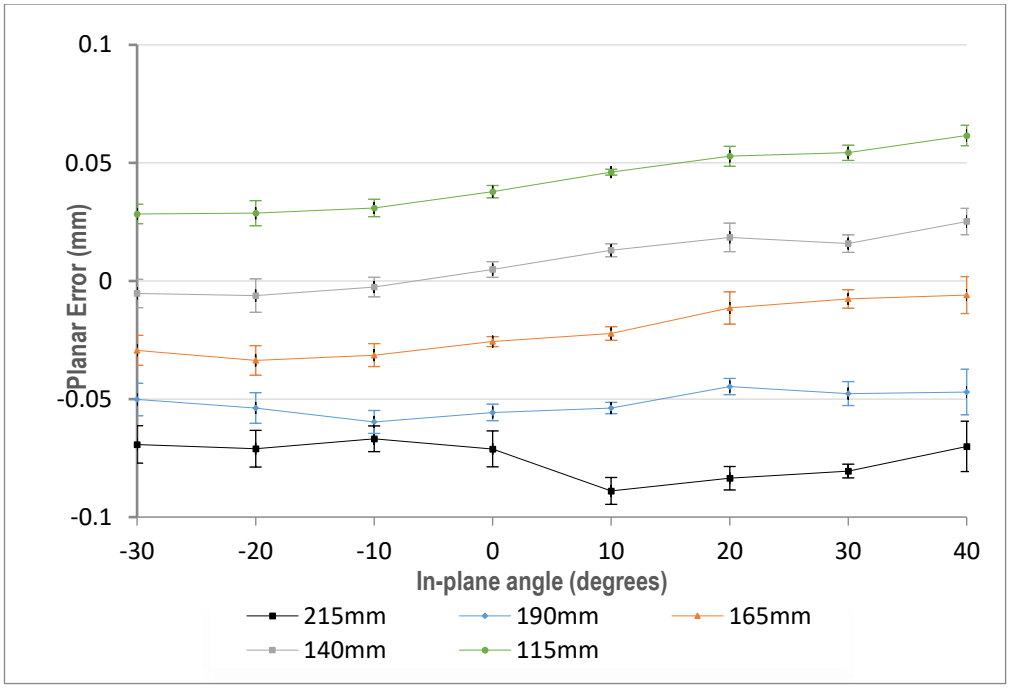

(a). Diffuse / matte white target error against in-plane angle

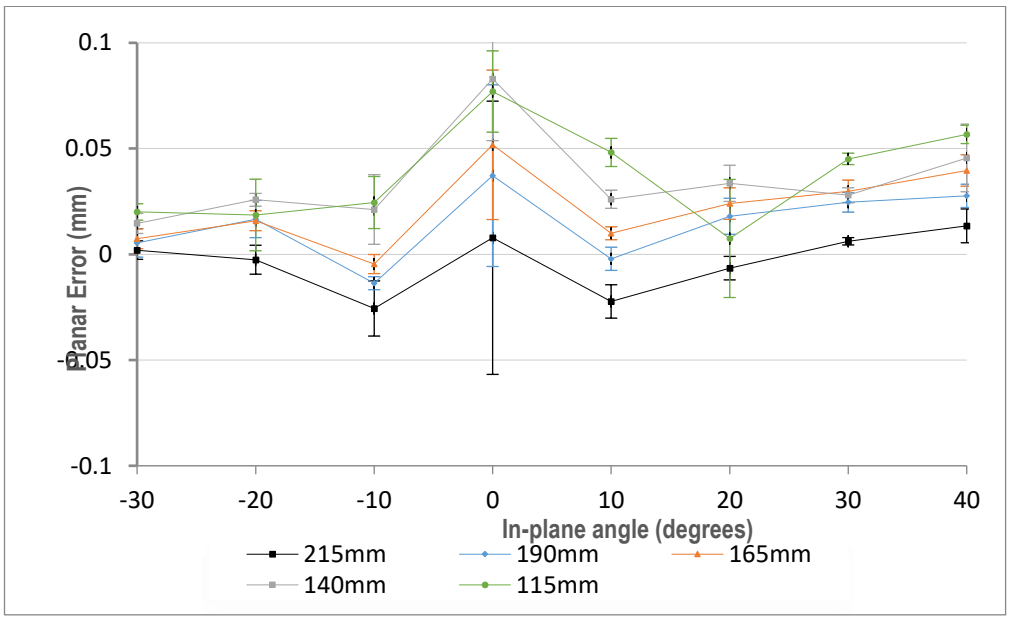

(b). Reflective target error against in-plane angle

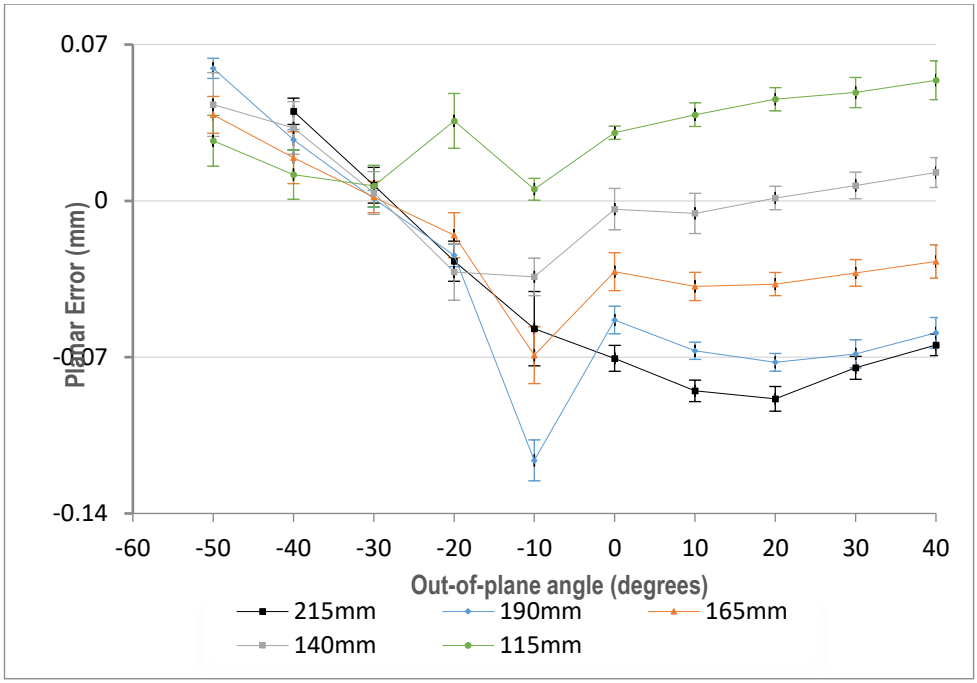

(c). Diffuse / matte white target error against out-of-plane angle

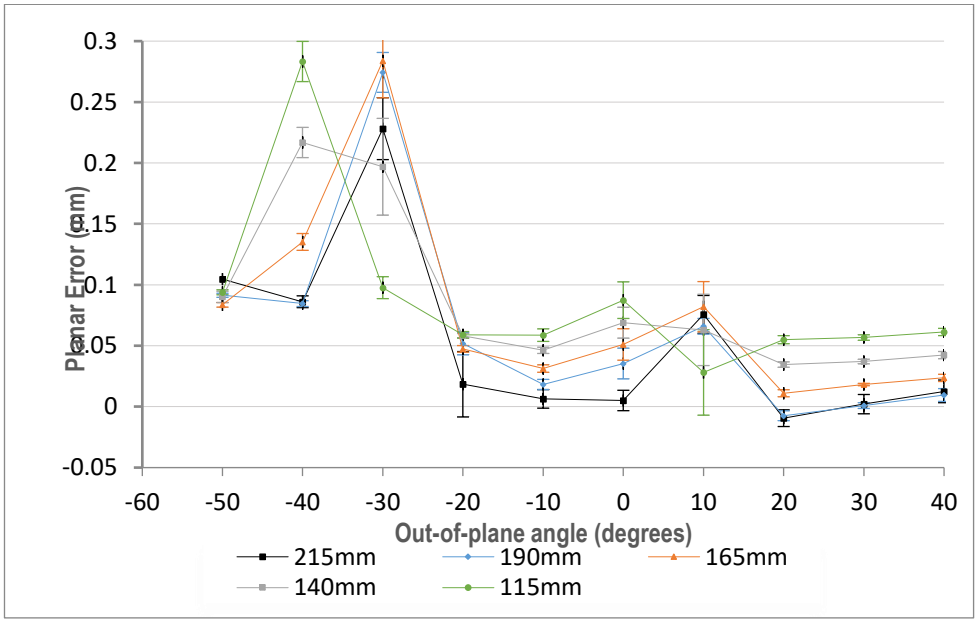

(d). Reflective target error against out-of-plane angle

Fig. 3.4. Scan error for various standoffs at different in-plane and out-of-plane angles with standard deviation error bars and data points joined for clarity.

It can be clearly seen in Fig. 3.4a that Lambertian target scans taken with varying in-plane angles (out-of-plane = 0°) show planar error to be dependent on scanner stand-off with in-plane angle having little

effect. Large scanner stand-offs show similar absolute error than near stand-offs, large stand-offs have negative errors and small stand-offs positive errors, with positive angles showing slightly greater error magnitudes than negative angles. suggest that in-plane positive angle scans are symmetric to in-plane negative scans. This has not been seen. There are differences in the microstructure of both the diffuse and reflective target which cause error not to be symmetrical.

Scans taken from the same target, but with varying out-of-plane (in-plane = 0°) Fig. 3.4c show similarly consistent results for positive scan angles only.

The reflective target scan results have some angles exhibiting the same characteristics as the Lambertian matte white target with varying in-plane angles, but in-plane scans of 0° (Fig 3.4b) and out-of-plane scans of -20° and scans from -20° to -50° (Fig. 3.4d) do not show this consistency.

3.4. Discussion of experimental laser line scan error measurement

As discussed in section 2.6. “Laser scanning error measurement” when the scanner beam is normal to the target surface the scan noise is at its greatest. This has been seen in the graphical views of the scan data Fig. 3.6 and Fig. 3.7. If the scanner beam has a half angle of β, a scanner in-plane angle of θ and stand-off of L, Fig. 3.5. If θ is less than β, there will be part of the line scan that is normal to the planar surface producing greater noise/data disruption. This disruption in the data is a distance D away from the experimental origin; where: -

$$D = L \times \sin\theta \text{ (while } \theta < \beta). \quad (3.1)$$

The scan beams half angle β was determined to be 19.00° (standard deviation 0.60°) from the largest and smallest X coordinates of the data points gained from all scans taken in the study, taking into account both scan angle and scanner stand-off.

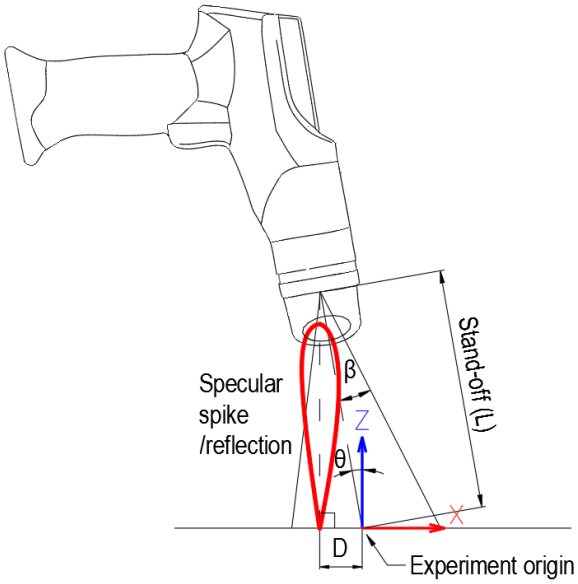

Fig. 3.5. Scanner geometry showing the section of beam normal to surface for in-plane scans.

Scan data having in-plane angles -10°, 0°, 10° gained at the 5 experimental stand-offs was combined within the Polyworks software to form an image of the data Fig. 3.6a. No manipulation of the scan data was required as all scans were taken with their beam centre traveling over the experimental origin along the Y axis Fig. 3.1 (each scan has a different colour). The scans shown have in-plane angles less than the scan beam half angle and so at various distances D along the combined data, part of the scan beams was normal to the target surface. At these points, disturbances are caused by the specular reflection . These areas of noise / disrupted data are clearly seen and their positions correspond to the calculated distance 'D' for the particular scan angle and stand-off. The same data is shown orthogonally viewed along the experimental Y direction Fig. 3.6b. This data disruption is not evident for scans taken from the Lambertian target Fig. 3.4a, but data disruption and greater experimental variation can clearly be seen between 10° and -10° for the reflective target Fig. 3.4b. This specular effect is sufficiently intense to cause disruption to scan passes taken not only at the smallest stand-offs, but not at 215 mm (the largest stand-off).

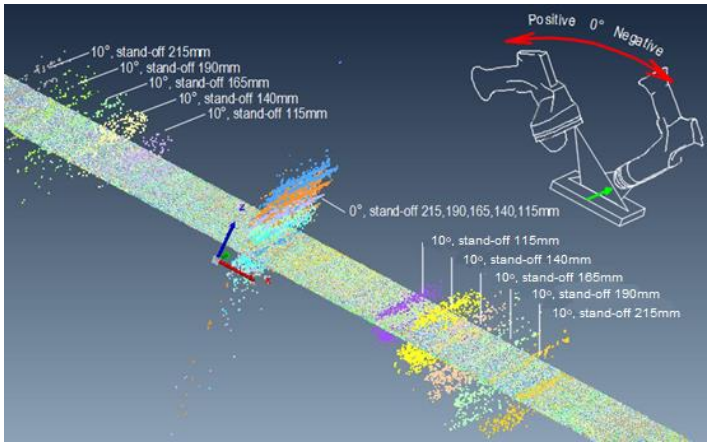

(a). Oblique view

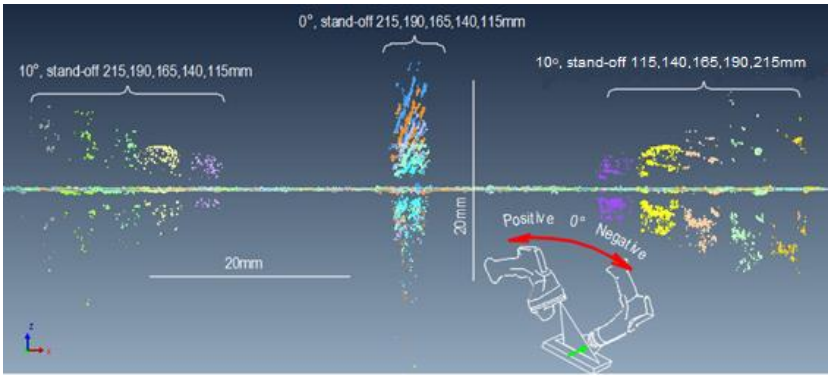

(b). Orthogonal view from negative Y direction.

Fig. 3.6. Scans taken of the reflective target with scan angles -10°, 0°& 10° at various stand-offs, with out-of-plane angle of 0°.

Scans varying out-of-plane Fig. 3.4c, for the matte white target with scan angles from 40˚ to 0˚ show measurement error change little with angle and confirm error is dependent on scanner stand-off, with large stand-off distances exhibit negative errors and small stand-offs positive errors. There is some deviation from this for all scans taken at negative angles less than 0˚.

Scans varying out-of-plane Fig. 3.4d for the reflective target with scan angles between 40˚ to 20˚, change little with angle and show error is dependent on scanner stand-off with error being mostly in the positive direction. From scan angle of 10˚ there is some disruption of scan data, but disturbance becomes considerable for -30˚ and -40˚ scans.

Scan data for all out-of-plane scans was combined within Polyworks software to form an image of the data Fig. 3.7a. As previous, no manipulation of the scan data was required as all scans were taken with their beam centre traveling over the experimental origin along the Y axis Fig. 3.1 experimental setup (each scan has a different colour). For clarity only data around the experimental origin is shown. This data has had 115 mm and 215 mm stand-off scans separated out and the scans for each angle placed side by side to display the data disruption for each individual scan. The data is viewed orthogonally along the experimental Y direction Fig. 3.7b.

The data in Fig. 3.7b shows a disturbance in all scans from 20˚ to -50˚, this disturbance has not translated to noticeable errors in all angles in the graphed representation of the data. Either the disturbed data is equally distributed above and below the fitted plane and the effect is self-cancelling, or the disturbance is small and within the experimental variance. For scan angles of -30˚, -40˚ and 10˚ all stand-offs show considerable data disruption both in the Polyworks image Fig. 3.7b and in the graphed error data Fig. 3.4d.

The disturbed data is caused by specular reflection , being returned to the CCD.

A matte target as used in this investigation reflects the laser beam uniformly in all directions. The laser scanning device is tuned to this level of received / reflected laser light. Reflective targets reflect the laser beam in a combination of ways from mirror like reflection to that exhibited from a matte surface. Speckle reflection results from the laser beam being scattered from the imperfections in the target surface microstructure. The scattered laser beams additively interfere with each other, increasing their intensity. This intense light returning to the scanner CCD may saturate the device so no return point is recorded. The light may be so intense, the CCD cannot identify the centroid of the returning light, so recording an incorrect target surface position. As light is scattered from the target surface micro imperfections, the laser beam may split and travel in different directions. The scattered beams emanate

from essentially the same point on the surface but are being scattered to different positions on the receiving CCD resulting in erroneous data.

Some of the data disruptions Fig. 3.7b produces gaps in the data; this appears to be the CCD becoming saturated. It can also be seen that stand-off affects this disruption. For out-of-plane scans of -50˚ there is less data disruption to the 215 mm stand-off than the 115 mm position. These effects are present on both reflective and Lambertian surfaces, but the effect is more pronounced on the reflective surface.

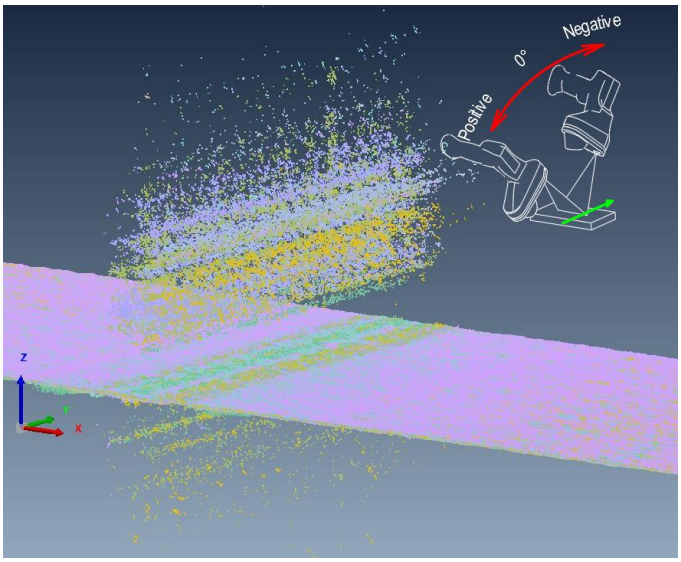

(a). Oblique view of 115 mm and 215 mm stand-off scans in their as scanned position

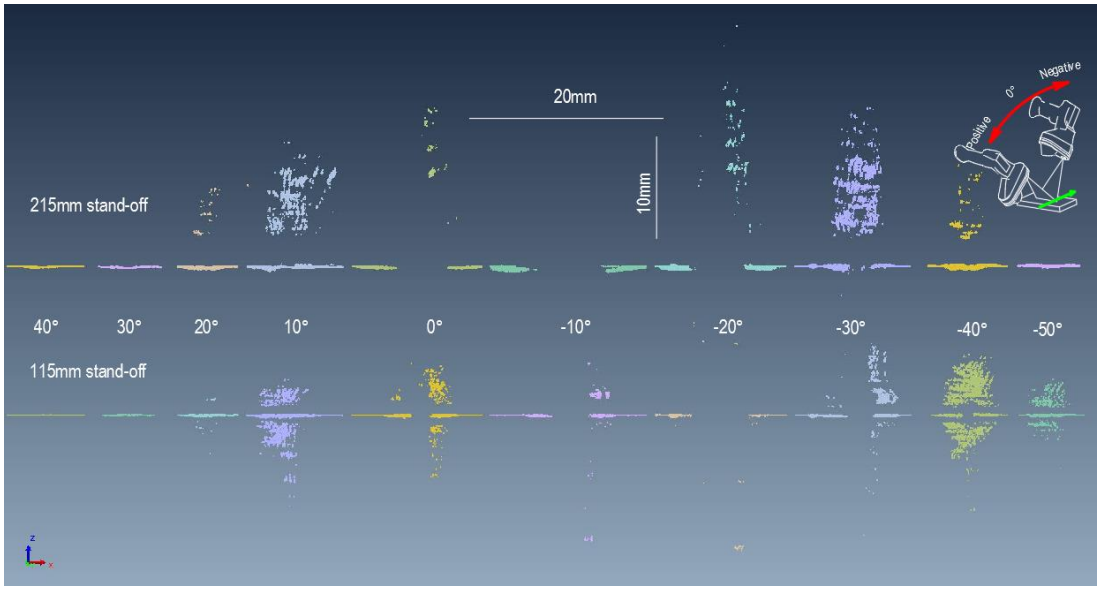

(b). Orthogonal view from negative Y: Scans separated (translated horizontally) to show disturbance.

Fig. 3.7. Scans taken with out-of-plane of 40° angle to -50° (in-plane of 0°) with 140 mm stand-off for the reflective target.

indicates how a specular lobe can disrupt the accuracy of laser light returning to the CCD. This disruption is dependent on scanner geometry, scanner out-of-plane angle and stand-off. The disruption caused by the specular reflection can be seen graphicly Fig. 3.6 and Fig. 3.7.

3.5 Summary

If the target surface is diffuse, scanner error would appear to be influenced by the systematic error of the scanner. If the surface microstructure causes speckle reflection, the scanner systematic error is outweighed by the accuracy of the errors in the returned light beam and the CCDs inability to accurately determine the centroid of the laser beam image. In general scanner error is more sensitive to laser head stand-off due to the changing geometry of the sent and received laser beam as stand-off changes. Largest stand-offs produce negative errors and the smallest stand-offs positive errors. This systematic error is only modified when speckle reflection influences scan error more than the laser head systematic error. If a diffuse material is being scanned, in-plane and our-of plane angles have little effect on the

scanner error, but as can be seen in Fig, 3,4, there are angles for both reflective and diffuse surfaces that cause speckle reflection, showing that at these angles any relationship between scanner error and scanner stand-off are lost. At this point the variance of the cloud point distribution has a greater influence on scanner error than the scanner systematic error.

surfaces may rise and fall relative to each other, so within the same scan pass, a variety of these in-plane and out-of-plane parameters may be experienced. It is unlikely that the full range of angles measured in this investigation will be experienced, as good scanning practice tries to keep the scanner as normal as possible to the target surface. The large negative and positive in-plane and out -of-plane angles would be difficult to achieve for a person with normal dexterity. It is also the case that the laser scanner tested has range finding lasers and an audible guide to keep the scanner stand-off at an ideal distance, so an assumption of 0.07 mm as a reasonable error for scan data seems reasonable. An ideal range of scanning angles would be to scan in-plane from -10 degrees to +10 degrees with a stand-off of 150 mm (the distance the laser on board range finder is set). If possible, out of plane setting other than small positive angles should be avoided.

Chapter 4. Hybrid probe tip compensation concepts

It has been seen in section 2.7. 'Tactile probing / analogue scanning error measurement' when measuring with a tactile probe, as the probe contacts the target, it triggers the static CMM to register the probes positions and so return a value of the probe centre to the CMM software based on the probe geometry established during qualification. In the case of the articulated arm tactile probe system used in this investigation, the probe is put into contact with the surface and the operator triggers the device to take the reading. As with the static CMM, the probe centre position is recorded based on the probe geometry established during qualification.

Where prior knowledge of the surface form is known, for example prismatic surfaces, probe compensation can be provided to give accurate surface information by offsetting this probe tip centre data. Where prior knowledge of the surface does not exist, probe tip compensation may be more of an approximation, formed using learning algorithms or predictions of the surface shape. This chapter will develop two hybrid systems that use laser scan data to inform tactile probe compensation.

Before any discussion of hybrid probe tip compensation methods can be take place, there must be a good understanding of the merits of laser scanning and tactile probing. In this investigation the laser scanner is attached to an articulated arm, and tactile probing is undertaken using a static CMM.

The arm mounted laser line scanner can gather substantial numbers of data points quickly (600K per second), but their accuracy is around an order less or more than tactile probing of a freeform object. Reflective surface finishes can be problematic, with speckle reflection producing erroneous data / outliers. The articulated arm allows the system to be portable and large objects to be laser scanned from multiple positions, with the different scans being aligned using overlapping data or reference objects temporarily attached to the target object. Laser scanning is a non-contact measuring technique, so delicate / flexible objects can be measured without damaging them. If the material to be scanned is crystalline then subsurface scattering of the data may be problematic.

Tactile probing on a static CMM can give measurements to a single micron. The maximum permissible error for the static CMM used in this investigation is 0.00185 mm for a 150 mm object. Data acquisition can be quite slow compared to laser scanning where depending on the type of probe being used and technique employed, 25 points a minute might be reasonable. A scanning probe can be added to the CMM. The probe does not leave the surface and records points at set intervals. In tactile scanning mode, probes can gather 100's of points per minute.

4.1. Rationale for the hybrid process of probe tip compensation

In section 2.7. 'Tactile probing / tactile scanning error measurement'; various methods to reduce probe approach error have been discussed. These will prove un-successful if the probe 'flank' contacts the surface, rather than the area of the probe that is intersected by the scan plane. The techniques proposed in this thesis are a hybrid system that combines tactile probing and laser scanning.

It is proposed that the free-form surface will be tactile probed / scanned on a CMM without the application of any learning or probe compensation. That is, the probe centre coordinates will be returned. The surface knowledge required to determine probe compensation will be provided by cloud point data gained from an articulated arm CMM equipped with a laser line scanner.

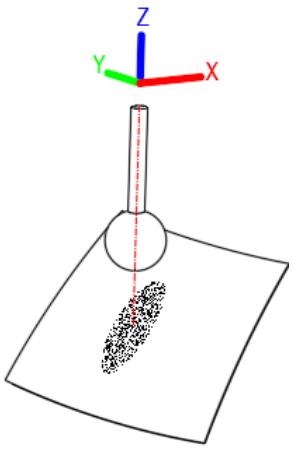

Fig. 4.1. Cloud point data of a surface directly below the probe (assuming the probe approach direction is along Z) has been isolated and represents the component of the surface capable of influencing the probe position.

Fig. 4.1 shows a free-form surface with a small subset of the laser scanned cloud point data representing the surface directly below the probe (assuming a 'Z' axis approach direction indicated by the red chain line).

4.2. Proposed probe tip compensation methods

Two methods for probe compensation are proposed. One method will modify the probe centre data that is returned when the probe tip is arrested by the work piece. The probe centre correction will be in the direction of the probe approach direction and follows the conventional correction shown in Fig. 2.10. The method will use a laser scan representation of the surface to estimate the steepest slope beneath the probe tip. It is the estimation of this slope that informs the probe tip compensation. This is shown as 'Z correction' Fig. 4.2 a.

The second method of probe tip compensation will determine the direction of the actual contact point of the probe with the target surface. As the probe contacts a free-form surface the contact point is the closest point on the surface to the probe centre. A laser scan representation of the target surface can be used to determine this closest point. The probe contact point will lie on this line such that a probe

compensation of the probe tip radius can be applied from the probe centre along this line. This is shown as 'Contact correction' Fig. 4.2 b.

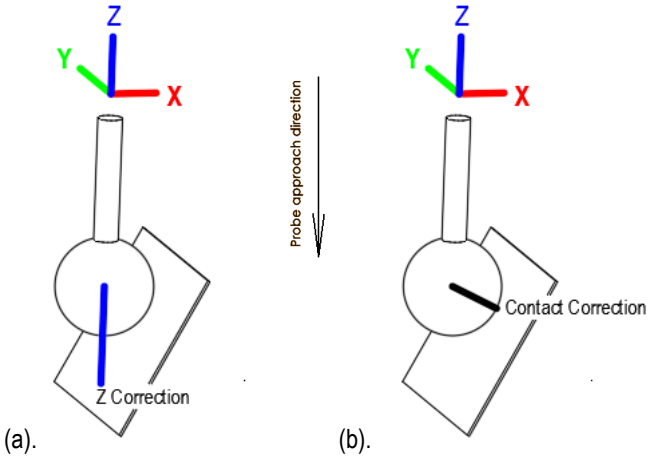

Fig. 4.2. (a). Probe compensation is in the 'Z' axis (approach) direction. (b). Probe compensation is in the direction of the probe to surface contact point.

Both proposed methods have their rationales detailed in this chapter and their methodologies developed and optimized in chapter 5. The overarching considerations used in both rationales are the same and are stated here in '4.2. Considerations used in forming hybrid probe compensation'.

4.3. Considerations used in forming hybrid probe compensation

The initial assumptions for measuring a free-form object are straight forward and obvious to a metrology technician experienced in the measurement of prismatic objects using tactile or laser scanning. These are: -

- The surface finish is of a resolution that can be tactile scanned by a suitable sized probe. The probe is not too large that it ignores relevant surface detail, or too small that it picks up surface finish effects rather than surface form.

- The material of construction is suitable for laser scanning. It does not produce sub surface scattering of laser light such as some crystalline materials do.
- The material of construction will not deform during the measurement process.
- The surface finish is appropriate for laser scanning, it is not so reflective that it cannot be scanned accurately without the aid of surface treatments used to make the surface matte.
- Surface features have a clear line of sight from the laser and to the receiving devise. i.e. there are no occluded features such as deep holes / grooves or re-entrant features.
- Features are accessible by the probe, over hangs, internal or re-entrant features that make probing impossible are not included.

The assumptions detailed relate to either touch trigger probing, tactile scanning or non-contact scanning. Problems occur when the two measuring practices are combined. The different systems are forming a virtual representation of the same surface, but with different dimensional and positional accuracies. It is well understood that tactile scanning and tactile touch trigger probing undertaken on a static CMM produce more accurate measurements than a laser line scanner mounted on an articulated arm. Other than these obvious issues, error can occur when combining data from different measuring systems into a common coordinate system as discussed in section '2.5. Working coordinate systems and alignment of coordinate systems'.

The accuracy of this data alignment from a machine coordinate system into a work piece coordinate system depends on the reliability of the best fit features formed from the data points, which depends on several criteria; these being: -

- The completeness of the feature being scanned. If the feature being scanned is relatively complete, that is in the case of a cylinder it has a full circumference or a sphere, a complete perimeter, when laser or tactile scanned there will be a greater proportion of the whole feature

to fit data to and so the best fit algorithm will produce a more accurate representation of the target object.

- The completeness of the data available: - Similar to the previous item, laser scanning of an object may be poorly undertaken with good practice guide lines not being followed , . The accuracy of best-fit features may depend on how much data is available and its ability to represent the entire feature. If only a small amount of data representing one end of a planar feature is available, the fitted plane is likely to be a less accurate representation of the surface than if data of the same density is available throughout the feature.
- The accuracy of the feature: - If the feature being scanned has not been accurately formed / machined then the accuracy of the best fit feature may be compromised. That is poor surface form or finish detail picked up by the laser scanner or probe may influence both the dimensional and geometric accuracy of the fitted feature.
- Scan noise: - Extraneous data has been discussed in chapter 2. This can be produced from surfaces that have a highly reflective finish or the use of poor scanning techniques. This can cause dimensional and geometric errors.

Accuracy of data set alignment with other data sets or CAD models is not part of this investigation, but it will be discussed in 'Chapter 8. Future work'.

To better understand the impact of data quality, i.e., noise, (erroneous data). A hemispherical test form of 150.032 mm diameter was laser scanned to generate 'raw' cloud point data and a polygonal mesh. The polygonal mesh was generated in real time and was analysed in both its cleaned and uncleaned forms. Fig. 4.3 shows deviation plots of the data sets from the hemisphere. The 'raw' un-cleaned cloud point data set, un-cleaned polygonal mesh and the cleaned polygonal mesh are shown Fig. 4.3a, Fig. 4.3b, Fig. 4.3c respectively. The data sets were also best fitted with spherical features to determine the influence of outliers on the dimensional accuracy of a best fit feature. The diametral accuracy of these best fit spheres and the standard deviation of the residuals are shown Table 4.1.

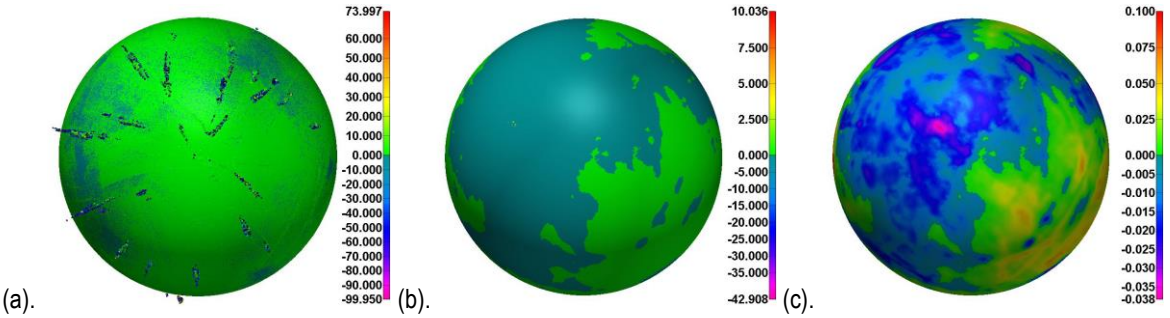

Fig. 4.3. Deviation plot of three data sets derived from laser scanning the same hemispherical form. (a). 'Raw' cloud point data, (b). Polygonal meshed in real time, with discrete areas of outlying mesh present, (c). Polygonal meshed in real time, with discrete areas of outlying mesh removed. Legends show deviation of data from a 150.032 mm reference hemisphere, with units in mm.

The cloud point data set has outliers at a greatest distance (73.997 mm) from the measured surface, with cleaned polygonal mesh data sets having the smallest (0.100 mm).

The underlying effect of meshing scan data is that it reduces the data point outliers, in essence cleaning the data of stray data points either automatically or by combining these stray points into small meshes making it easier to manually remove the stray data not connected to the main body representing the target. It can be seen from Table 4.1 that these un-cleaned outliers can influence the dimensional accuracy of the fitted spherical feature for the cloud point data set.

Table 4.1. Details the dimensional accuracy of the three data sets.

* Hemisphere diameter measured at 150.031 and 150.033mm. Nominal diameter taken as 150.032mm ** Not shown in Fig. 4.3	Best fit sphere diam. (mm)	Best fit diameter Error (mm) *	STD Of best fit residuals (mm)	Deviation mean
Real time Polygonal meshed (not cleaned)	147.686	2.346	4.951	-1.334
Manual formed Polygonal meshed (not cleaned) **	149.084	0.948	4.173	-0.768
Cloud point data	149.942	0.090	2.793	-0.205
Manual formed Polygonal meshed (cleaned) **	150.005	0.027	0.216	-0.009
Real time Polygonal meshed (cleaned)	150.043	0.011	0.857	0.03

Polygonal meshed data produced the most accurate dimensional representation of the hemispherical features size, with data produced in real time not only being the most accurate but being the most convenient way of obtaining data.

The most effective and efficient way of gaining a cloud point data set of an object would appear to be to form a real time mesh as laser scanning progresses. Once laser scanning is complete and the mesh is finalised, software tools can be used to automatically select areas of floating mesh and triangles containing polygonal topological errors. The resultant 'cleaned' polygonal mesh can be exported as a cloud point data set.

It is apparent from the data that the digital representation of the surface produced by laser scanning has errors. These errors may not simply be from the scanning process and the inherent problems of surface finish, sub surface scattering, scanner orientation and the like, but also the way the scan data has been processed.

Scan data error may derive from the amount of manipulation that is required in the reverse engineering / metrology process being used. It may not always be convenient to have data sets in the machine coordinate system in which they were derived. It may be more convenient or an essential part of the process to manipulate the data, translating and rotating it from a machine coordinate system into a more usable work piece coordinate system.

If a product is being reverse engineered with no requirement for validation against the original design form, there may be no requirement to manipulate the coordinate systems. If the process is being used primarily for quality control, then direct comparisons of the digital surface representation to a CAD model in the same coordinate system may be essential, requiring data sets to be aligned with reference to CAD models or other reference data sets.

This investigation is concerned with using laser scanned data to provide the surface knowledge capable of allowing accurate probe compensation to be made when measuring free-form surfaces. To

this end laser scan data representation of the surface is required to be in the same coordinate system as the tactile probed data; such that alignment of laser scanned cloud point data to tactile probed data must be considered as a source of error. It is also the case that if the scan data is to fill the gap of there being no prior knowledge of model features; then erroneous data (outliers) may be problematic.

In essence dimensional errors in a cloud point representation of a surface can involve individual points or groups of local points that are offset from the original due to inaccuracies in the scanning process. Or whole data sets that are displaced (translated / rotated) due to registration issues. Highly exaggerated and simplified errors in the digital data are shown in Fig. 4.4 where red dots represent the cloud point data and black lines the actual surface. For clarity, only cloud point data to one side of the actual surface is shown.

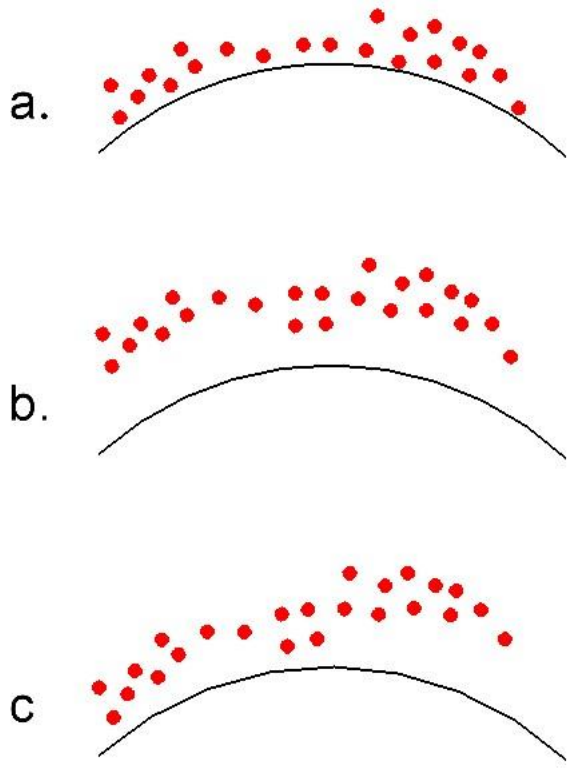

Fig. 4.4. A simplified representation of laser scan data for a curved surface from. (a). data is representing laser scanner error / normal variance. (b). & (c). cloud point data of the surface feature is displaced from the surface as per a registration / alignment issue.

Examples Fig. 4.4a, depict a conventional variance between individua cloud point data points and the surface. These errors are likely to be produced from the inherent laser scanner accuracy issues that were discussed in section '3.2 Experimental measurement of scanner error'. Fig. 4.4b, and Fig. 4.4c, show a displacement of the whole cloud point data set from the surface with Fig. 4.4b showing a translation and Fig. 4.4c, a rotation. Both issues are likely to be caused by the data alignment process when moving from a machine coordinate system to a work piece coordinate system.

Previous discussions have considered cloud point data error at a feature level and comparisons have been made between the accuracy of this data and actual surfaces. If as previously discussed, a cloud point data representation of a surface is to be used to determine probe compensation where there is no knowledge of the actual surface form, then data coverage and density may be an added consideration.

If a CAD model of the surface is present or the surface can be derived from an equation there is continuous and infinite knowledge of the surface between its bounding edges. If cloud point data is being used to represent this unknown surface, then only a finite number of data points representing the surface are available.

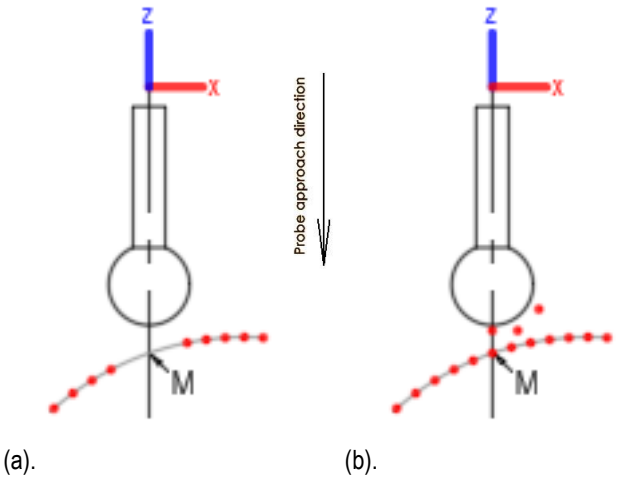

(a). (b).

Fig. 4.5. A simplified representation of a probe approaching the target surface (grey line) along the 'Z' axis. (a). indicates a lack of data coverage at the theoretical measurement point and (b). shows extraneous data / outliers.

Fig. 4.5 shows an exaggerated pictorial view where the probe approaches the work piece surface along the 'Z' axis with 'M' being the intended point to be measured. As there is no prior information of the surface available, cloud point data (red dots) are used to represent the surface and so provide this information. If there are gaps in the cloud point data Fig. 4.5a, or there are outlier points Fig. 4.5b for reasons such as local areas of the surface being highly reflective, then probe compensation will become more difficult. Sparse data points may also be due to bad scanning technique, too rapid travel across the work piece or incorrect scanner settings.

4.4. Rational for probe compensation in the probe approach direction

Initially the problem will be examined in 2D space, on the 'Z – X' plane Fig. 4.6b. There is no surface knowledge connecting contact point 'C' to the intended measurement location 'M'.

The main premise of the hypothesis is that the probe diameter is assumed to be relatively small compared to the form being measured and that that the curved target surface below the probe will approximate to a straight line as the probe tip decreases in size. To examine the validity of the

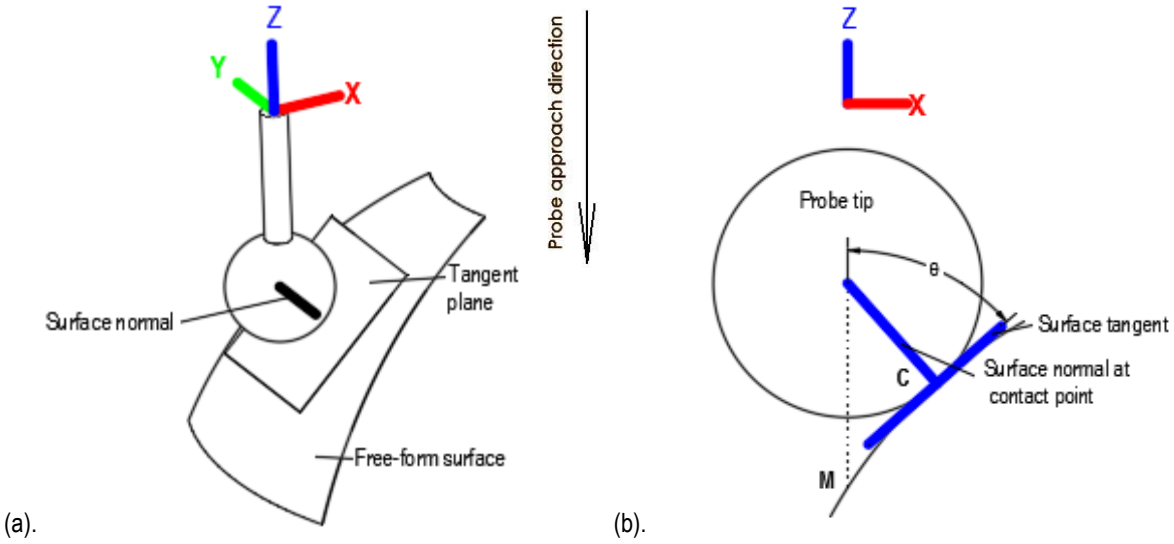

(a). (b).

Fig. 4.6. (a). & (b). Probe surface normal and tangency at the probes point of contact sketched in 3D and 2D respectively.

assumption it is assumed that the free-form surface is in fact a convex spherical surface Fig. 4.7a and a cross section is taken at a longitude of 0º. The probe size relative to the measured form has been shown to an unrealistic ratio for clarity.

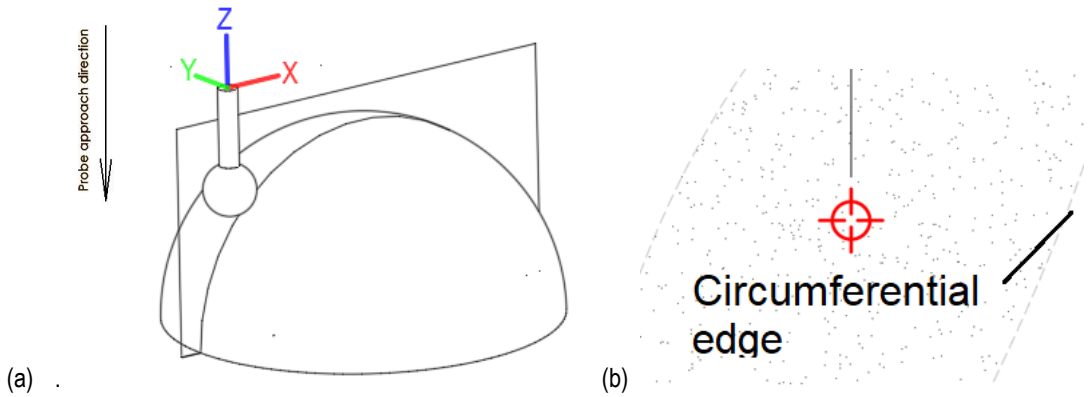

(a) . (b)

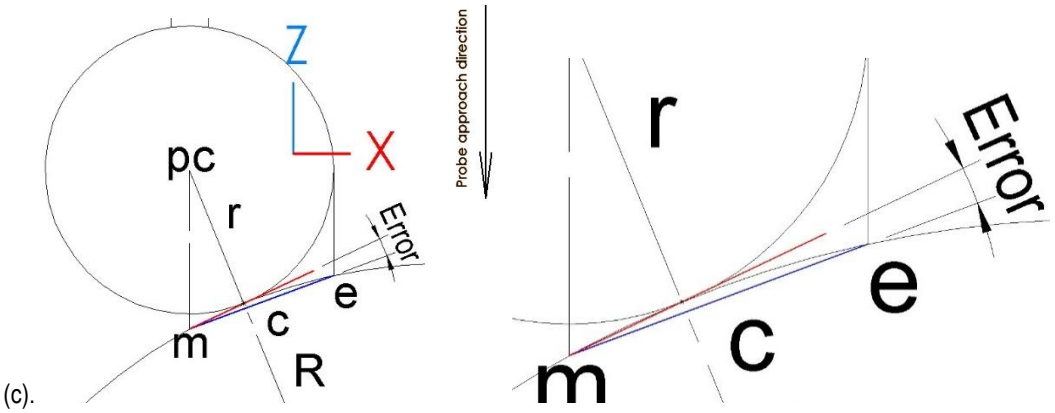

Fig. 4.7. Details a probe contacting a spherical form. (a). shows the cross section position at longitude of 0º, image. (b) details scan perimeter, (c). details the cross section on plane 'Z – X'. The ratio of probe size to work piece has been exaggerated for clarity.

The image shows a probe of radius 'r' and spherical target object of radius 'R', point 'pc' describes the probe centre. Point 'c' the probe / target surface contact point, 'm' the position being measured (intersection of the probe axis and the target surface). Point 'e' is a point on the target surface, directly below the probe 'circumferential edge', with the extended red line segment 'mc' describing a straight line between the probe anticipated contact point 'm' and the actual contact point 'c'.

The blue line '$\overline{me}$' represents the estimated target surface slope that can potentially influence the probe 'Z' axis position. The 'Error' angle is the difference between the 2 lines '$\overline{me}$' and '$\overline{mc}$'.

As the probe radius gets smaller relative to the surface feature; red line 'mc' approaches the blue line '$\overline{me}$'. This can be seen Fig. 4.8. View 'a' has a relatively large probe to measured feature diameter and view 'c' a relatively small probe diameter to measured feature diameter.

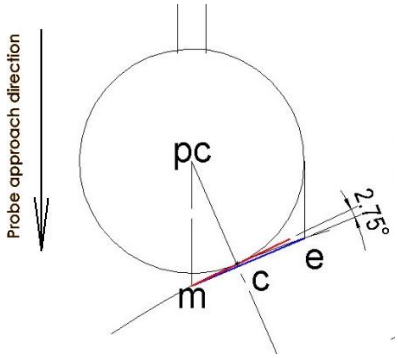

Fig. 4.8. depicts the error in angle terms associated with the hypothesis. For clarity probe size is shown the same size in all images with surface topology changed.

Fig. 4.8 shows the angle error associated with the hypothesis and Table 4. 1. Shows the error angle for different target form to probe tip diameter ratios.

Table 4.2. Details the hypothesis error (angle) for a spherical target object as sphere diameter rises. Relative work to probe size is indicated as a ratio for the geometry shown in Fig. 4.7

Ratio of work dia. to probe dia.	Error angle (degrees)
1.67	11.11
3.33	5.65
8.33	2.3
16.67	1.16
33.33	0.58
66.67	0.29
133.33	0.15
266.67	0.07

When the probe diameter is relatively small compared to the measured features diameter, we can estimate the probe compensation in the Z direction by assuming the surface to be measured is a straight line. This assumption is detailed in Fig. 4.9 and equation 4.1 through 4.2 detail the compensation value required.

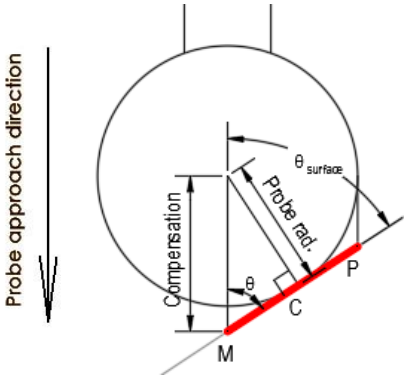

Fig. 4.9. Probe compensation.

$$Probe\ Rad\ = Compensation\ x\ \sin\theta_{surface} \tag{4.1}$$

Rearrange

$$Compensation\ = \left(\frac{Probe\ radius}{\sin\theta_{surface}}\right) \tag{4.2}$$

In essence this is the same as equation (2.1), except the probe tip radius has not been subtracted. As detailed previously in section '2.7. Tactile probing / tactile scanning error measurement', when probing three dimensional surfaces the probe flank (outside of the two-dimensional 'X – Z' scan plane being discussed here) may be the point of contact with the target surface rather than point 'C', so the compensation equations cannot return the correct probe compensation. The compensation method being developed here uses laser scan cloud point data to provide the surface knowledge required to estimate the flank contact point, which can then be used to calculate probe compensation.

The scan data is assumed to follow the target surface form or be a constant offset from it. As was seen in Fig. 4.4a, the correction hypothesis assumes the surface representation to be parallel to or a match to the surface. The assumption only needs to hold for the small patch of cloud point data directly below the probe relative to its approach direction and because the probe is relatively small compared to the object being measured, the assumption seems reasonable.

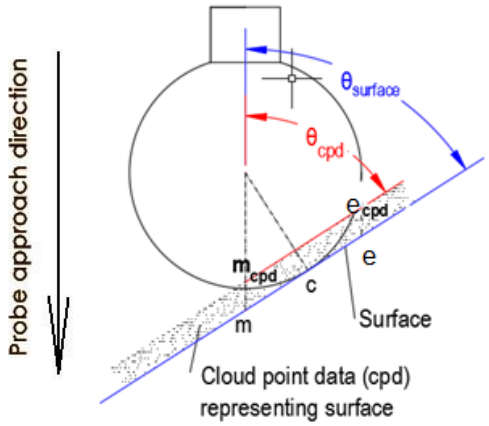

Fig. 4.10. Laser scan cloud point data parallel to the actual surface is used to determine surface tangency and so surface normal.

If the probe diameter is small compared to the surface curvature and the offset scan data is considered to be parallel to the surface, we can substitute θ_{cpd}; into equation (4.2), giving:

$$Compensation\ \left(\frac{Probe\ radius}{\sin\theta_{cpd}}\right) \tag{4.3}$$

Up to this point the discussion has been related to a two dimensional representation of the probe and work surface seen on the 'Z – X' scan plane, where any probe 'flank' contact outside of this view plane has been ignored.

If a series of radiating lines like spokes in a wheel were to be considered, joining the theoretical probe surface contact point 'm' with points around the perimeter of the local laser scanned points below the probe tip Fig. 4.11, the line '$\overline{me}$' that influences the probe position is the one that has the smallest angle between '$\overline{me}$' and the probe approach direction. That is the steepest radiating line.

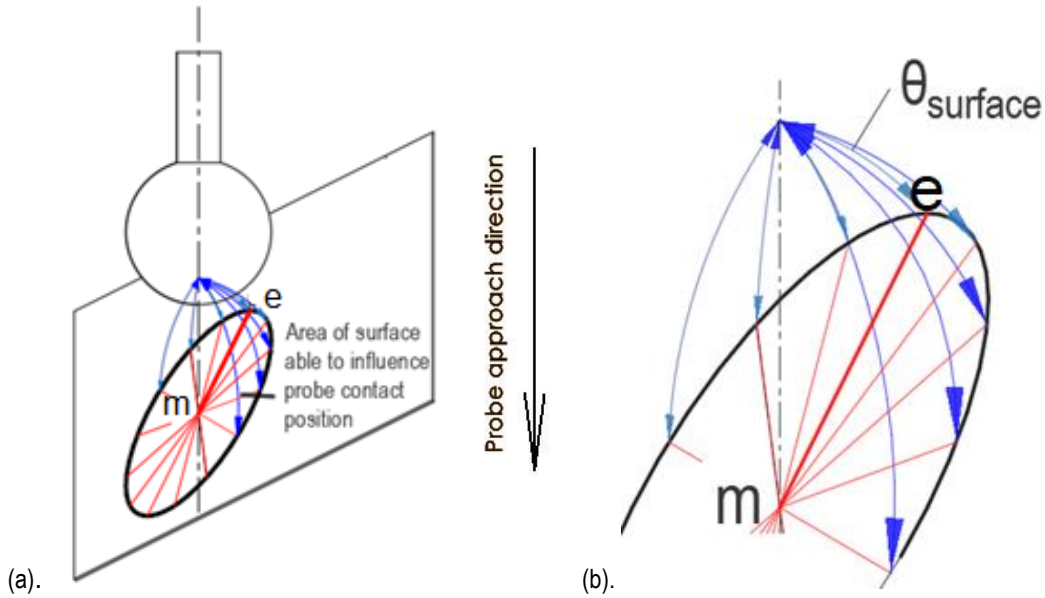

Fig. 4.11. (a). Rationale for finding the area of the target surface that the probe contacts when approaching in the 'Z' direction. (b). An enlarged view.

In this example the thick red line '$\overline{me}$' and angle $\theta_{surface}$ represent the line of contact with the probe and its angle from the vertical respectively. If the cloud point data is considered rather than the actual surface, θ_{cpd} can be viewed as equivalent to $\theta_{surface}$. So, the smallest value of θ_{cpd} can be used in equation (4.3).

Problems probing the apex of convex forms has not been considered here but will be discussed later.

4.5 Rationale for probe compensation in the direction of probe contact point normal

As with the method proposed in section '4.3. Rational for probe compensation in the probe approach direction' this rationale uses contactless laser scan data of a target surface to correct contact probed data.

It has been seen Fig. 4.6b that where a probe tip contacts a surface during tactile scanning, the surface normal passes through the probe centre and the 'probe to surface' contact point.

This means that if cloud point data forms a good representation of the actual surface (the scan data is accurate and has few or no outliers) or the scan data is relatively parallel to the actual surface (offset produced by data set alignments). The closest cloud point to the probe centre should be a good representation of the actual contact point direction. This should hold no matter what degree of offset the scan data has as shown by the red dots Fig. 4.12. The closest point to the probe centre, i.e. the one that best represents the actual probe contact point would lie on the surface contact normal shown. Scan data points are shown to the outside of the target surface only as is depicted in Fig. 4.4a, although depending on the target surface finish and laser scanner stand-off some scan data can be recorded below the target surface. Fig. 3.4a shows laser scanner stand-offs of 215 mm and 190 mm as having -0.070 mm and -0.050 errors respectively.

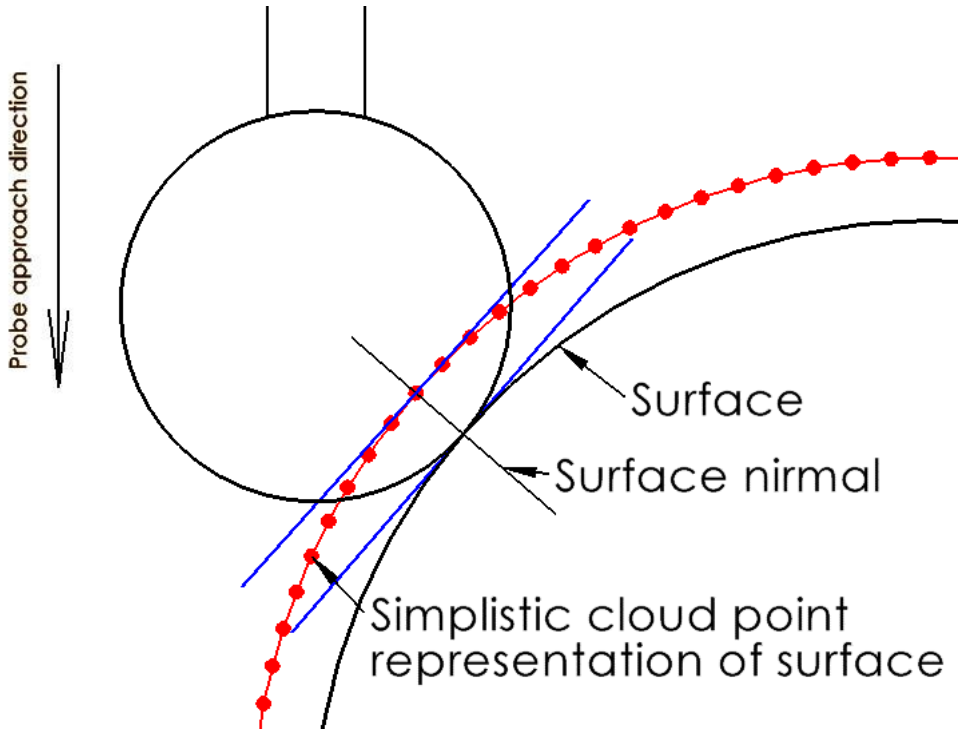

Fig. 4.12. Cloud point data representation of the surface has an offset error which can be above or below the actual surface (shown as red dots).

If a cloud point data displacement through miss alignment of the whole data set during coordinate system alignment occurs, the above may not hold true. If we assume a free-form surface to be replaced

by a sphere, the probe error using this hypothesis can be estimated. Fig. 4.13 shows a probe taking a tactile measurement of a spherical feature whose centre is (0,0). A cloud point representation is detailed as a red dashed circle that is displaced from the actual measured feature by a 'scan displacement error' 'd' to point 'D' in the negative 'X' direction. The displaced scans have centre coordinates (-d,0,0). The probe to measured object size ratio and the cloud point data displacement have been highly exaggerated for clarity.

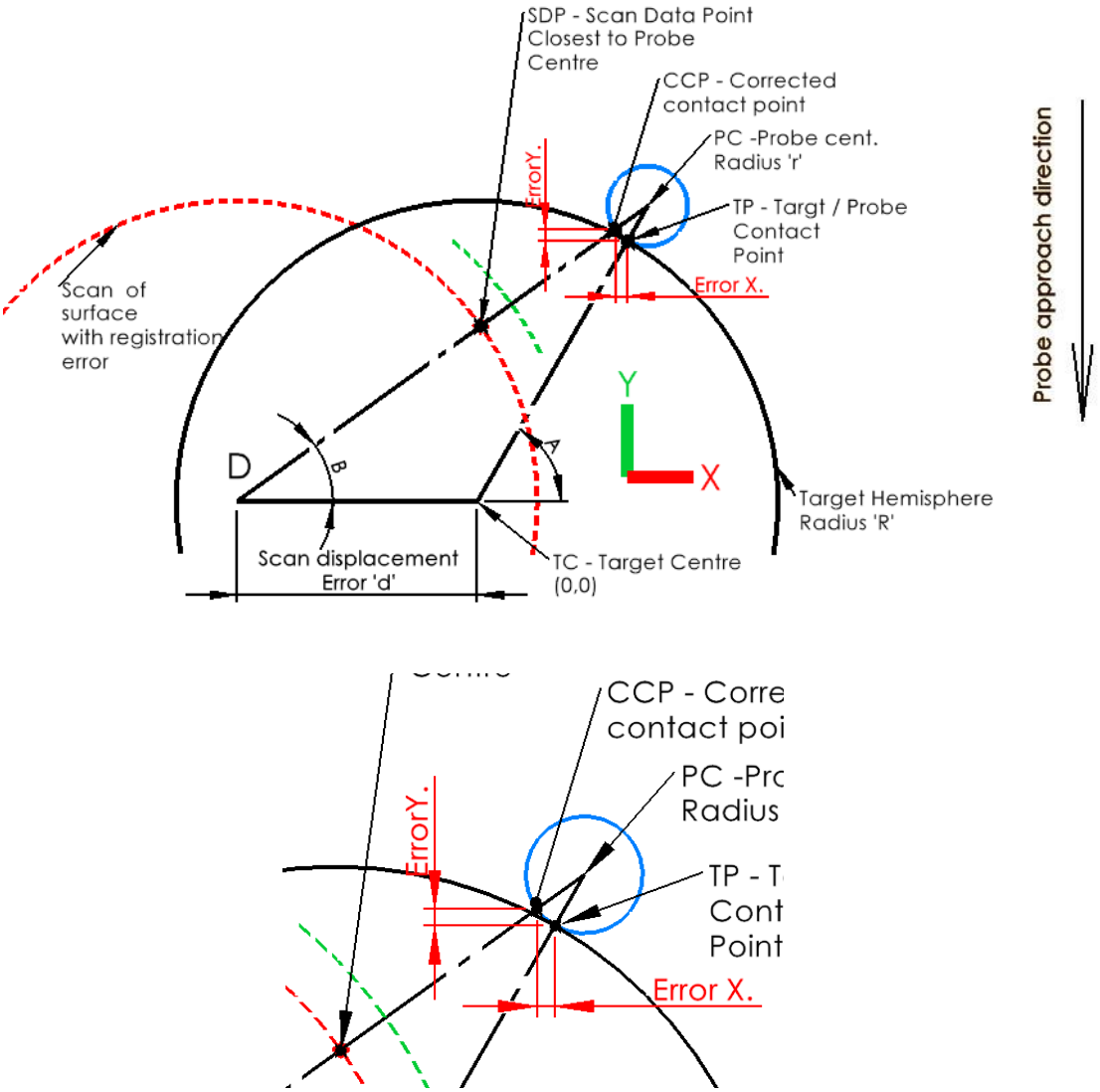

Fig. 4.13. Cloud point data displaced in the scan alignment process. For clarity probe size and displacement value have been exaggerated and an enlarged view added.

The probe contacts the surface at point 'TP' the closest point on the actual surface to the probe centre.

If the cloud point data representation is displaced by a distance 'd' the closest cloud point data to the probe centre lies on the virtual cloud point surface normal 'D – PC'. It can be seen that if the proposed probe correction hypothesis corrects the probe along this cloud point normal by an amount equal to the probe radius, the corrected contact point will be point 'CCP'. The error associated with a cloud point alignment displacement is shown as the distance between this point 'CCP' and the actual target / probe contact point 'TP'.

Points 'PC' describe the probe centre point, 'r' the probe radius, 'R' the target sphere radius. Suffix's 'x' and 'y' represent the horizontal and vertical directions respectively.

$$PC_x = (R + r)\cos \mathrm{A} \quad (4.4)$$

$$PC_y = (R + r)\sin \mathrm{A} \quad (4.5)$$

$$\text{Angle B} = \tan^{-1}(PC_y / (PC_x + \mathrm{d})) \quad (4.6)$$

$$\mathrm{TP}_x = Rcos(A) \quad (4.7)$$

$$\mathrm{TP}_y = Rsin(A) \quad 4.8)$$

$$\mathrm{CCP}_x = PC_x - r\cos B \quad (4.9)$$

$$\mathrm{CCP}_y = PC_y - r\sin B \quad 4.10)$$

$$\text{Error Horiz.} = TP_x - CCP_x \quad 4.11)$$

$$\text{Error Vert.} = TP_y - CCP_y \quad (4.12)$$

Substituting for TP and CCP

$$\text{Error Horiz.} = RCos(A) - (PC_x - r\cos B) \quad (4.13)$$

$$\text{Error Vert.} = RSin(A) - (PC_y - r\sin B) \quad (4.14)$$

By Pythagoras the magnitude of the error is: -

$$\text{Linear Error} = \sqrt{(\text{Error Horiz}^2 + \text{Error Vert}^2)} \quad (4.15)$$

For a hemispherical form of 150 mm diameter (R = 75 mm) being measured with a 6 mm diameter probe tip (r = 3 mm) at 85° from the 'X' axis, (A), a cloud point alignment displacement of 0.050 mm (d),

the correction error of the hypothesis would be 0.002 mm in 'X', 0.0002mm in 'Y' and 0.002mm error magnitude.

It can be seen from Fig 4.13 that the accuracy of a probe tip compensation method using laser scanned data of a surface to inform the correction is dependent on how accurately the scanned data represents the target surface and how accurately the scanned data is aligned to the target surface. The probe tip correction in the surface contact direction realized in Chapter 5 must overcome these issues.

If scan data error were added to the scan alignment error (green dashed curve in Fig. 4.13 - enlarged view) this would not add to the error of the compensation method as the two data sets are concentric for the hemispherical form depicted. It may be the case that scanner error is not a constant offset from the surface for a sphere or the surface of a free form object. That is, it is not concentric for the sphere example used in Fig. 4.13 and it would not be a 'curve offset' for a freeform object. It has been seen in section 3.3 'Results of experimental laser line scan error measurement' that laser stand-off contributes to measurement error. When scanning a freeform or spherical objects it is impossible to maintain a constant stand-off between full width of the laser beam and the target surface.

Although a prismatic spherical form is used to develop the probe tip correction in the surface contact normal direction, there is no reason why the compensation solution should not apply to any freeform surface

4.6 Summary

Two probe tip correction methods have been proposed for the correction of tactile scanned data of a surface form by the use of a less accurate laser scanned cloud point representation of the same surface. The accuracy of the systems discussed is based on the cloud point data not only being a relatively sound representation of the surface being measured, but also the cloud point data must be

accurately aligned with the tactile data. The assumptions discussed not only rely on there being sufficient data present but just as importantly there being a lack of outlier data points. Before these proposed systems can be tested on actual measured forms, data manipulation processes and routines must be developed. This is detailed in chapter 5.

Chapter 5. Realization and initial testing of probe compensation methods

The two systems proposed for applying tactile probe compensation detailed in chapter 4 have been discussed in broad detail. To develop the methodologies further there must be some basic understanding of the data structures used. Tactile probed and cloud point data in its most basic form is the 'X', 'Y', 'Z', coordinates of the measured points. In some cases, this data may be accompanied by surface normal information if the data is in the form of a polygonal mesh.

The probe compensation rationales discussed both take relatively inaccurate laser scan data and align it with highly accurate tactile scanned probe centre data. It is understood that the probe centre data does not represent the free-form surface well as it needs correction in either the probe approach direction or in the probe surface contact normal direction. The laser scanned cloud point data is a representation of the actual surface.

For convenience only, the tactile scanned data set has been aligned to the target form. The cloud point and tactile probed data has planar features best fitted to the faces to be used in the alignment process. The translation of laser scanned data onto tactile probed data is accomplished using the 'perpendicular' planes method. The work piece coordinate system is set such that the 'Z' direction is vertical (as with most CMM) and the other orthogonal axes follow the right-hand rule.

The initial process for setting up the data followed the same process for both compensation methods; this is shown in Fig. 5.1. For the convenience of data manipulation, the tactile scanning probe is operating in the 'X – Z' scan plane, with discrete measured points being taken at the probe positions shown. If data points are gained with no software learning techniques or no probe compensation applied as discussed in chapter 2, then the blue dots Fig. 5.1a represent the theoretical points being measured. The red points are the actual contact points where the flank of the probe contacts the work piece and the green dots the centre of the probe. This situation is complicated further. If the probe

has an oblique approach direction relative to the surface, this situation is further complicated by the need to consider probe deflection error.

It is the probe centre measured coordinates that are initially returned from tactile probing / tactile scanning. Fig. 5.1b shows a point cloud data surface representation returned from an arm mounted laser line scanner, with image Fig. 5.1c showing the cloud point data and probe centre points aligned together in the hemisphere work piece coordinate system.

The cloud point data subsets that represent the surface of the target object directly below the probe (in the 'Z' direction) that are capable of influencing the probe at each of the five discrete measurement locations are identified and separated out Fig.5.1d. These influencing data sets are extended slightly larger than the probe diameter. If there is no exact data point representing the surface at the perimeter of the probe data set, the procedures may need to look slightly beyond the probe radius for guiding cloud point data points.

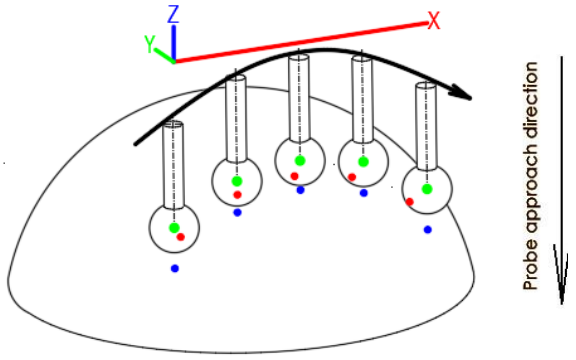

(a).

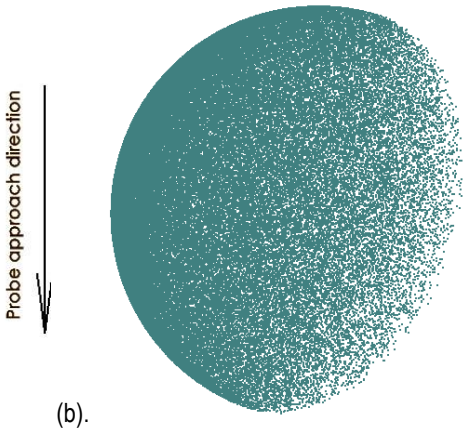

(b).

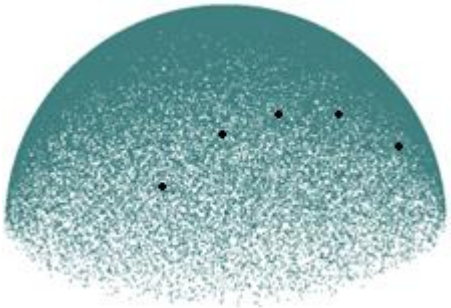

(c).

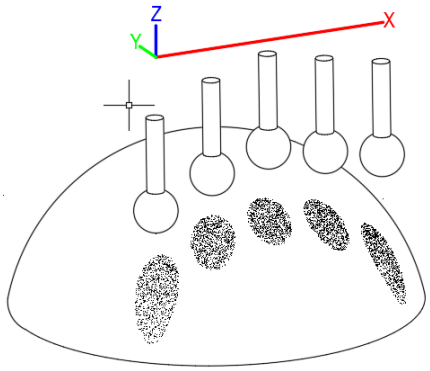

(d).

Fig. 5.1. Probe size has been exaggerated for clarity, (a). shows tactile scan points, (b). Cloud point data in the mobile arms coordinate system, (c). the combined data sets aligned to the tactile probed work piece coordinate system. (d). the influencing cloud point data sets at each discrete measurement point separated out.

5.1 Development of probe compensation in the probe approach direction

The main process in developing a probe centre compensation while maintaining the 'X' and 'Y' coordinates is to determine the area of the surface below the probe that can influence the probe's contact position. This has been estimated as the smallest angle $\theta_{surface}$ where $\theta_{surface}$ is the angle between the vertical 'Z' axis and line '$\overline{me}$' which is going to influence the probe contact position, see Fig. 4.11.

The cloud point data is to be used as a digital representation of the actual surface form. Some of the difficulties involved with this have been discussed in detail, see section 4.2. 'Considerations used in forming hybrid probe compensation'. Even if a perfect cloud point data representation of the measured surface is available, it must be remembered that the actual surface is continuous between its boundary edges, whereas cloud point data consists of a finite number of data points that may not give full coverage of the surface, even if the individual points within a cloud point data set were highly accurate and sat precisely on the actual surface. If the data set is to be considered a replacement for the actual surface, any gaps in the cloud point can only be filled from estimates generated by interpolation of existing data points. It can be seen in Fig. 5.2 that the position where the probe 'Z' axis intersects the surface (as highlighted by the red cross hairs in the enlarged view), that there is no data point. It can also be seen that around the perimeter of the cloud point data, there are areas where the data is relatively sparse. Section 3.2. 'Experimental measurement of scanner error' detailed how scanner accuracy was dependant on scanner stand-off. It was also evident target surface microstructure

caused specular reflection saturating the CCD (gaps in data coverage) or scattering the laser beam to cause erroneous data / outliers.

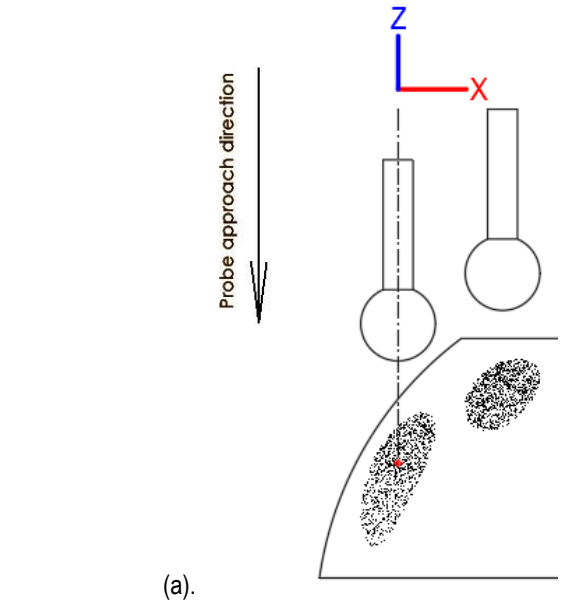

(a).

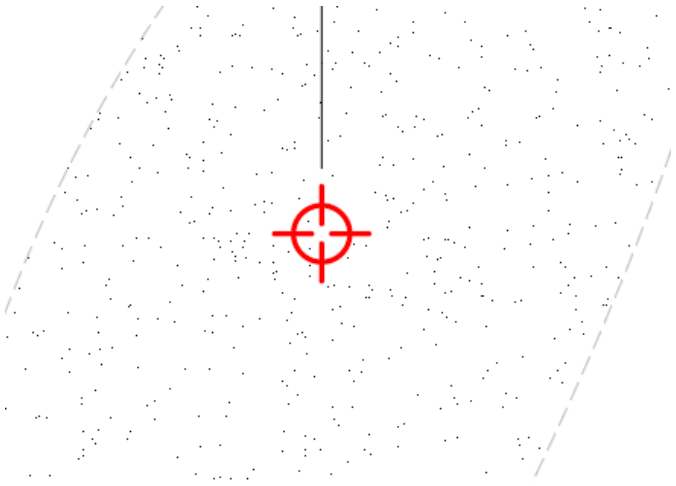

(b).

Fig. 5.2. (a). Shows the cloud point data representing the actual surface form. (b) illustrates those areas of sparse date around the perimeter and directly below the probe centre.

To determine the angle that line '$\overline{me}$' has to the vertical, (Fig. 4.11): work must be undertaken in three-dimensional space to determine the point where the probe axis penetrates the cloud point representation of the surface. A plane may be formed using three points local to the axis penetration

point Fig. 5.3. At each tactile probed point, the 'X', 'Y', 'Z' coordinates are known for the probe centre point. What is not known is the 'Z' value that the probe axis passes through the surface data.

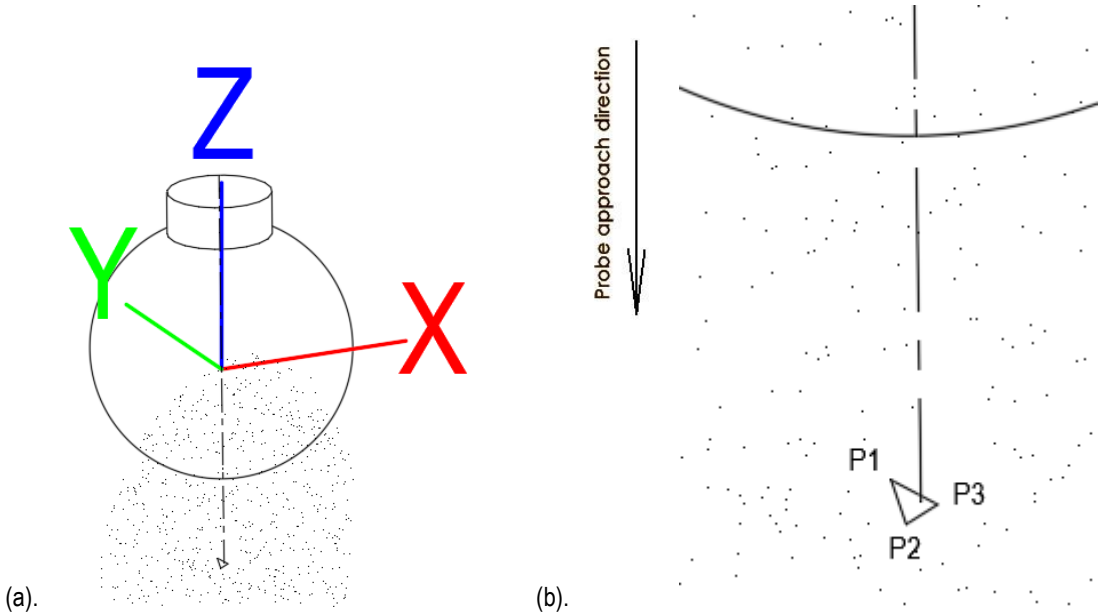

(a). (b).

Fig. 5.3. (a). Probe centre points are taken when tactile probing. (b). No cloud point exists at the exact point the probe axis intersects the data.

Using data points close to the probe axis, a plane may be formed to estimate the local surface. From this plane, the estimated penetration point of 'Z' can be calculated. Selection of the best data to form the plane has been ignored at present but will receive a separate discussion later in this section.

A plane is depicted in $\mathbb{R}3$ Fig 5.4. The plane contains a point 'p_0' with coordinates $x_0,\ y_0,\ z_0$ and a non-zero normal vector '$\vec{n}$' with components $\langle a, b, c \rangle$. and a point 'any point' with coordinates $(x,\ y,\ z)$.

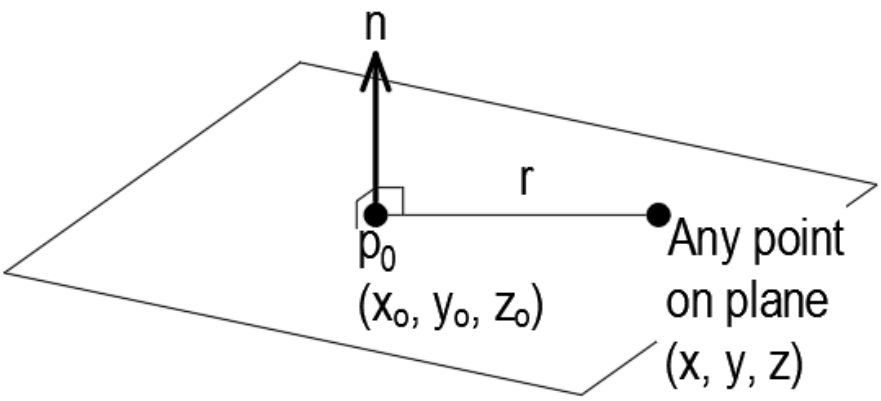

Fig. 5.4 A plane is in $\mathbb{R}3$ with a known point P_0 and a normal vector n and an additional point anywhere on the plane other than on point P_0. Based on .

The position vector $\vec{r}$ to any point on the plain is: -

$$\vec{r} = \langle x - x_0,\ y - y_0,\ z - z_0 \rangle \tag{5.1}$$

The normal vector '$\vec{n}$' is orthogonal (normal) to any vector on the plane. If vector '$\vec{n}$' is orthogonal to '$\vec{r}$', the 'dot' or scalar product of the two vectors is zero ($A \cdot \mathrm{B} = |A||B|\mathrm{Cos}\theta$) where ($\mathrm{Cos}90^o = 0$)).

So: -

$$\vec{n} \cdot \vec{r} = 0 \tag{5.2}$$

The vector equation for a plane through a point P_0 $(x_0,\ y_0,\ z_0)$ with a normal vector $\overrightarrow{n}$ with components of $\overrightarrow{n} = \langle \mathrm{a}, \mathrm{b}, \mathrm{c} \rangle$ is obtained by substituting "$\vec{n}$" and "$\vec{r}$" into equation (5.2).

$$\langle \mathrm{a}, \mathrm{b}, \mathrm{c} \rangle \cdot \langle x - x_0,\ y - y_0,\ z - z_0 \rangle = 0 \tag{5.3}$$

Completing the 'Dot Product' vector multiplication to form the scalar equation of a plane.

$$\mathrm{a}(x - x_0) + \mathrm{b}(y - y_0) + \mathrm{c}(z - z_0) = 0 \tag{5.4}$$

To determine a plane in three-dimensional space, three points are required which are non-collinear, (they do not lie on the same line). Fig. 5.5 shows three points 'Q', 'R', 'S', in $\mathbb{R}3$. The points are non-collinear, vectors $\overrightarrow{QR}$ and $\overrightarrow{QS}$ are nonzero and are not parallel.

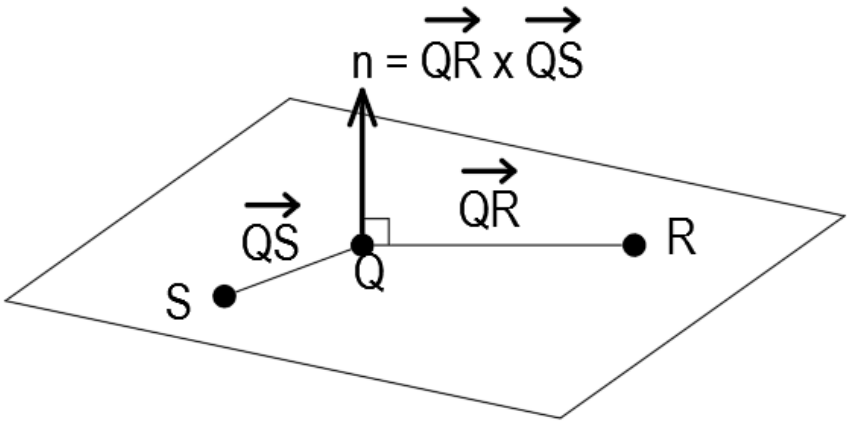

Fig. 5.5. Three non-collinear points lying on a plane in $\mathbb{R}3$. Based on .

The cross product vector will always be orthogonal to the plane containing the original two vectors. So, vector 'n' can be determined as it is normal to vectors $\overrightarrow{QR}$ and $\overrightarrow{QS}$.

$$\vec{n} = \overrightarrow{QR} \times \overrightarrow{QS} \tag{5.5}$$

Points 'Q', 'R', 'S' lie on the plane possessing the normal vector '$\vec{n}'$. The components $\langle \mathrm{a}, \mathrm{b}, \mathrm{c} \rangle$ of normal vector '$\vec{n}$' can be substituted into equation (5.4) along with $x_0,\ y_0,\ z_0$ of any one of the 3 points 'Q', 'R', or 'S'.

Once the plane equation is determined, the probe axis 'X', 'Y' coordinates can be used in the equation and the equation solved for the one remaining unknown, the 'Z' coordinate of the point on the plane where the probe axis intersects the plane.

The determination of this intersection point is relatively straight forward. What is a little more involved is selecting the three points used to determine the plane that will yield the most accurate results. The ability of the plane to represent the missing cloud point data is very much dependent on the three data

points chosen to form the plane. Fig. 5.6 shows how the combination of the measured forms curvature and selection of data points can cause errors. The green plane quite accurately defines the forms local surface where the probe 'Z' axis intersects it. The three green data points used to form the plane are close to the intersection point and when connected as a triangle, the blue axis forming the intersection point falls within the triangle formed by the three green points.

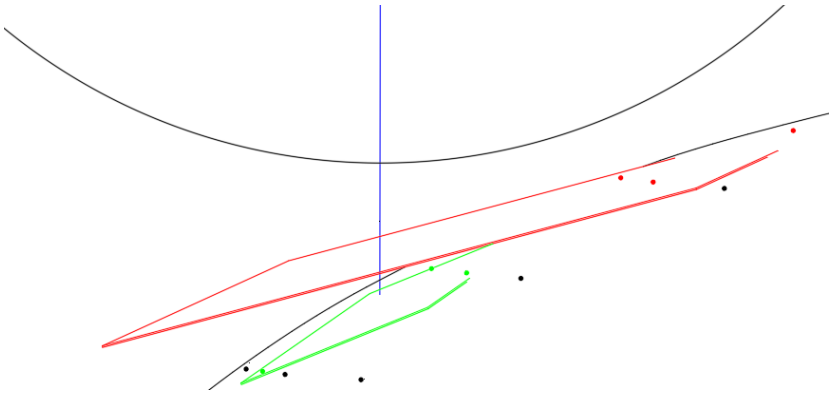

Fig. 5.6. A magnified probe tip with blue line representing its axis.

For illustration purposes. the red plane was formed from three red points to one side of the intersection point and not the closest points available. The red plane does not fit the cloud point data set well. It overhangs the data points, with 'daylight' between the plane's underside and the other data points. To reduce this error a data point selection procedure was formed to ensure that not only the closest points to the probe axis were selected, but also the selected points when connected by a triangle that 'encircles' the intersection point of the 'Z' axis.

To see this more clearly, the subset of cloud point data will be discussed and documented using its 'X' and 'Y' coordinates only as in Fig. 5.6 which shows the surface representation of the cloud point data projected onto a plan view (all data points have the same 'Z' value).

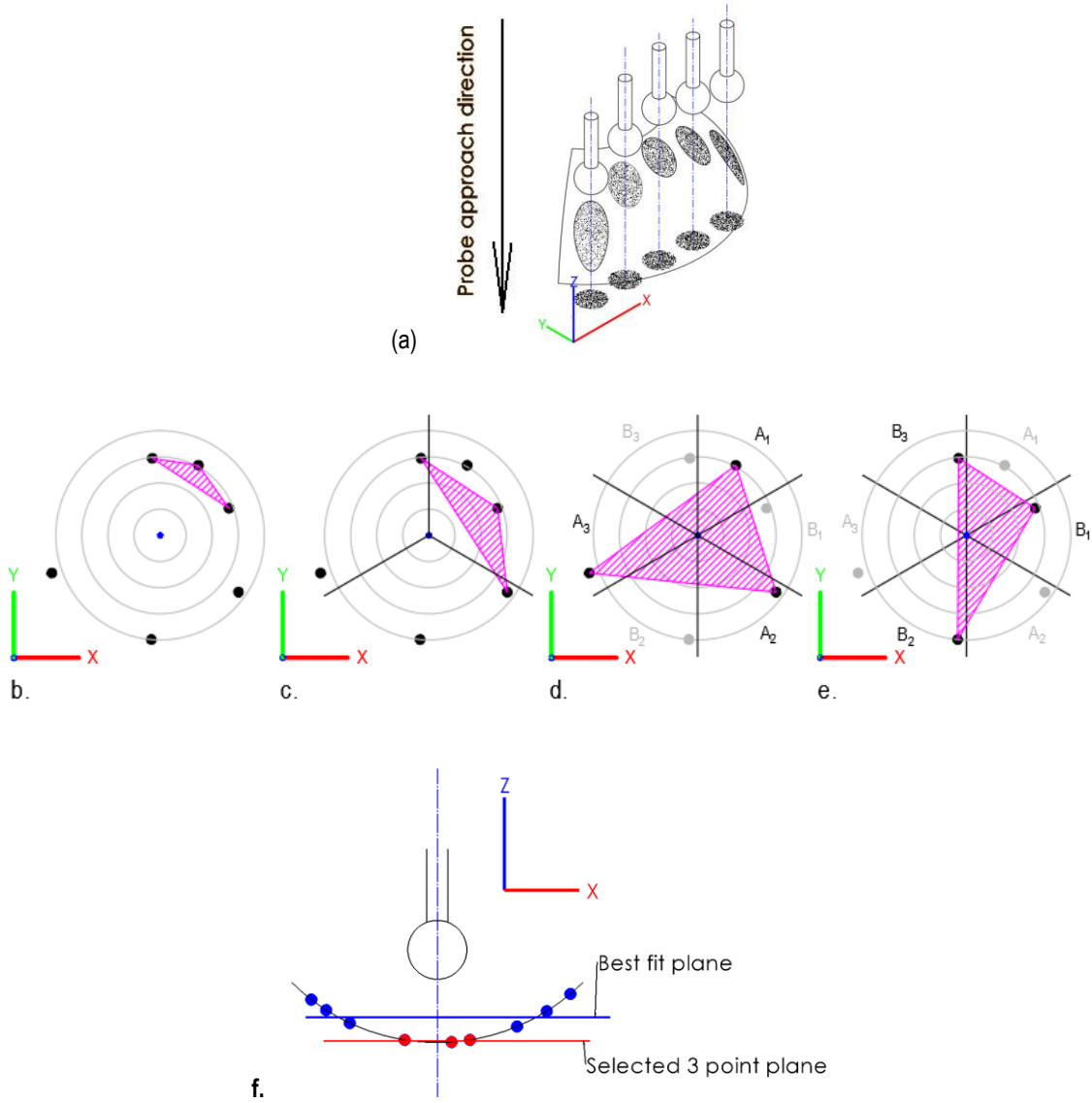

Fig. 5.7. Cloud point data used to determine the plane that intersects the probe axis. (a). Cloud point data influencing probe position is shown in plan view, (b). Plane formed from the 3 data points closest to 'Z' axis, (c). Data set split into 3 segments and closest point from each segment used to form a plane. (d). Data set split into 6 segments. (e). closest data points in segment set 'B' used to form a plane. (f) shows an alternative best fit method.

Fig. 5.7b, c, d, e, are enlarged to show the central data points surrounding the blue dot representing the probe axis as viewed from above. Grey concentric rings are shown simply as a visual aid to indicate the distance that data points are away from the probe axis. The magenta triangle joins the points selected to form the plane and give an indication whether the probe axis is within the point's triangular boundary or not.

Fig. 5.7b. uses the 3 closest points to the probe axis. This does not satisfy the need that the points surround the probe axis. It was considered that splitting the data points into 3 equal segments with the closest data point in each segment being used to form the plane would satisfy the selection requirements. Fig. 5.7c shows this not to be the case as the probe axis falling outside the triangle boundary can still occur. Fig. 5.7d and Fig. 5.7e shows the method used to identify the three most suitable points. The data is separated into six equal segments, 'A_1 to A_3' and 'B_1 to B_3' with segments 'A' alternated with segments 'B'. The closest point to the 'Z' axis in each segment from data set 'A' or data set 'B' are selected. The probe 'Z' axis falls on or within each boundary triangle. To decide which set of points (segment 'A' or segment 'B') is used; the distance of points from segment 'A' points to the 'Z' axis are summed and compared to the sum of distance of points from segment 'B' points to the Z axis. The set of points with the smallest combined distance will be used to determine the plane detailed in equation (5.4).

An alternative method could be to use a plane best fit technique on a larger number of surrounding points Fig. 5.7f, but it seemed more accurate to select the three most appropriate points as is seen in Fig. 5.6, rather than best fitting of a plane using a greater number of points. The greater the number of points included in the plane best fit, the further the points are away from the probe 'Z' axis. The scan data is a representation of a freeform curved target surface, so the wider the range of points selected, the more likely the intersection point of the 'Z' axis and scan data representation of the surface is offset in the 'Z' direction (blue line) from that using a plane generated by the three points selected in Fig. 5.7f. (red line). The red plane gives a better 'Z' intersection value than the best fit plane.

To gain point 'e' the highest point of line '$\overline{me}$' is a little more involved. It is assumed that the highest point in the data set will be on the perimeter of the cloud point data set capable of influencing the probes position. That is the data on the steepest line radiating from the newly found point 'm'. Sparse or missing data as depicted in Fig. 5.2 and Fig. 5.3 can make this difficult to determine. There may not be a full set of data points around the perimeter at the exact probe radius and at the point representing

the highest point on the surface patch capable of influencing the probe vertical position. To accommodate these issues as discussed earlier a slightly larger radius than the probe may be used to determine the subset of cloud points capable of influencing the probe position, allowing points both within and very slightly beyond the probe radius to be used in the point location estimate. When determining point 'm' previously the 'X' and 'Y' coordinates of the probe axis were known and so calculation for point 'm' was straightforward. Because point 'e' could be anywhere on the cloud point data perimeter, work has to be undertaken to estimate its 'X' and 'Y' coordinates. This is done by placing a series of points on the perimeter of the individual 'probe' data sets at intervals of 0.5˚. 'Z' Values were determined using the same system as for finding point 'm'. From this series of perimeter points and the use of basic trigonometry, the angle of line '$\overline{me}$' for each point can be determined. The line having the smallest angle to vertical is assumed as having the greatest influence on the probe vertical position when approaching the surface. This angle θ_{cpd} can be substituted into equation (4.3) to calculate probe compensation in the 'Z' direction.

The pseudo code for the procedure is detailed below.

Isolate the subset of cloud data points capable of influencing the probe vertical position plus a small margin (using probe 'X' and 'Y' coordinates and probe radius).

Determine the distance (in the 'X' – 'Y' plane) of each point in the subset from the probe axis.

Sort the cloud point subset in ascending order of distance from the probe axis.

Taking a plan view from the positive 'Z' direction determine the angular position of each data point in the cloud point subset relative to the probe centre point in the 'X' -'Y' plane (positive X as 0° / 360°, negative Y as 90°, negative X as 180°, positive Y as 270°).

Working in the X' -'Y' plane determine from the cloud point data subset, the 3 points that have the smallest combined distance from the probe X' -'Y' coordinates and when joined together form a boundary triangle around the probe axis

From the three points, determine the equation of the plane that is an estimate of the surface where the probe 'Z' axis intersects the surface

Using the probe X' -'Y' coordinates and plane equation obtain the 'Z' coordinate (point 'm')

Working in the X' -'Y' plane, set up a series of points at the probe radius away from the probe 'Z' axis at intervals of 0.5°. For each point determine the 'Z' coordinate of the point that is estimated to lie on the surface using previously used procedure.

For each of the formed points calculate the angle from vertical of the line formed between it and previously calculated point 'm'.'

Determine the perimeter point that has the smallest angle to the 'Z' (vertical) axis. This is point 'p'.

Using the smallest angle to vertical of line '$\overline{me}$' calculate probe 'z' using equation (4.3).

5.2 Development of probe compensation in the direction of probe contact normal

As with developing a probe centre compensation while maintaining the 'X' and 'Y' ordinates in section 4.3; cloud point data taken from an arm mounted laser scanner is used as a representation of the actual surface. The broad details of the process have been discussed in section '4.4 Rational for probe compensation in the direction of surface normal' and expressly detailed in Fig. 4.13. The surface normal at the contact point of the probe and the target surface passes through the probe centre. With the assumption that the cloud point data has no issue with outliers or sparse data, the contact point compensation is calculated by firstly determining the closest cloud point data point to the probe centre. It is the probes contact with this area of the target surface that has arrested the probe and determined the recorded centre position of the tactile probe. The surface normal equation can then be determined using the single closest laser scanned data point and probe centre coordinate. The surface normal equation can be used to determine the estimated contact point by offsetting the probe radius from the recorded probe centre point along this newly calculated normal direction.

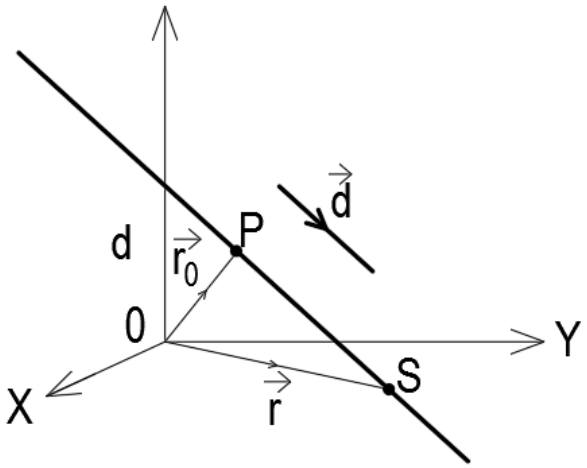

Fig. 5.8. Shows a line that passes through a specific point 'P' with position vector $\overrightarrow{r_o}$ and is parallel to direction vector $\vec{d}$. Point 'S' is any point on the line with position vector $\vec{r}$. Based on .

Fig. 5.8 shows a line passing through two points 'P' and 'S' in $\mathbb{R}3$ with their position vectors being $\overrightarrow{r_0}$ and $\vec{r}$ respectively. Through vector addition it can be seen that: -

$$\overrightarrow{0S} = \overrightarrow{0P} + \overrightarrow{PS} \tag{5.6}$$

The estimated surface contact point 'C' is unknown, but the vector from probe tip centre to the closest scan data point can be easily determined: -

$$\vec{r} = \vec{r}_0 + \overrightarrow{PS} \tag{5.7}$$

The estimated contact point 'C' lies on vector $\overrightarrow{PS}$. Its estimated position is some scalar multiple 't' of $\overrightarrow{PS}$ away from the probe tip radius Fig. 5.9: -

$$\vec{r} = \vec{r}_0 + t \times \overrightarrow{PS} \tag{5.8}$$

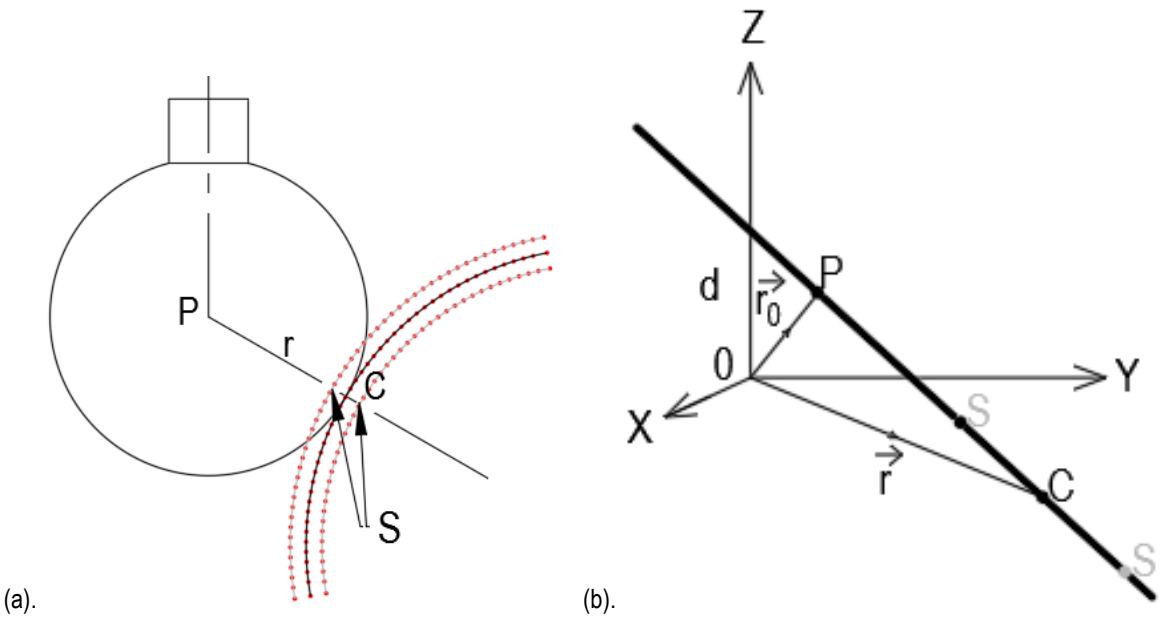

Fig. 5.9. (a). The probe and object being measured from a cloud point data representations of the surface laying above, below and on the actual object surface. (b). Shows the same arrangement in vector form. Point 'S' is shown in grey to represent its possible positions relative to 'C'.

The juxtaposition of probe, measured object and cloud point representations of the surface at the instance the probe centre point is returned as a tactile probed data point is shown Fig. 5.9a, with the vector representation Fig. 5.9b. Because the origin is positioned at the (0, 0, 0) coordinate of the work coordinate system, position vectors $\overrightarrow{r_0}$ and $\vec{r}$ can be represented by the coordinates of the probe centre 'P' and the unknown probe to surface contact point 'C' respectively. We thus know the probe centre and the closest laser scanned data point that lies on contact normal $\overrightarrow{PS}$.

It has been stated that scan data points representing the actual surface can be potentially above or below the surface (positive and negative surface scan data error). It is known that the estimated contact of probe and surface is distance 'r' (the probe tip radius) away from the recorded probe centre point 'P' and the laser scanned cloud point best representing the probed surface is distance $\left|\overrightarrow{PS}\right|$ away from the probe centre, so scalar 't' can be determined as: -

$$t = \left(r \,/\left|\overrightarrow{PS}\right|\right) \tag{5.9}$$

Where $\left|\overrightarrow{PS}\right| = \sqrt{(S_x - P_x)^2 + \left(S_y - P_y\right)^2 + (S_z - P_z)^2}$ (5.10)

Substituting for 't' into equation (5.8): -

$$\vec{r} = \vec{r}_0 + \left(r / \left|\overrightarrow{PS}\right|\right)\overrightarrow{PS} \quad (5.11)$$

In coordinate terms this may be written as:

$$\begin{pmatrix} C_x \\ C_y \\ C_z \end{pmatrix} = \begin{pmatrix} P_x \\ P_y \\ P_z \end{pmatrix} + \left(\frac{Probe\ Radius}{\sqrt{(S_x - P_x)^2 + \left(S_y - P_y\right)^2 + (S_z - P_z)^2}} \right) \text{x} \begin{pmatrix} S_x - P_x \\ S_y - P_y \\ S_z - P_z \end{pmatrix} \quad 5.12)$$

The compensation for the probe centre point along the normal is not given as a correction of the probe centre 'X', 'Y', 'Z' coordinates in the probe approach direction, but as an estimate of the probe / surface contact point.

The pseudo code is detailed below.

Isolate the subset of cloud data points capable of influencing the probe contact position using probe 'X', 'Y' and 'Z' coordinates and probe radius).

Determine the distance of each point in the data subset from the probes measured position (Probe centre point).

Sort the cloud point subset in ascending order of distance from the probe centre point.

Determine the closest scanned cloud point to the probe centre.

Calculate the surface normal vector $\overrightarrow{PS}$.

Calculate scalar 't'.

Using equation (5.12) calculate the estimated probe to surface contact position.

5.3 Checking probe tip correction algorithms using virtual data

Before the algorithms developed in sections 5.1 and 5.2 were checked on a real object using actual tactile probed and laser scan cloud point data, it was considered prudent to ensure the principles were appropriate, the mathematical equations correct and the code for calculating the correction worked correctly. To this end virtual data of a hemispherical form was generated mathematically as well as a series of tactile probe centre points representing 2 mm, 4 mm and 6 mm probes touching the surface along a set of 'scan planes.

Data was generated to represent a 150 mm diameter hemispherical surface form. Looking at the data in the '-Z' direction as per Fig. 5.7a. The origin of the static CMM coordinate system was set to the hemisphere centre. The 'X' and 'Y' hemisphere virtual cloud point data (*vcpd*); 'X_{vcpd}' and 'Y_{vcpd}' values laying within the 150 mm diameter circle being generated pseudo randomly*. The 'Z_{vcpd}' coordinate value being calculated using Pythagoras to produce points to represent the hemisphere surface: -

$$Z_{vcpd} = \sqrt{\left(\frac{150}{2}\right)^2 - X^2{}_{vcpd} - Y^2{}_{vcpd}} \tag{5.13}$$

The virtual tactile probe points (*vp*)were generated as a set of 177 points taken at 10 mm intervals along the 'Z – X' scan plane and the scan planes being parallel and at 10 mm spacing in the 'Y' direction. The probe tip centre 'Z' ordinate 'Z_{vp}' value calculated as: -

$$Z_{vp} = \sqrt{\left(\frac{150 + probe\ tip\ radius}{2}\right)^2 - X^2{}_{vp} - Y^2{}_{vp}} \tag{5.14}$$

It was unclear how many cloud point data points would be suitable. A series of virtual data sets varying from one million to four million points in one million point intervals was generated.

* Data was generated using Microsoft Excell and Microsoft Visual Basic for Applications (VBA). Random numbers are Pseudo-random and are generated from a seed value based on the system clock.

For each virtual probe tip diameter and each of the four virtual cloud point data sets, the two probe tip correction algorithms developed in section 5.1 and 5.2 were applied and the probe tip corrections calculated. The probe tip compensated results were transferred to Polyworks metrology software and through a spherical best fit procedure, sphere diameters from the corrected data sets were calculated.

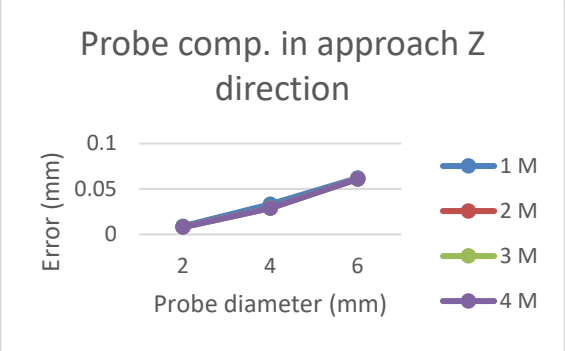

(a). Error of sphere diameter for probe tip compensation in the 'Z' approach direction for 2 mm, 4 mm, 6 mm probe tips.

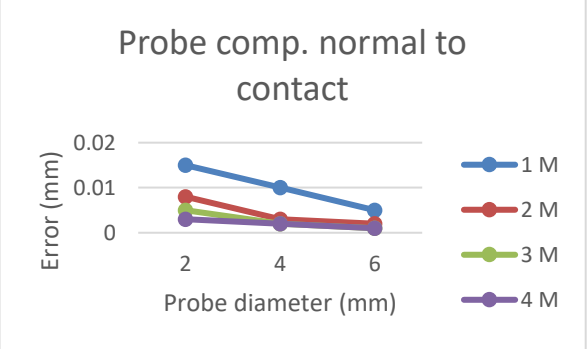

(b). Error of sphere diameter for probe tip compensation in the direction of surface normal for 2 mm, 4 mm, 6 mm probe tips.

Fig. 5.10. Details the dimensional accuracy of the probe tip corrected methods developed in sections 5.1 and 5.2 when 'perfect' mathematically generated virtual scan cloud point and probe data are used. Results are shown for four data sets ranging from 1 million to 4 million cloud point data in steps of 1 million. Probe sizes of 2 mm, 4 mm and 6 mm have been probe tip compensated.

Probe tip compensation in the probe approach direction ('Z') for perfect data: -

- Measured diameter error of the virtual object decreases as probe diameter decreases. For a 6 mm, 4mm and 2 mm diameter probe using 1M scan points. The diameter best fit error was 0.062 mm, 0,033 mm, 0.009 mm respectively.
- The best fit diameter error of the virtual measured object changes very little with the cloud point density (scan point numbers) used in this preview. The graphs lie on top of each other. For the 2 mm probe, the diameter best fit error for a 2mm diameter probe with 1M, 2M, 3M, and 4 M scan points is 0.009 mm, 0.008 mm, 0.008 mm, and 0.008 mm respectively

For probe compensation in the direction of surface normal direction (finding the actual contact point): -

- The best fit diameter error of the virtual measured object decreases with increasing cloud point density (scan point numbers) used in this preview. For a 4M, 3M, 2M and 1M data points and a 4mm diameter probe. The diameter best fit error was 0.002 mm, 0,002 mm, 0.003 mm and 0.010 mm respectively.
- Measured diameter error of the virtual product decreases as probe tip diameter increases. For a 6 mm, 4mm and 2 mm diameter probe using 1M scan points. The diameter best fit error was 0.015 mm, 0,010 mm, 0.005 mm respectively.
- Measured diameter error is less sensitive to probe tip diameter as virtual cloud point density increases (flatter graphs).

The diameter measurement errors on the whole are less when using the probe compensation in the contact surface normal direction (0.001 mm to 0.015 mm) compared to compensation using the 'Z' approach direction method (0.001 mm to 0.061 mm), although the variance of the sphere best fit residuals (standard deviation) are similar (Table A1 Appendix A).

The dimensional errors at the high end of this range are considerably outside those expected from tactile probing. At the lower end of the error range, errors are comparable or less than those expected from tactile probing.

The 'perfect' virtual data used to preview the hypotheses differs from actual data which has both tactile probing and laser scanner error. Although the tactile probe data is anticipated to closely resemble the mathematically generated data. The cloud point data is highly likely to be offset from the actual object due to laser scanning error and with some displacement error associated with alignment processes associated with transferring the cloud point data from a machine coordinate system to a work piece coordinate system. These issues will be addressed in section 6.6 'The accuracy of hybrid compensation based on the contact normal of the probe' by adding simulated laser scanner error and alignment error into the data used for validating the probe compensation hypothesis.

It may also be the case that scan density of an actual scanned object may be less consistent than that produced using two random number generators for 'X' and 'Y' coordinates. Surface finish, scanner beam angle to surface normal and difficulty accessing the surface may contribute to areas of sparse or relatively abundant cloud point data points.

These differences between the perfect mathematically produced data and actual data require that the probe tip compensation methods be undertaken on data taken from an actual metrology project that fully exposes them to the full range of measurement errors and alignment issues. It would be possible to simulate some of these issues, but a greater understanding of cloud point coverage would be needed. Chapter 6. details the use of the probe tip compensation methodologies using data generated from an actual part.

5.4 Summary

The two probe tip compensation methods proposed in Chapter 4 have been fully formulated and checked using virtual data of a hemispherical target model. Different probe diameters have been simulated. The probe tip compensation in the normal direction to the probe tip / target surface contact point has shown the greatest potential for producing accurate probe tip compensation. The following chapter will test the two methodologies using data gained for an actual hemispherical form. To better mimic scanning of a free-form feature, the normal direction compensation method will be further tested using simulated data gained from a Bézier curve generated surface.

Chapter 6. Experimental checking of probe compensation methodologies

To determine the accuracy of the developed probe tip compensation methods, measurements were undertaken on a spherical object. To have the ability to validate the compensation methods, full prior knowledge of the surface form is a necessity, although this prior surface knowledge would not be used in generating probe compensations. The prior knowledge would only be used to validate the compensated measurements against the known original form. The experimental setup used to check the methodologies developed in section '5.1 Development of probe compensation in the probe approach direction' and '5.2 Development of probe compensation in the surface normal' require the use of measuring equipment found in a modern metrology laboratory. The equipment and software used in this validation is detailed here.

6.1 Experimental equipment, artefacts and software

The equipment used to validate the tactile probe compensation routines is as follows:

- Hexagon Global S Blue 9.12.8 static CMM equipped with a tactile scanning probe and HP-L-106 laser scanner head. *
- 2 mm, 4 mm and 6 mm Silicon Nitride probes **
- Faro V6 HD Laser line probe and touch trigger probe mounted on a Faro Edge seven axis arm (2.7 meter version).
- Taylor Hobson - Form Talysurf PGI 1500E.

The software used in the investigation includes: -

- the CMM on board metrology software PC-DIMIS Version 2018 R2.

- Polyworks version 2018 reverse engineering and metrology software used to gain laser line scan point data, align tactile and optically gained data and to output best fit feature / deviation measurements.
- Microsoft Excel and the accompanying Visual Basic for applications used as the programming environment to calculate probe compensation.

The measured object was: -

- An aluminium cylindrical form with turned hemispherical end and milled alignment features machined perpendicular to the forms base and cylindrical axis (detailed in appendix B) and seen in Fig. 6.1.

All measurements were undertaken in a temperature-controlled metrology laboratory, with the temperature held between 20°C and 21°C. Additional precautions were undertaken by using a temperature compensation probe attached to the target object when tactile scanning and having the laser scanner arm temperature compensator activated.

The static CMM and articulated arm CMM had current calibration certificates.

Prior to use both the static CMM and articulated arm CMM were put through their compensation procedures.

* The stated accuracy of the Hexagon Global S Blue 9.12.8 static CMM is dependent on the size of the object being measured. If L is the measured objects length in mms. The maximum permissible error of the CMM is calculated as being: -

$$0.0014mm + 0.003\left(\frac{L}{1000}\right)mm \tag{6.1}$$

** To tactile scan aluminium objects, Silicon Nitride probes were used rather than the more common ruby tipped versions. Ruby contains Aluminium Oxide and so there is chance of 'pickup' when contacting an Aluminium target. Silicon Nitride probes are also more wear resistant than Ruby probes, so are suitable for tactile scanning.

6.2. Experimental methodology

The hemispherical form shown in Fig. 6.1 was selected as the initial test form to verify the accuracy of the probe compensation methodologies developed in section '5.1 Development of probe compensation in the probe approach direction' and '5.2 Development of probe compensation in the probe compensation in the direction of surface normal'. An aluminium form was machined from bar stock using a CNC mill-turn lathe. The hemispherical and cylindrical features were turned, and the four equally spaced rebates were milled with no additional finishing process being applied.

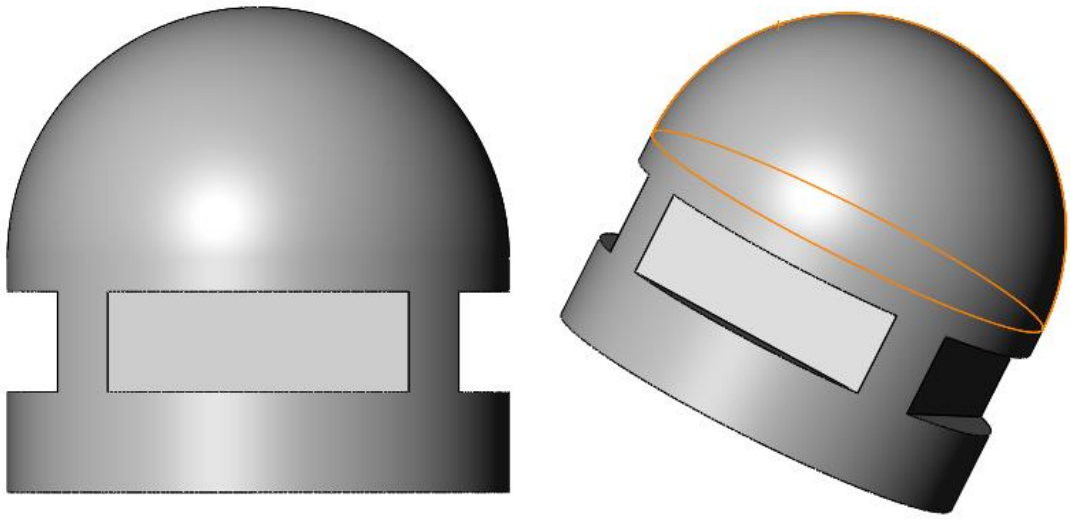

Fig. 6.1. The test form.

To validate the compensation methods, full prior knowledge of the surface form is a necessity. The prior knowledge would only be used to validate the compensated measurements against the known

original form. To this end the hemispherical form with full prior knowledge of the surface features in the form of a CAD model and the ability to derive each surface by simple equations was used.

Only the hemispherical feature was used in the hybrid probe compensation validation process.

The form was considered a good starting model for several reasons as detailed here: -

- The surface finish of the machined objects is typical of what would be seen in a metrology lab and so would give an appropriate challenge to the CMM when tactile scanning the form and an appropriate challenge to the arm mounted laser scanner when optically scanning the surface.
- Only the hemispherical surface was to be used to represent a free-form surface so there were no re-entrant or occluded features to contend with.
- Two of the fhe four rebates and the object base were sufficient prismatic features to align the laser scan data to the tactile scanned data.
- The hemispherical form has an infinite number of surface normals to be corrected ranging from horizontal to vertical.

The experimental setup is shown in Fig. 6.2

(a).  *(b).* 

Fig. 6.2. Experimental setup (a). showing the static CMM with the hemispherical form being probed in a series of parallel tactile scans. (b). An arm mounted laser line scanner.

Initially the test form was measured on the moving bridge CMM to gain its actual size. One hundred points were touch trigger probed with a 'Z' axis approach and using a spherical best fit algorithm present in the on-board CMM software, the diameter was determined. The test object was probed using 2 mm, 4 mm and 6 mm diameter probes. A diameter of 150.032 mm was returned for the hemispherical feature (.

From the CMM maximum permissible error (MPE) information detailed in equation (6.1) the measurement accuracy expected from a 150 mm object is 0.00185 mm. (0.0014 + 3 x (150 / 1000)).

The four perpendicular rebates cut in the cylindrical base and the tops of the parallels the test form was mounted on were tactile probed. Using the CMM on-board software the CMM machine coordinate system was aligned to the work piece. The coordinate system origin was set at the hemisphere centre and the 'X-Z' plane and 'Y-Z' plane set to the hemisphere front and right cut features respectively with the 'X-Y' plane being set to the base of the test form. It is understood that if the test form had truly

been a free-form surface / body, this may not have been possible. The work piece coordinate system was set as described for convenience purposes to aid code checking. As algorithms are developed checks are made at each stage, not only to identify syntax and program flow errors, but also mathematical errors. With the coordinate system arranged as suggested, issues in columns of data points are easier to identify.

A series of tactile parallel scan planes ('X-Z') were set up on the CMM keeping the 'Y' coordinate nominally constant; that is the probe vertical axis was constrained in a 'Z-X' scan plane as indicated Fig. 4.7a. Parallel scan paths were taken in the 'Y' direction at 10 mm intervals to give full coverage of the hemisphere. Measurements were undertaken as a series of tactile scans over the hemispherical test form surface with discrete points being measured at intervals of nominally 4 mm. No probe compensation or learning was applied. Probe centre points were returned. The touch probe operation was undertaken with a variety of probe diameters (2 mm, 4 mm, 6 mm).

For each probe diameter, some 800 probe points were taken over the 15 parallel scan planes.

It is understood that this was not the best measurement practice. The most accurate probe approach direction is normal to the surface, this is not only to reduce probe compensation error, but to reduce the chance of probe stylus deflection. To have a normal probe approach direction, there would need to be some surface prior knowledge. We are assuming no prior knowledge in this investigation, so a 'Z' axis approach was still employed.

Once the measurements had been obtained, the whole data set was exported from the CMM software to PolyWorks metrology software where best fit algorithms were used to fit planes to the data points representing the four registration rebates and the test form base surface Fig. 6.3. Although only two of the registration rebate features are required for alignment, all four were probed. The planes used for the alignment were 'CMM Base', 'CMM Front' and CMM Left. The alignment method used was the

'Perpendicular planes' method . The planes can be aligned in a particular order, or they can be aligned based on a weighting for each pair off planes. In this work, the planes were aligned with the CMM Base' aligned first, 'CMM Front' aligned second and CMM Left aligned last.

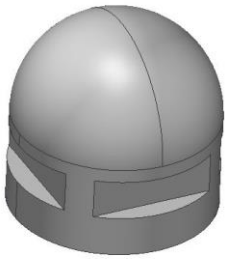

(a).

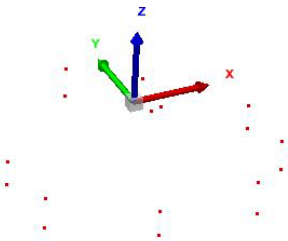

(b).

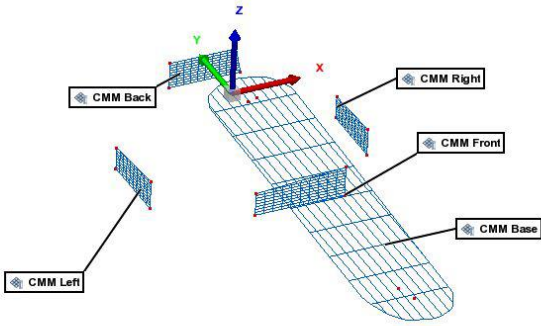

(c).

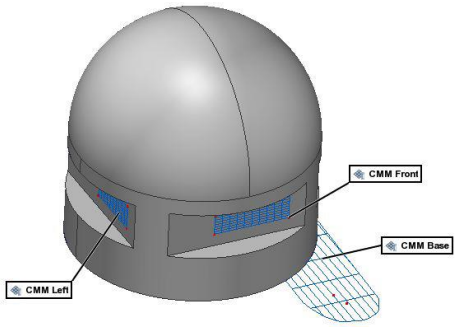

(d).

Fig. 6.3. Details the formation of registration features (planes) from probed data. (a). The test form, (b). Touch trigger probe points taken of the four cut features around the cylindrical feature and the top surface of the parallels that the form was mounted on. (c). Planes have been best fitted to the tactile probed data points (red dots). (d). planes combined with CAD model for clarity.

The same target object was laser scanned. Care was taken to gain coverage of the whole object including the orthogonal rebates and the tops of the parallels that the test form was mounted on. To ensure lack of scan coverage did not pose problems, the laser line scanner was set to 'extra fine' resolution.

To aid scan data cleaning the cloud points were meshed in real time with spurious floating mesh data being isolated and deleted at the end of the mesh finalisation process. The polygonal mesh was then converted to cloud point data within the Polyworks metrology software. For comparison purposes, the test form was also scanned to cloud point data directly. Cleaning of raw cloud point data can prove difficult as discussed in section '2.3. Reverse engineering data capture and processing'. This data is likely to hold outlier data points as can be seen in Fig. 2.7a which may affect the accuracy of any probe tip compensation calculations. On completion of probe tip compensation, both compensated data sets were reimported into the Polyworks project for a spherical bet fit process to determine the diameter of the compensated forms.

Fig. 6.4 shows the Cloud point data alignment workflow described here with cloud point fitted planes shown as red nets to contrast the planes fitted to tactile probed CMM data, shown as blue nets.

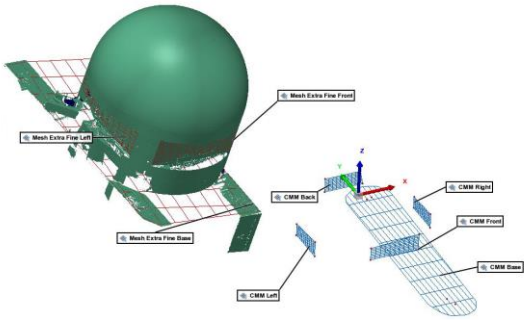
Mesh Extra Fine Front
Mesh Extra Fine Left
CMM Back
CMM Right
CMM Front
Mesh Extra Fine Base
CMM Base
CMM Left

(a).

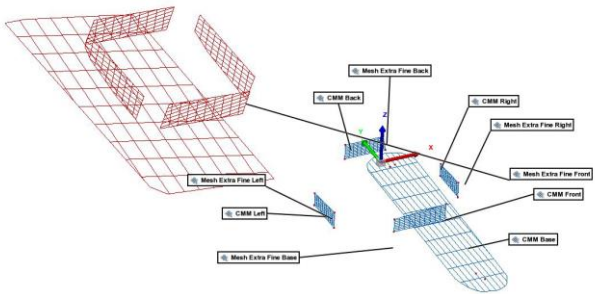
Mesh Extra Fine Back
CMM Back
CMM Right
Mesh Extra Fine Right
Mesh Extra Fine Front
Mesh Extra Fine Left
CMM Front
CMM Left
CMM Base
Mesh Extra Fine Base

(b).

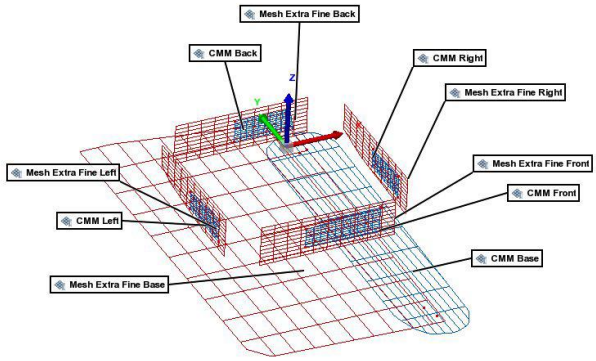
Mesh Extra Fine Back
CMM Back
CMM Right
Mesh Extra Fine Right
Mesh Extra Fine Front
Mesh Extra Fine Left
CMM Front
CMM Left
CMM Base
Mesh Extra Fine Base

(c).

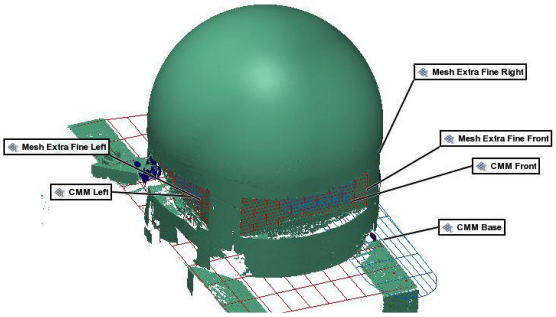
Mesh Extra Fine Right
Mesh Extra Fine Left
Mesh Extra Fine Front
CMM Front
CMM Left
CMM Base

(d).

(e). 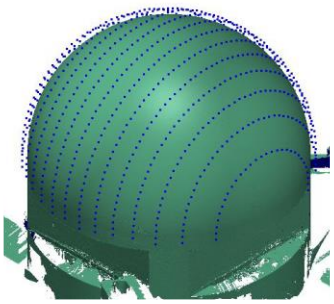

Fig. 6.4. Details the process of Cloud point data alignment onto the tactile probed data work piece coordinate system. (a). Cloud point data (green image) is imported into the tactile probed project; planes are fitted to the registration features and base shown as a red mesh. (b). Shows the juxtaposition of the imported cloud point data in its machine coordinate system and the tactile probed data work piece coordinate system. (c). Laser scanned cloud point data and associated planes translated onto tactile probed data using planes for alignment. (d). Scan data and tactile probed data in same coordinate system. (e). Scan points returned from 6 mm diameter probe centre, requiring probe compensation.

Both proposed probe tip compensation methods require the less accurate laser scanner generated cloud point data to be in the same coordinate system as the tactile probed data. Planar features analogous to those fitted to the tactile probe data ('Mesh Base', 'Mesh Front' and Mesh Left) were best fitted to the cloud point data using the planar feature best fit procedure.

Alignment of the cloud point data set onto the CMM data set was accomplished by rotation and translation of the Cloud point data and associated planes such that the 'Mesh base' plane, 'Mesh front' plane, 'Mesh left' plane became coincident with the 'CMM base' plane, the 'CMM front' plane and the 'Mesh left' plane respectively Fig. 6.4(c), using the 'Aligning Perpendicular planes' method discussed above and detailed in ..

Accurate alignment of coordinate systems is best carried out on planes that are perpendicular, which may not be the case when the plane is formed from a best fit to cloud point data. This is a little bit of a 'black box' process hidden within the metrology software. To some extent the decision process is taken

out of the operators control by automating the process. These issues and their impact on the accuracy of probe tip compensation will be discussed later.

Once alignment of the cloud point data set to the tactile probed data set was completed Fig. 6.4d. The cloud point data could be used as a substitute for prior knowledge of the surface form and probe tip correction could be performed on the probed data Fig. 6.4e.

The corrected probe contact points were calculated from the reoriented cloud point data using equations (4.3) and (5.12) for the probe compensation in the probe approach direction and probe compensation in the direction of surface normal methods respectively. The procedure was undertaken for raw cloud point data and data polygonaly meshed in real time.

6.3 Experimental accuracy results

Although not part of this investigation, the on board static CMM laser scanner was used to scan the target form and the data used as a comparison to that achieved by the articulated arm mounted laser scanner. A spherical feature best fit was applied to both the static CMM mounted laser scanner derived cloud point data and articulated arm laser line scanner derived data. Table 6.1 details the diameter measurements returned for the two laser scanners. The diameter error has been determined as the diameter difference between the tactile scanned hemisphere diameter (150.032 mm) determined in section 4.2. 'Considerations used in forming hybrid probe compensation' and the laser scanned best fit sphere diameters. Both data sets were for 'raw' cloud point data (uncleaned).

Table 6-1. Details static CMM onboard laser scanner and arm mounted laser scanner measurement for hemispherical form.

	Form dia. best fit (mm)	Error (mm) Hemisphere diameter 150.032 mm	STD Of best fit residuals (mm)
CMM laser scan	150.042	0.010	0.0419
Faro arm scan	150.08	0.048	0.0093

It can be seen from Table 6-1 that the Static CMM mounted laser scanner produced a more accurate diameter measurement than the articulated arm mounted laser scanner, with diameter accuracy from the static on board CMM being of the order 5 times more accurate. This accuracy level could prove fruitful for investigations detailed in '8.2 Future work' section of the thesis. It must be commented that the diameter accuracy is only one consideration. Before any use of the static CMM laser scanner is proposed, data deviation maps would show if the data were a good representation of the target feature form.

Fig. 6.5 details the dimensional accuracy of the probe tip correction methods developed in sections 5.1 and 5.2 when applied to uncleaned cloud point data and to scan data that is meshed in 'real time' and is then subsequently cleaned. Full data values with standard deviations can be seen in Appendix A.-Table 2.

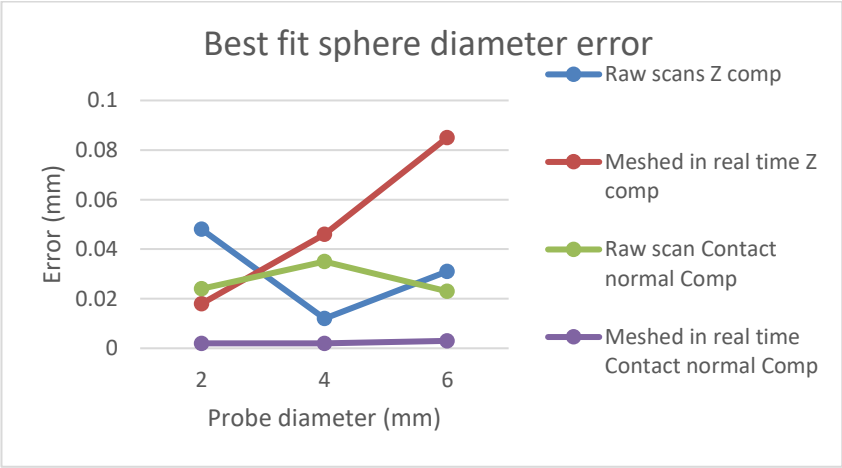

Fig. 6.5. Hemispherical form dimensional (diameter) accuracy.

Fig. 6.5 shows raw cloud point data to be in general less consistent than meshed data: -

- For diameter accuracy, compensated polygonal meshed data in the contact normal direction gave more accurate results than that compensated in the 'Z' direction. 0.018 mm diameter compensation error in the 'Z' direction was recorded for a 2mm probe tip. The equivalent error in the surface contact direction was 0.002 mm.
- For diameter accuracy, compensated data in the contact normal direction using polygonal meshed data gives more accurate results than using raw cloud point data. For a 6 mm diameter probe, compensation errors in the surface contact direction were 0.033 mm and 0,003 mm for raw cloud point data and polygonally meshed data respectively. Using real time meshing of data is the recommended data gathering workflow. It not only produces more accurate probe compensation, but it is also less subjective than having to select every outlier cloud point to be removed for cleaning.
- Smaller probe diameters give better probe compensation when compensation is in the 'Z' direction. For data meshed in real time the compensation error for a 2 mm diameter and 6 mm diameter probe tip was 0.018 mm and 0.085 mm respectively. This could be a limiting factor for the 'Z direction compensation method. Small probes can record surface detail rather than surface form, so using a larger probe to ensure surface detail is filtered out could be problematic for this method.
- Probe diameter has little effect on probe compensation in the 'Z' direction when using scan data meshed in real time for these experimental parameters. This is shown by the flatness of the graph. It is thought that there is sufficient scan data point density for probe diameter to not have an effect. For the probe compensation in the surface contact direction to be robust, scan density will need to be considered. It may be the case that heuristics are developed that categorise surface topology and inform the user of the scan density requirements for the target feature being considered.

When probing the hemispherical form to gain a best fit diameter, the approach direction was along the 'Z' axis. This was not best practice. The most appropriate direction is normal to the component surface. This is not only from a probe compensation perspective, but to keep probe stylus deflection to a minimum. As the probe approaches an oblique surface it may deflect or 'skid'. For good practice, this procedure should be corrected if the investigation is repeated.

6.4 The effect of cloud point density on the accuracy of hybrid compensation methods

The effect of cloud point density / sparse data on the accuracy of probe tip compensation using the proposed hybrid techniques has been discussed in Chapter '4 Development of probe compensation methods'. For probe tip compensation in the 'Z' direction, precautions have been made by forming planes to represent the target surface where there is sparse data points Fig. 5.7, but no such precautions can be made for probe correction using the surface normal method. The surface normal compensation method relies on locating the closest point to the probe tip and not a substitute for this point. Section 8.2 'Future work' does discuss potential filtering methods and ways to use a group of data points rather than a single point.

To determine the effect data density has on the probe tip compensation, laser scans were taken of the same hemispherical form as used above. The laser scanner was set to 'Extra fine' resolution to ensure a large number of data points were recorded and real time meshing employed to clean the scans of noise and to aid the removal of any floating spurious meshes. The resulting mesh model was aligned with the tactile probed data as detailed above and all mesh points other than those associated with the hemispherical form were deleted, resulting in nominally 8M points concerned with the probe tip compensation process. Within the PolyWorks software environment a triangle reduction tool is available to reduce un-necessary triangles in areas of low curvature. This tool was used systematically to nominally halve the number of triangles to form a series of polygonal models of reducing density

from 8M vertices to 25,000 vertices (10 data sets). Each data set was then exported as data points and used as a 'virtual surface form' to calculate probe tip compensation for 2 mm. 4 mm and 6 mm diameter probes with the results shown Fig. 6.6.

For comparison purposes only, data sets were also generated mathematically for a 150.032 mm hemisphere such that a comparison between mathematically generated data and actual data could be made. The number of data points generated in the mathematical data sets matched those from the laser scanned data sets (8M to 25,000 data points in 10 sets). Diameter error was calculated for both compensation methods with results shown Fig. 6.6 and Fig. 6.7. For both data sets points are joined for clarity. It is well understood that if any heuristics are developed to help determine the minimum number of data points that are required to ensure the compensation methods can function correctly. Data point density would be a better metric than number of data points.

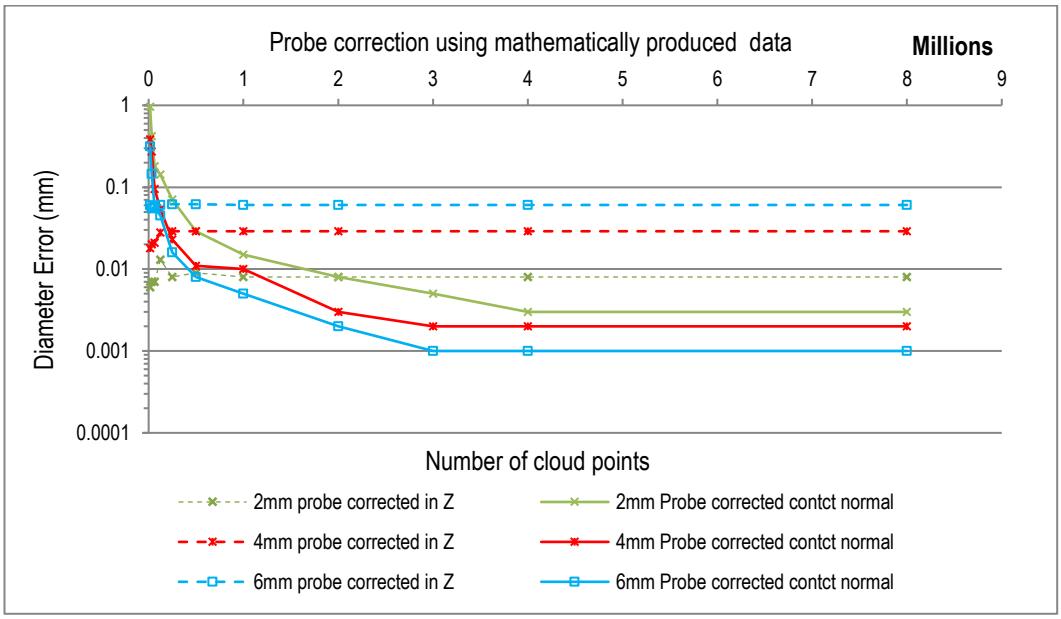

Fig. 6.6. Probe tip compensation detailed using mathematically generated data.

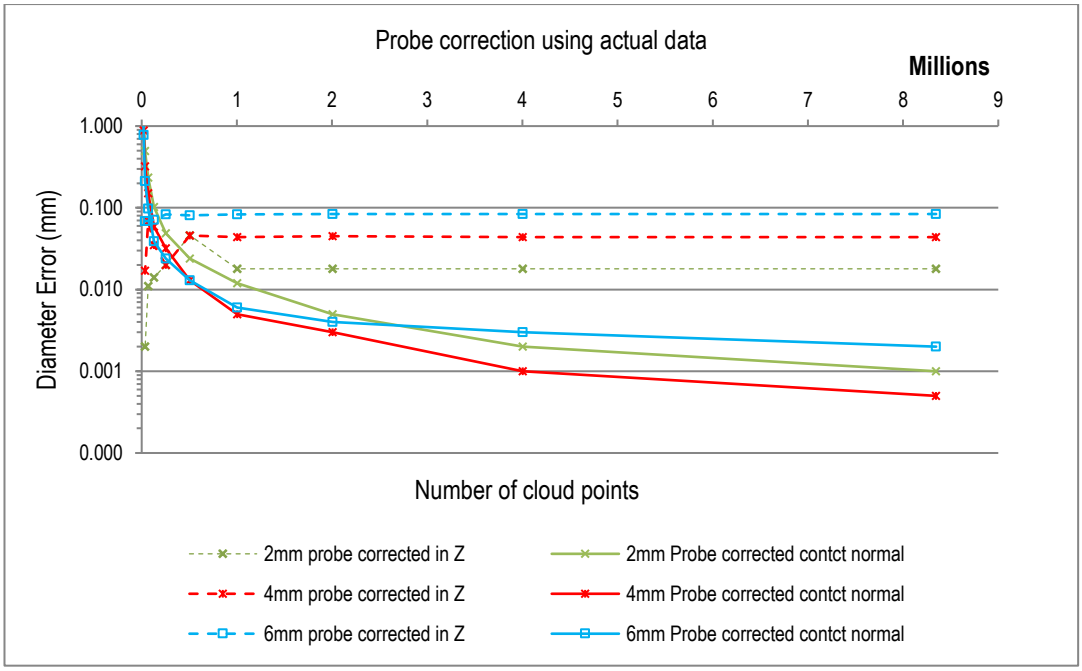

Fig. 6.7. Probe tip compensation detailed using actual data.

6.5. Discussion of results

Fig. 6.6 and Fig. 6.7 show the effect of laser scan data density on the accuracy of the two hybrid tip compensation methods developed. They show that: -

- Theoretical data and actual scan data produced very similar shaped graphs.
- Compensation along contact point probe normal gives smallest error for both theoretical and actual data. Typical 'Z' direction compensation errors are between 0.008 mm and 0.060 mm while data compensated in the contact normal direction gives errors typically between 0.001 mm and 0.005 mm.
- Compensation along the Z axis gives erratic results at low scan densities for both theoretical and actual date.
- Actual data compensation is similar to theoretical data counterpart.

- For compensation in the contact normal direction, both actual data and theoretical data have an increasing degree of accuracy as number of scan data points rise, but with diminishing returns.

6.6 The accuracy of hybrid compensation based on the contact normal of the probe

It can be seen in section '6.3 Experimental accuracy results' that the proposed probe tip compensation method estimating the compensation in the direction of probe vertical travel is considerably less accurate than that proposing compensation normal to the probe / target surface contact. There were other obvious drawbacks to the less accurate method, for example if a probe landed on the apex of a surface form such as cone. The estimated line of effect '$\overline{me}$' would point downwards bellow the actual contact point with no influence on the probe position, so additional data checks would need applying to the data to identify such issues. For the accuracy issue discussed the compensation method in the probe approach direction is investigated no further.

A hemispherical form was used to test the probe tip compensation methods developed in this thesis. Unlike a free-form surface, the hemispherical form has a single value of curvature. Modern CAD modelling software packages use 'base sketches' which are lofted, swept, extruded etc. to form surfaces. For non-prismatic surfaces, the 'base sketches' can be in the form of Bézier curves / 'splines. These are used to generate all manner of products ranging from household and industrial goods like injection moulded products, pump cases, turbine blades and the like.

Probe tip compensation was validated on a Bézier curve generated surface with varying curvature along the scan plane. Although the Bézier curves generating non prismatic forms may be described as 'free-form', their start and end points as well as their control points are known, so any point on the curve can be defined using the parametric equation (6.2) where 0 <= t <= 1.

$$B(t) = \sum_{i=0}^{n} C_i^n (1-t)^{n-1} t^i P_i \quad (6.2)$$

Where the Binomial coefficient C_i^n is:

$$C_i^n = \frac{n!}{i!(n-i)!} \quad (6.3)$$

Equation (6.2) can be expanded to form a cubic Bezier curve as shown in equation (6.4). Where P_0 and P_3 are start and end points respectively and P_1 and P_2 are control points Fig. 6.8.

$$B(t) = (1-t)^3 P_0 + 3(1-t)^2 t P_1 + 3(1-t) t^2 P_2 + t^3 P_3 \quad (6.4)$$

The X and Z coordinates are calculated as per equations 6.5 and 6.6 respectively.

$$B(t)_x = (1-t)^3 P_{0x} + 3(1-t)^2 t P_{1x} + 3(1-t) t^2 P_{2x} + t^3 P_{3x} \quad (6.5)$$

$$B(t)_z = (1-t)^3 P_{0z} + 3(1-t)^2 t P_{1z} + 3(1-t) t^2 P_{2z} + t^3 P_{3z} \quad (6.6)$$

The use of Bézier curves to generate a free-form object has the same advantage as the hemispherical form in that any point on the surface can be calculated. This allows tactile probing errors to be easily identified.

Unlike the previous methodology, an actual product has not been produced. Production of a complex surface introduces manufacturing challenges and is not only difficult to produce accurately, but due to its non-prismatic form it is difficult to validate the machined surface. There are also issues with surface finish and cusps from machining tool radii not matching the designed product.

To eliminate these issues, a virtual product was produced using the form shown in Fig. 6.8.

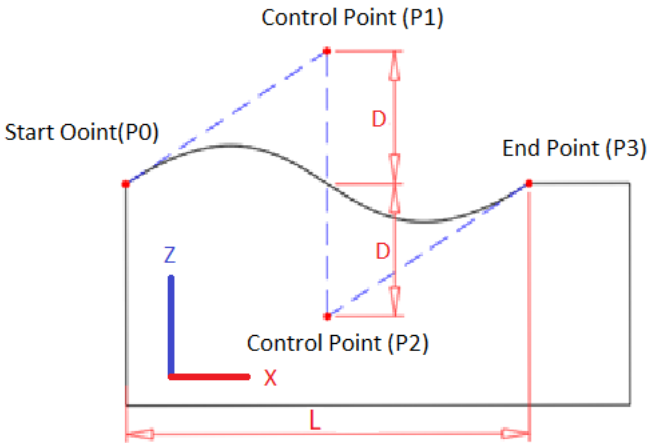

Fig. 6.8. Bezier curve generated test form. The form has curve length 'L' of 50 mm and dimension 'D' of 15 mm.

To form the virtual simulation, three sets of data were generated: -

- One representing the probe tip centre data simulating that derived from tactile probing,
- One set representing the target surface to check probe compensation against and
- One representing the arm mounted laser scanner data representation of the target surface.

The tactile probe data points were generated at nominally 0.5 mm intervals ($P_3 – P_0$ in the X direction divided by 100). From these contact points, tangent values were generated by taking the first differential of equations (6.5) and (6.6) with respect to 't' resulting in equations (6.7) and (6.8). Probe centre data was calculated by offsetting the surface contact point 'A' by the probe radius in the surface normal direction as depicted in Fig 6.9.

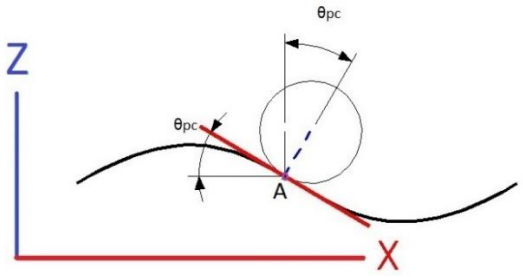

Fig. 6.9. Shows the probe centre point being derived from an arbitrary probe contact point 'A'.

The surface tangent angle to the 'X' axis is θ_{pc} is derived from the change in 'X' and 'Z' at the contact point. The first differential of the Bézier curves are: -

$$B'^{(t)_x} = 3(1-t)^2(P_{1x} - P_{0x}) + 6(1-t)t(P_{2x} - P_{1x})\ 3t^2(P_{3x} - P_{2x}) \quad (6.7)$$

$$B'^{(t)_z} = 3(1-t)^2(P_{1z} - P_{0z}) + 6(1-t)t(P_{2z} - P_{1z})\ 3t^2(P_{3z} - P_{2z}) \quad (6.8)$$

At the probe / surface contact point the tangent angle to the #X' axis is θ_{pc} is derived by trigonometry, using opposite / adjacent: -

$$\theta_{pc} = \tan^{-1}\left(\frac{B'^{(t)_z}}{B'^{(t)x}}\right) \quad (6.9)$$

With the probe centre coordinates being P_{centx} and P_{centz} ; the probe / surface contact coordinates being P_{contx} and P_{contz} and probe radius as r: -

$$P_{centx} = P_{contx} + \sin(\theta_{pc}).r \quad (6.10)$$

$$P_{centz} = P_{contz} + \cos(\theta_{pc}).r \quad (6.11)$$

The procedure is laid out graphically in Fig. 6.10. and discussed in more detail below.

(a).

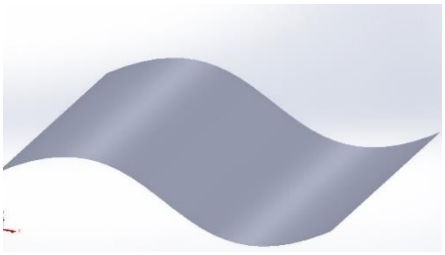

(b).

(c). 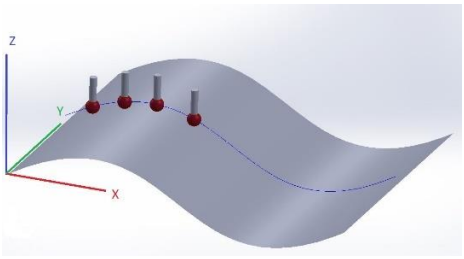

Fig. 6.10. Details the workflow for checking the accuracy of the proposed probe tip compensation in the probe contact normal direction. (a). reference surface generated from Bézier equations. (b). Laser scan data representing reference surface. (c). Probe positions of the reference surface. Contact points between probe and reference surface generated mathematically to determine probe centre point.

To form a virtual representation of the target object, surface data was generated using 250,000 data points generated at equal intervals in the 'X' direction (nominally 0.0002 mm) using equations (6.5) and (6.6).

Rather than aligning corrected probe contact points to the CAD model of the Bézier curve to determine errors of the correction method, corrected probe points were compared against this dense data set. Alignment to the CAD model was not used as this, although unlikely could introduce error in the data set alignment process. The maximum radius at the peak and trough of the Bézier curve form is 16.78mm. With a point spacing of nominally 0.0002 mm in the 'X' direction the maximum deviation from the surface to a line joining two adjacent points is approximately 0.0000000012 mm. If compensation error is measured from this estimation of the 'perfect' surface, it will have a minor effect on our compensation error calculation which has been seen to be a single micron level.

The coordinates in the 'Y' direction were generated randomly to form a virtual Bézier surface 4 mm wide.

A set of 250,000 data points representing the arm mounted laser scanner cloud point data set of the target surface was generated in the same manner, but a number of treatments were applied to represent laser scanner and registration errors.

- The points were left ‘as is’ to represent perfect scan data and a transformation added to the data set as a whole to mimic a data alignment / registration error.
- Each data point was moved in the ‘Z’ (Vertical) direction a random distance between ‘0’ and an upper value to represent scan data variance.
- Each data point was moved in the ‘Z’ (Vertical) direction a random distance between ‘0’ and an upper limit to represent scan data variance, then the whole data set was translated in a combined ‘X’ and ‘Z’ direction to mimic a scan registration error.

By not linking the three data point sets there is no prior knowledge of the surface form when calculating the probe compensation. As has been discussed in section’5.4 Summary’ Random numbers generated using Microsoft Excel and Microsoft VBA are Pseudo-random and are generated from a seed value based on the system clock.

Chapter 3 ‘Accuracy investigation of arm mounted laser line scanning’ shows that laser scan error is dependent on laser unit stand-off, in plane and out of plane angle as well as reflectivity of the surface being scanned. The planar error found in the tests seemed appropriate to represent good and bad scanning practices for both diffuse and reflective surfaces.

Fig. 3.4 shows the maximum planar errors to be in general between ±0.070 mm, except for reflective target error with out-of-plane angles of between -20° to -50° Fig 3.4d. It must be remembered that these planar errors were generated by fitting a relatively large plane (in terms of probe size) from raw cloud point data that had not been cleaned or meshed, so it seemed a fair assumption that if good scanning practice were to be used, scanning as close to normal in both the in-plane and out-of-plane directions and using a mid-standoff the scanner would return a worst accuracy well below this 0.070mm value. It is not forgotten that speckle reflection, sub surface scattering and reflection from surface error can cause outlier data points. This could have an adverse effect on probe tip correction algorithm, which uses the closest data point to the probe tip to calculate the surface contact normal compensation. In this instance it will be assumed that cloud point data would have been polygonally meshed in real time,

removing outlying data and then converted back to a cloud point data set. It is also the case that modern metrology software has onboard filtering routines for the removal of outliers. This issue will also be discussed in '8.2. Future work' section of this thesis, where it may be more appropriate to include multiple sample points closest to the probe centre in the compensation calculation. This could allow any small number of spurious outlier points to be eliminated by the larger number of scans that represent the target surface more accurately.

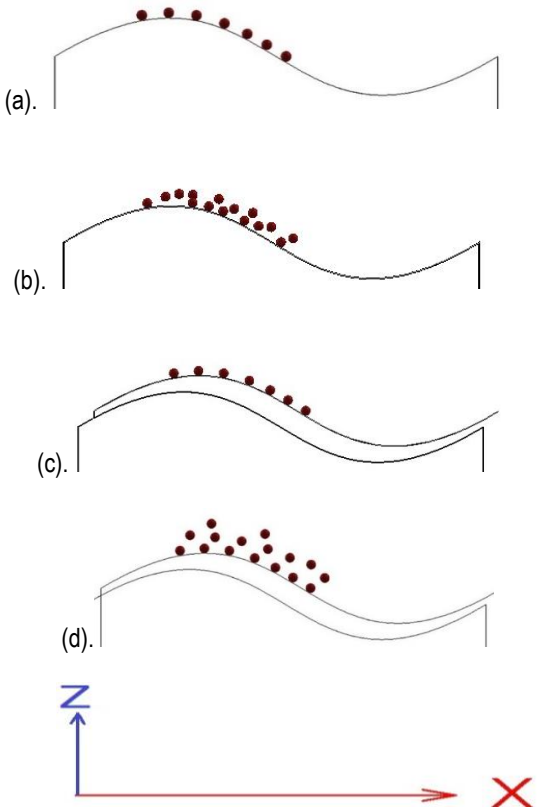

Fig. 6.11. Details the scan treatments applied to represent actual data. (a). perfect scan data, matching the virtual target surface exactly. (b). random error applied to the scan data representing the virtual target reference surface. (c). perfect scan data displaced in the 'X' and 'Z' directions to represent scan registration error. (d). random error added to scan data as well as a 'X' and 'Z' scan registration error.

To simulate scan registration error, a combined shift in the data set of 0.1 mm in both the 'X' and 'Z' has been applied. Scan alignment error measurement is not part of this investigation, so a figure larger than that anticipated is used.

To simulate scan data variance a 0.000 mm to 0.070 mm random movement in the Z direction was applied to each data point.

To simulate scan registration and scan data variance error a combined shift in the data set of 0.1 mm in both the 'X' and 'Z' has been applied, combined with a 0.000 mm to 0.070 mm random movement in the Z direction for each data point. These three separate simulations are depicted pictorially in Fig. 6.11b, c, d.

For each investigation the probe compensation in the 'normal direction' was applied to the 100 probe centre points and the error calculated between the compensated (calculated contact point) and the closest data points that represent the 'mathematical' target surface. To determine the closest point in the data set representing the 'mathematical' target surface, the two closest points P1 and P2 Fig. 6.12, one before the probe contact point and one past the contact point were determined.

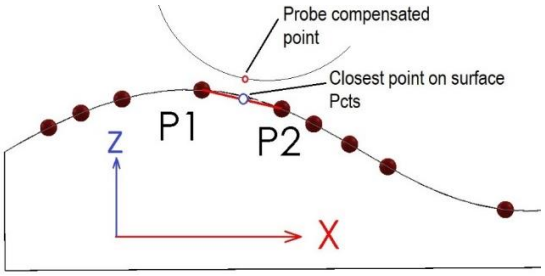

Fig. 6.12. Shows interpolation of the 2 closest points to determine probe contact point coordinates.

The closest surface point 'P_{cts} vertically below in the 'Z' direction is the calculated contact point on the target surface data set was determined by interpolation using equation (6.13) and (6.14).

$$P_{ctsx} = P1_x + \left(\frac{(\text{Compensated Probe}_x - P1_x)}{P1_x - P2_x}\right) * (P1_x - P2_x) \quad (6.12)$$

$$P_{ctsz} = P1_z + \left(\frac{(\text{Compensated Probe}_x - P1_x)}{P1_x - P2_x}\right) * (P1_z - P2_z) \quad (6.13)$$

Compensation error measured between the target surface data set and the probe compensation point can be determined in different directions ('X', 'Y', magnitude) but in this case has been calculated using

Pythagoras. Because 'P_{cts} is interpolated, it is vertically below the calculated contact point, and all 'Y' data points are taken as being on the scan plane. Although Pythagoras gives the magnitude of the error, in this case it will return the error in the 'Z' direction as error in 'Y' and 'Z' are zero. This will be discussed later in 'Chapter 8.2. Future work'

$$Error = \sqrt{(Pctsz - CompensatedPoint_z)^2 + (Pctsx - CompensatedPoint_x)^2} \quad (6.14)$$

The simulations were run with 2 mm, 4 mm and 6 mm probe diameters. The error reported is the average of the compensated probe point individual errors for the 100 probed points. Compensated data points, standard deviation and min and max statistics are seen in the appendix Table A-3 to A-5.

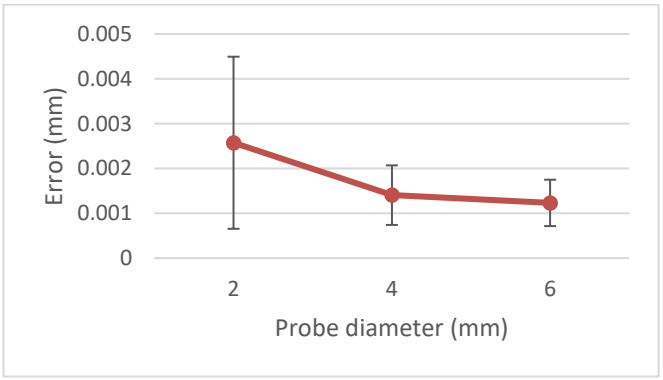

(a). 0 to 0.07 mm random error added to virtual cloud point data. No displacement of the whole data set.

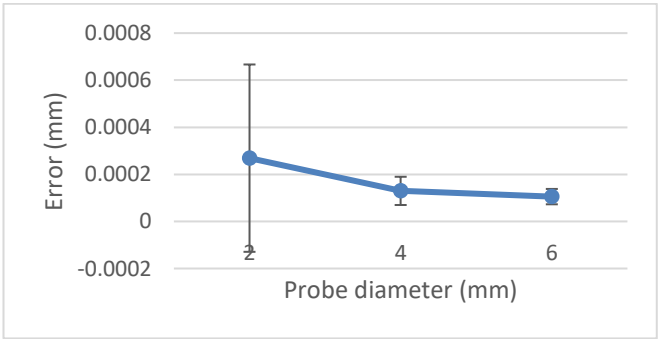

(b). No scan point data error added, 0.1 mm displacement of the whole date set in the X and Z direction

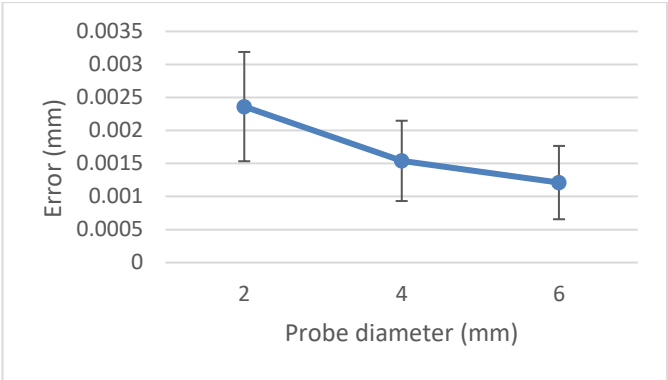

(c). 0 to 0.07 mm random error added to virtual cloud point data and a 0.1 mm displacement of the whole date set in X and Z direction.

Fig. 6.13. Results for errors calculated from Probe tip compensation compared to a perfect data surface.

Summary data for the graphs shown in Fig 6.13. is detailed in the appendix (Tables A-3, A-4, A-5). The information includes error standard deviation, minimum and maximum values.

Fig. 6.13 graphs show that after probe tip correction in the normal direction of the contact point: errors of less than 0.0025 mm were achieved between the actual surface representation and the calculated contact point, with the larger virtual probes delivering the most accurate results of less than 0.0015 mm.

Scans that were incorporated with a 0 to 0.070 mm random scanner error show the greatest error and have very similar values to scans with a combined random scanner and an alignment displacement error. Scans having a simulated alignment displacement error only, having the least error of around an order less. It can be seen that there is a greater error standard deviation for data generated from the smaller 2 mm probe.

In Fig. 6.14, the 'hatched' blue cloud point is the data point that is closest to both the small blue probe tip and the large red probe tip centre. 'Angle Small probe' is larger than 'Angle Large probe'. The smaller angle produces a correction vector closest to the probe actual contact normal indicating the larger probe tip will produce potentially the most accurate compensation results. If the cloud point data

point closest to the probe centre was on the contact point surface normal, this error would be zero. Probe tip diameter has less influence on compensation error, the closer the selected cloud point data point is to the surface / probe contact normal.

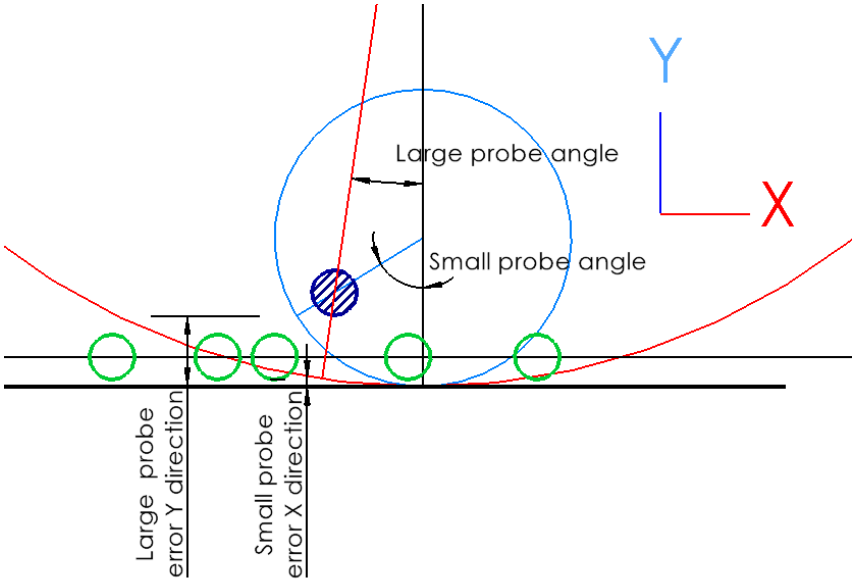

a.

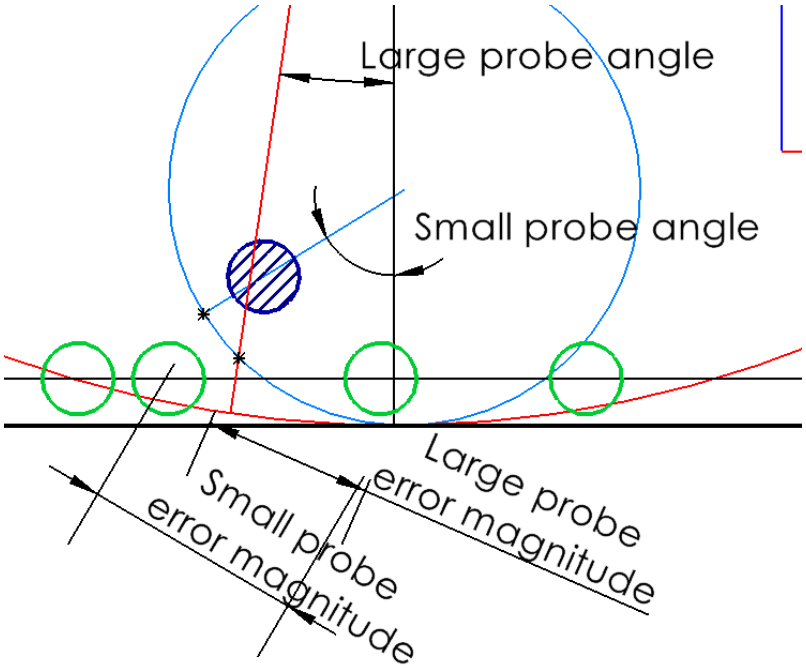

b.

Fig. 6.14. The effect of probe diameter on compensated error. Geometry has been greatly exaggerated for clarity.

6.7 Summary

When using actual laser scan cloud point data to represent the target surface, the probe tip compensation method in the normal direction of the contact point of probe and surface proved more reliable and accurate than compensation in the 'Z' (vertical) direction. Within the bounds of the experimental procedure, coordinate system alignment accuracy had little effect on surface contact normal direction compensation. One of the largest influences on accuracy for this method appears to be probe tip diameter. Probe tip compensation showed good accuracy levels comparable to the accuracy of a static CMM measuring prismatic objects.

Chapter 7. Discussion of results

7.1 Discussion of Arm mounted laser scanner accuracy

It has been suggested by that shiny reflective surfaces produce less accurate results than matte surfaces. When a planar feature is fitted to the laser scan data, the accuracy of the planes fitted to data from reflective targets in some instances are superior to those derived from matte surfaces. Scan stand-offs of 215 mm and 190 mm with out-of-plane angles between 0 degrees and -20 degrees have systematic errors of 0.010 to -0.024 mm and-0.064 to 0.099mm respectively. This is not to suggest that cloud point data sets derived from highly reflective surfaces are more accurate. The large numbers of cloud point data points that reflect with accurate data positions may outweigh the erroneous data points. It can also be seen that the data point spikes are highly concentrated, occupying only a small area of the scan width and so their detrimental effect on accuracy may be greatly reduced or 'positive' and 'negative' spurious data may have a cancelling effect on each other. More work scanning and fitting of prismatic features to other surface feature forms would be required before such statements could be validated. It does appear that reflective surfaces can cause a speckle reflection that saturate the laser scanner receiving device result in a gap in the cloud point data coverage and cause erroneous data points (noise) to be produced for both reflective and diffuse targets (-30 degree out-of-plane angles at stand-offs varying from 115mm to 215mm).

As with previous work on static CMM laser scanners, arm mounted laser scanner accuracy is dependent on both laser stand-off from the target, and angular orientation to the target. At some extreme angles higher inaccuracies were seen, but these were at positions that would be difficult to achieve with a conventional workpiece and by an operator with normal dexterity. It must also be remembered that the arm mounted laser scanner unit is equipped with both a visual laser range finder system and an audio signal to help maintain optimal scanner orientation and stand-off to target surface.

A conservative / poor scanner accuracy of 0.07 mm error was taken forward from laser scanner results to be used in testing of the probe tip compensation methods.

7.2 Discussion hybrid probe tip compensation methods

7.2.1 Using virtual hemispherical scan data

Of the two probe compensation error methods developed in this thesis, 'Z' direction probe compensation (in the approach direction) attempted to find the steepest area of the target surface directly below the probe to estimate the intended probe surface contact point Fig. 4.11. Error and uncertainty were added to this methodology by assuming a straight line form under the probe tip, even though the system did attempt to determine probe flank contact. It can be seen in Fig. 5.10a that as probe tip diameter increases from 2 mm to 6 mm, the probe tip compensation error increases from 0.008 mm to 0.060 mm for the test hemisphere diameter. This is to be expected as the assumption that the surface influencing the probe contact point is a straight line does not hold as well over larger probe diameters.

Increasing the cloud point data count from 1million points to 4 million points has had negligible effect on the recorded diametral error. It is assumed that 1 million data points spread over the target hemisphere gave sufficient data point density, such that increasing the number had no improving effect.

Probe compensation in the normal direction to the probe tip contact point showed that the larger 6 mm diameter probe tip produced more accurate probe tip compensation than the 2 mm probe tip.

As scan data density increased to 4 million data points covering the test hemisphere form; tip correction accuracy also increased. At 4 million data points the compensation error for the 2 mm probe, the 4 mm probe and 6 mm probe gave hemisphere diametral errors of 0.003 mm, 0.002 mm and 0.001 mm

respectively. Results showed that with sufficient scan density, the contact normal compensation was more accurate than compensation in the 'Z' (approach) direction.

7.2.2 Using actual hemispherical scan data

Both polygonal meshed and cloud point data were used. The most accurate probe tip compensation was obtained using the surface contact normal method with data that had been polytonally meshed. Diametral accuracies of 0.002 mm, 0.001 mm and 0.003 mm for the hemisphere were achieved for 2 mm, 4 mm and 6mm probe respectively. Raw cloud point data scans for the same tip compensation technique produced hemispherical diameter errors of around a factor or more worse presumably because the data was uncleaned. It is thought that as scan density rises, compensation error is less sensitive to probe diameter increases, that is there is more chance of a mass of data points around the surface contact normal.

For probe compensation in the Z direction matters were not cut and dry, with probe tip compensation using raw cloud point data being in some cases more accurate than polytonally meshed data. This highlighted some instability in the method.

7.2.3 Effect of scan density on probe tip compensation accuracy

The effect of cloud point data on the accuracy of probe tip compensation during the measurement of a target hemisphere has been examined using theoretical and mathematically generated data. Very similar shaped graphs were generated with scan density having less influence on compensation accuracy as scan density increased.

Compensation along the Z axis gives erratic results at low scan densities for both theoretical and actual data. Sufficient scan density is an essential prerequisite for accurate probe tip compensation, but above a certain level there are diminishing returns when actual data is being considered.

No matter what the scan density was, the probe tip correction was most accurate using the surface contact normal method, with results being over an order of magnitude superior to compensation calculated in the approach direction.

7. 3. Discussion of Hybrid probe tip compensation normal to probe tip contact point on a pseudo free-form Bézier curve generated surface

Probe tip compensation in the 'Z' approach direction has proved less reliable and less accurate than the compensation in the surface contact normal direction. For this reason, the proposed probe tip compensation method was taken no further.

The probe tip correction in the normal direction to probe and target surface contact uses data rather than an estimate to calculate the probe tip compensation direction / actual contact point. Assuming the surface beneath a probe equates to a straight line is probably true at very small probe diameters, but results show this assumption to be miss guided as probe diameter increases.

One of the main hurdles to accurate probe tip compensation appears to be laser scan cloud point data density and the effect of data outliers. Poor data can give a false direction for probe tip compensation.

The results show the probe compensation in the surface contact normal direction to be very accurate and confirm that correction is more accurate when using a 6 mm diameter probe rather than a 2 mm probe. The reason for this is shown graphicly Fig. 6.14.

Physical displacement of the data set as might be found with a scan registration error caused little compensation error: 0.000105 mm was recorded for a 6 mm diameter probe. Combining a randomised scan error and a displacement error for a 6 mm diameter probe produced a compensation error of 0.00121 mm.

It is thought that the scan displacement error may need reconsidering and a rotation adding rather than a translation. Putting a translation in the 'X' and 'Z' direction of 0.1 mm has had little effect on the compensation error. It is thought that the data displacement in 2 directions has created offset data that is relatively 'parallel' to the original surface as per Fig. 7.1 a. Obviously, the displaced Bezier curve cannot be parallel along its whole length, but if the displaced data is considered as a series of small individual areas around the probe correction points, the displaced data is close to being parallel to the surface. This relatively parallel displaced data will have little effect on probe compensation accuracy as discussed in previous sections and repeated Fig. 7.1 a. The random data applied to the data set adds more variance. There is more chance of a stray data point (green point off of the actual contact normal line) influencing the correction calculation, see Fig. 7.1 b. Point 'G' becomes the corrected probe contact point rather than 'A'

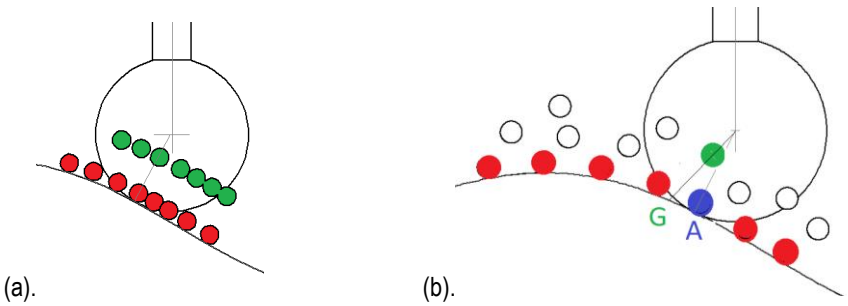

(a). (b).

Fig. 7.1. (a). Red cloud point data representing the target surface has been displaced on mass to simulate a coordinate alignment error. The offset data does not change the compensation. (b). The data points randomised to simulate scan data shows the blue cloud point data point indicating the correct correction point A, but the green randomly generated point is closest to probe centre, so G is the calculated compensation point and not A.

Not having a three dimensional actual freeform model to validate the probe compensation is a serious limitation to the investigation. The accurate machining and validation of such a model has been discussed at length. A partial solution could be to form a Bezier curve driven model in both the 'X' and 'Y' directions, forming a surface with double curvature. The surface would have all the benefits of the Bezier model used in this investigation, but it would have the advantage of producing probe to surface contact off of the scan plane. That is, it would promote probe flank contact.

How laser scan cloud point data is obtained / the clean-up treatment can influence how accurately the data represents the target surface. Meshing the data in real time has the effect of filtering out erroneous data points as the meshing algorithms can be set to ignore outliers which are outside the parameters set by the user. There may be issues with the meshing algorithm forming small mesh segments that 'float' in space, but deleting mesh patches not attached to the main polygonal mesh body is relatively easy. The operator simply selects the main body(s) of meshed data that represents the target surface well; inverts the selection to highlight all outlying data, then deletes that poor data. Or software settings can be used to automatically delete software clusters that outlie the main body of scan data.

Raw cloud point data is more difficult to clean as there is no interlinking of data points. The software operator must make a value judgement for every data point.

To some degree this issue seems to have been ignored when producing theoretical scan data to test the probe tip compensation, because user intervention or settings within the CMM onboard software can be used to rectify this situation. This will be discussed in '8.2 Future work' section, concerned with developing a more advanced strategy for selecting the data used in determining the probe tip compensation direction.

The surface generated from a Bézier curve does not fall into the quite tight definitions of a prismatic feature , . Although it is represented mathematically. In this investigation if there is no prior knowledge of the surface used to determine probe tip compensation and no CMM onboard software learning

algorithms are used, then the surface could be considered free-form. Although the surface used has only curvature in a single direction, this has been considered sufficient to represent a free-form surface. This topic will be expanded in the ‘‘8.2 Future work’ section that follows.

Chapter 8. Conclusions and Future work

8.1 Thesis conclusions

This thesis has carried out an investigation into the measurement accuracy levels achievable by an arm mounted laser scanner. No other research has been found on this subject. Arm mounted laser scanner accuracy has been shown to be dependent on laser stand-off, in-plane and out-of-plane angle and target surface reflectivity.

Reverse engineering has been discussed in some detail. It is the case that there is less known design intent when reverse engineering an existing product compared to validating a new product. The lack of surface / feature prior knowledge in the reverse engineering process does not mean probe tip correction is to be used exclusively for reverse engineering. It can also be used when measuring any free-form surface. There are a number of definitions of free-form surface varying from any surface feature that is not a prismatic (such as planar, cylindrical, spherical or conical features) to features that cannot be expressed by a simple mathematical expression. This thesis would suggest that when measuring a product, other than the most obvious machined flat or cylindrical faces, any face or feature where there is no prior knowledge of the surface topology may need to be treated as free-form. This is especially true when reverse engineering a product that has worked well for many years. It may have a good performance because.

- It was designed well, or
- Because of the hand crafting / manufacturing idiosyncrasies that formed it or
- How it has worn or deformed over its life.

It is a requirement of the reverse engineering process to capture all of this detail, rather than assuming what the original designer intended. The probe tip correction method developed can be used to more accurately carry out this process as worn / hand crafted faces and features are likely to be freeform rather than prismatic.

Of the two methods developed to produce probe tip correction from laser scan data of a target surface, the method of estimating the steepest slope of the surface directly below the probe tip proved unsuccessful.

Estimating the probe contact position with the target surface using the scan cloud point data points closest to the probe centre produced promising results.

Other systems like learning algorithms base their prediction of probing direction on previous tactile probed data points or base their approach direction on prior surface knowledge in the form of a CAD model. Alignment of a CAD model to a target object on a CMM can prove problematic / inaccurate depending on the features available for alignment.

The system developed in this thesis uses a less accurate surface representation provided by non-contact laser scanned cloud point data to inform probe tip compensation. The results have proved reliable using actual scan data on a hemispherical prismatic part and highly reliable with theoretical data from a free-form Bézier curve generated surface. The technique has proved robust, producing results with best accuracy equivalent to the maximum permissible error (MPE) of the CMM or better. For the static CMM used in this investigation. Levels of accuracy of 0.001mm have been seen. This degree of accuracy enables free-form objects to be measured with a level of accuracy achieved by the CMM measuring prismatic parts with their accompanying surface prior knowledge.

No other work has used such a hybrid system or achieved accuracy levels seen by the developed methodology when measuring free-form features.

This proposed method of probe tip correction seems only to have problems with stray / outlying data contained in the data set. This should not prove problematic as there are a number of tools contained within the laser scanner software and CMM onboard software that can combat the outlier data point problem. Other solutions to this issue have been put forward and are discussed next in the '8.2 Future work' section.

8.2 Future work

Further work could be undertaken to better understand how target surface finish affects the size and orientation of the speckle lobe and how the speckle lobe affects scan data accuracy for different scan angles and stand-offs. This work could be further extended to see if this process characterisation can be used to predict and enhance overall data accuracy for both metrology and reverse engineering purposes.

Removal of outlying scan data points or reducing outlier data influence is an important objective. More detailed information on the accuracy of cloud point data, rather than accuracy of fitted prismatic features to cloud point data could prove very useful enhancing probe compensation accuracy. If a good understanding of cloud data point error from the target surface is available, then it becomes relatively straight forward to identify if the closest point to the probe centre is a true representation of the surface or if it is more likely to be an outlier which should be ignored. That is, erroneous data points in the local vicinity of the probe lie further from the surface than anticipated, which implies they lie closer to the probe centre than anticipated and so should not be considered in the probe compensation calculation.

It has been seen that probe tip compensation in the probe / surface contact normal direction has shown good potential, producing error results at single micron level. Compensation error levels of 0.003 mm (STD residuals best fit 0.004mm) have been seen when applied to a hemispherical actual form and 0.0012 mm error (STD residuals best fit 0.001mm). The surface contact normal compensation method uses the closest data point to the probe centre to form its compensation. When using data from a virtual free-form target, increasing probe tip diameter decreases error due to the trigonometry involved Fig. 6.16. This could prove problematic if target surface features demand a small probe be used for contact measurement.

A possible improvement to the compensation algorithm could be to take a weighting of the cloud point data points closest to the probe centre. This could reduce the influence of problematic outlier data.

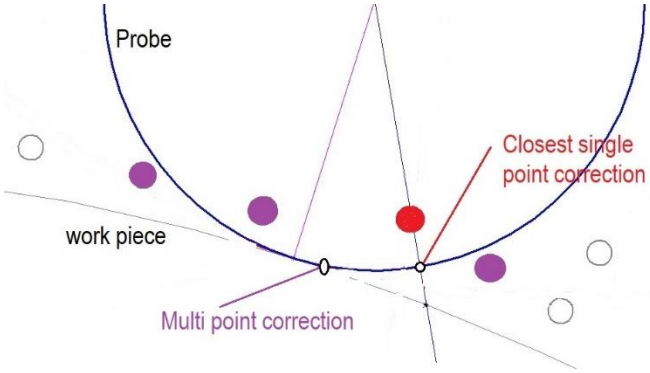

Fig. 8.1. An adaption of Fig. 6.15. Use multiple points to determine contact normal direction.

As can be seen in Fig. 8.1, rather than using the single closest 'red' data point; if the scan data selection was expanded to select the closest four data points to the probe centre, the calculated contact point may be closer to the actual probe contact point and the error could be reduced. It could be the case that the angles of the direction vector from probe centre to several of the closest point pairs could be used to discarded outliers or an arbitrary 'proposed' direction vector could be optimized using 'least squares' residuals of the angles from the proposed vector to all local scan data points being considered.

It has been seen in Chapter 3 that high numbers of cloud point data outliers and saturation of the laser scanner receiving device can occur when scanning normal to highly reflective surfaces. Sparse and plentiful data may give very different results, such that it may be the case that scanning heuristics need to be developed to ensure there is a sufficient cloud point coverage.

It has been shown that how laser scanned cloud point data is obtained / the clean-up treatment can influence how accurately the data represents the target surface. Stray data points reflected from secondary features, sub surface scattering or reflection from surface finish defects may have a detrimental effect on probe tip compensation. Meshing the data in real time has the effect of filtering out erroneous data points as the meshing algorithms can be set to ignore outliers which are outside parameters set by the user. Software settings can also be used to automatically delete clusters that outlie the main body of the meshed data. So further work may be required to qualify the CMM onboard software tools for eliminating outliers.

The use of laser scanners mounted on a static CMM may not be widespread due to the expense of the equipment, the need for a quite large CMM unit to be able to accommodate a laser scanner and its articulation mechanism, or existing CMMs may not be suitable to have laser scanners retrofitted because of software / computing constraints. If a static CMM is equipped with an onboard laser scanner. Laser scan data is likely to be considerably more accurate and give a better surface representation than data gathered by a portable arm mounted system Table 6.1. Data gathered from an integrated static CMM system would not need cloud point data manipulation to align probed data and laser scan data. All measurements / data could stay in the CMM machine coordinate system (one coordinate system only). Arm mounted laser scanner derived cloud point data taken in a different coordinate system to the tactile probed data, must use a variety of prismatic features (planes, axis of cylindrical features) for the alignment algorithms to align the different data sets. Free-form objects like car bodywork panels, may not have any prismatic features to align the coordinate systems.

Using a static CMM equipped for tactile probing and laser scanning could give a considerable advantage when calculating probe compensation using the hybrid method developed in this thesis. Not only is the laser cloud point data more accurate than the arm mounted equivalent, but the single coordinate system would reduce the time required to manipulate data. This may need an additional expense of having a polygonal meshing module included in the onboard CMM software.

To some degree Alignment error has been ignored in this thesis and very little research on this area has been found . A good understanding of the effect scan noise and poor data coverage have on transferring data from one coordinate system to another could prove useful, if the tactile probed and laser scanned data have to be gained from different equipment.

It could be the case that laser scan data is only taken from areas where tactile probing is to be undertaken, reducing scanning time, and data processing. This could prove a fruitful area for future

work for both prismatic and free-form target objects, although there are still considerable issues in verifying probe compensation techniques when free-form objects are being measured.

Verification of measurement results for a free-form object is difficult and has been discussed at length earlier. report that the ability to produce complex surfaces is out pacing the ability to confidently measure them. This makes it difficult to verify the accuracy of the probe tip compensation method developed.

The cloud point data gained from the static CMM on board laser scanner could be meshed in real time and the normal of polygonal mesh triangles closest to the probe centre used to produce an appropriate probe approach direction. This concept may be a little over simplistic as there could be issues with the small size of the triangular mesh elements having inclinations that do not exactly match the general surface form. If this were the case, work could be undertaken to look at mesh smoothing algorithms or an aggregation of the surface normals of these closest triangles.

Due to the difficulty of determining the accuracy of measuring processes based around non-prismatic, free-form surfaces. The accuracy of the target model (usually machined) cannot be taken for granted. Even when using the most up to date machining centres and tools, inaccuracies can creep into the process. Work holding strategies applying undue forces can cause distortion. Incorrect tool sizes can leave cusps and hollows as well as multi position machining introducing errors each time the work piece needs moving to gain access to material that still requires removal.

When validating such a model or the measuring process discussed in this thesis, these potential inaccuracies prove problematic. If the source CAD model is used as a reference, it is unclear if any deviation from the CAD model is due to the inaccuracies of the machining process, shortcomings in the measuring process or data set alignment issues.

It Is proposed that planar and cylindrical items produced to a high degree of accuracy (flatness and cylindricity respectively) are distributed at various angles to each other to form a setup where all

surfaces are fully and accurately defined through static CMM measurement and the fitting of prismatic features to the measured data.

Tactile probing / scanning can follow probe paths passing across the different features. Prior knowledge of the surface topology can be ignored when testing measuring strategies. This setup would promote probe tip flank contact in areas similar to free-form objects.

In essence this is like the National Physics laboratory free-form model, but it may be that potentially more accurate control can be applied to the surfaces. Grinding of planner and cylindrical faces can be used and internal and external features can be replicated by the juxtaposition of the various components. This would not be a portable solution to the problem and appears to not have features of varying curvature, but traversing a probe over a conical surface or obliquely over a cylindrical surface could rectify this situation by describing parabolic or elliptical paths.

Chapter 9. References

Bešić, I., Van Gestel, N., Kruth, J.-P., Bleys, P., & Hodolič, J. (2011). Accuracy improvement of laser line scanning for feature measurements on CMM. *Optics and Lasers in Engineering*, 49: 1274–1280.

Coleman, D., & Waters, F. (1997). *Fundamentals of Touch Trigger Probing.* Touch Trigger Press. Retrieved from Found in Flack Good Practice Guide 41

Martínez-Pellitero, S., Barreiro, J., Cuesta, E., & Fernández-Abia, A. I. (2018). Knowledge base model for automatic probe orientation and configuration planning with CMMs. *Robotics and Computer–Integrated Manufacturing*, 49 285–300.

Vukašinović , N., Bračun, D., Možina, J., & Duhovnik, J. (2010). The influence of incident angle, object colour and distance on CNC laser scanning. *The International Journal of Advanced Manufacturing Technology*, 50: 265–274.

Ainsworth I, I., Ristic , M., & Brujic, D. (2000). CAD-Based Measurement Path Planning for Free-Form Shapes Using Contact Probes. *Advanced Manufacturing Technology*, 16:23–31.

Bernardini, F., Rushmeier, H., Martin, I. M., Mittleman., J., & Taubin, G. (2002). Building a digital model of Michelangelo's Florentine Pieta. *IEEE Computer Graphics and Applications*, 22:59-67.

Boeller, W., Vincent, M. B., & Marbs, A. (n.d.). Investigating laser scanner accuracy. Retrieved October 15, 2022, from https://www.researchgate.net/publication/246536800_Investigating_laser_scanner_accuracy

Bostock, L., & Chanbler, S. (1983). *Applied Mathematics 2.* Stanley Thornes (publishers) Ltd.

British Standards. (2016). *ISO 10360-12:2016 'Geometrical product specifications (GPS) — Acceptance and reverification tests for coordinate measuring systems (CMS) Part 12: Articulated arm coordinate measurement machines' (CMM).* Retrieved October 15, 2022

Corral, M. (2022, Aug 15). Vector Calculus 2022. Schoolcraft College, Boston. Retrieved October 15, 2022, from http://www.mechmath.net

Feng, H.-Y., Liu, Y., & Xi , F. (2001). Analysis of digitizing errors of a laser scanning system. *Journal of the International Societies for Precision Engineering and Nano-technology*, 25:185–91.

Flack, D. (2014). *Good Practice Guide No. 43* (Vol. No 43).

Flack, D. (2014). *Measurement Good Practice Guide No. 41* (Vol. No. 41; CMM measurement strategies). Engineering Measurement Division National Physical Laboratory.

Flack, D., Claverley, J., & Leach, R. (2014). *Coordinate Metrology; Fundamental Principles of Engineering Nanometrology (Chapter 9)* (Second edition ed.). Elsevier Inc.

Flack, D;. (2001 Updated May 2014). *Measurement Good Practice Guide No. 42; CMM Verification.* ;Engineering Measurement Division National Physical Laboratory.

Forest , J., Salvi, J., Cabruja , E., & Pous , C. (2004). Laser stripe peak detector for 3D scanners. A FIR filter approach. *IEEE*, 0-7695-2128-2/04.

Garcia, J. F. (2015, December). Un-building blocks: a model of reverse engineering and applicable heuristics. *DOCTOR OF PHILOSOPHY IN SYSTEMS ENGINEERING*. Dudley Knox Library / Naval Postgraduate School. Retrieved from https://apps.dtic.mil/sti/pdfs/ADA632187.pdf

Hu, P., Zhou, H., Chen, J., Lee, C., Tang, K., Yang, J., & Shen, S. (2018). Automatic-generation-of-efficient-and-interference interference-free five-axis scanning path for free-form surface inspection. *Computer-Aided Design*, 98 24–38.

Isheil, A., Gonnet, J. P., Joannic, D., & Fontaine, J. F. (2011). Systematic error correction of a 3D laser scanning measurement device. *Optics and Lasers in Engineering* , 49:16–24.

ISO 10360-1. (2001). *ISO 10360-1:2001 'Geometrical Product Specifications (GPS) — Acceptance and reverification tests for coordinate measuring machines (CMM) — Part 1: Vocabulary' (CMM).*

ISO 10360-12. (2016). *ISO 10360-12:2016 Geometrical product specifications (GPS) - Acceptance and reverification tests for coordinate measuring systems (CMS) - Part 12: Articulated arm coordinate measurement machines (CMM)* (Vols. Part 12: Articulated arm coordinate measurement machines (CMM) (ISO 10360-12:2016)). BSI Standards Limited 2016.

ISO 10360-2. (2009). *Geometrical product specifications (GPS) — Acceptance and reverification tests for coordinate measuring machines (CMM).* London: BSI publications.

Javed, M. A., Won, S.-h. P., Khamesee, M. B., Melek, W. W., & Owen, W. (2013). A_laser_scanning_based_reverse_engineering_system_for_3D_model_generation. *IEEE* , 978-1-4799-0224-8/13.

Kempster, M. H. (1982). *An Introducton to Jig and tool design.* London Sydney Aukland Toronto: Hodder & Stoughton.

Korosec, M., Duhovnik, J., & Vukasinovic, N. (2010). Identification and optimization of key process parameters in noncontact laser scanning for reverse engineering. *Computer-Aided Design* , 42:744–748.

Lartigue, C., Contri, A., & Bourdet, P. (2002). Digitised point quality in relation with point exploitation. . *Measurement*, 32:193–203.

Lecrivain, G. M., Kennedy, I., & Slaouti , A. (2007). A Hybrid Methodology for the Creation of High Quality Surfaces for Reverse Engineering Applications. *Proceedings of the World Congress on Engineering 2007*, *2*, pp. 2 - 4.

Li , Y. F., & Liu , Z. G. (2003). Method for determining the probing points for efficient measurement and reconstruction of freeform surfaces. *Meas. Sci. Technol. 14 128, 14*, 1280-1288.

Li, C. J., Zhang, Z., Miyaki, T., Imamura, T., & Fujiwa, H. (2009). Processing Specular Reflection Components of Chrome-plated Surface by Multi-Image Reconstruction Method. *International Journal of Computer Information Systems and Industrial Management Applications (IJCISIM) http://www.mirlabs.org/ijcisim*, 1:303-311.

Li, J. C., Zhang, Z., Miyaki, T., Imamura, T., & Fujiwa, H. (2009). Processing Specular Reflection Components of Chrome-plated Surface by Multi-Image Reconstruction Method. *International Journal of Computer Information Systems and Industrial Management Applications*, 1:303-311.

Lou, S., Brown, S. B., Sun, W., Zeng, W., Jiang, X., & Scott, P. J. (2019). An investigation of the mechanical filtering effect of tactile CMM in the measurement of additively manufactured parts. *Measurment, 144*, 173-182.

Lou, S., Zeng, W.-H., Jiang, X.-Q., & Scott, P. J. (2013). Robust Filtration Techniques in Geometrical Metrology and Their Comparison. *International Journal of Automation and Computing*, 1-8.

Mahboubkhah, M., Aliakbari, M., & Burvill, C. (2018). An investigation on measurement accuracy of digitizing methods in turbine blade reverse engineering. *Journal of Engineering Manufacture*, Vol. 232(9) 1653–1671.

McCarthy, M. B., Brown, S. B., Evenden, A., & Robinson, A. D. (2011). NPL freeform artefact for verification of non-contact measuring systems. *The International Society for Optical Engineering*, DOI: 10.1117/12.876705.

Menq, C., & Chen, F. L. (1996). Curve and surface approximation form CMM measurement data. *Computers ind. Engng. 1996:30 2 211-225*, 30 2 211-225.

Mian, S. H., Mannan, M. A., & Al-Ahmari, A. M. (2014). The influence of surface topology on the quality of the point cloud data acquired with laser line scanning probe. *Sensor Review*, 34-3:255-265.

Muralikrishnan, B., Ren, W., Everett, D., Stanfield, E., & Doiron, T. (2012). Performance evaluation experiments on a laser spot triangulation probe. *;Measurement*, 45 333-343.

Nayar, S. K., Ikeuchi , K., & Kanade, T. (1991). Surface reflection: physical and geometrical perspectives. *IEEE Trans. on Pattern Analysis and Machine Intelligence*, 13,7,611-634.

Neumann , H. J. (1990). *Coordinate Metrology – Technology and applications.* Carl Zeiss company.

PC-Dmis. (2019). PC-Dmis Help files. Hexagon Metrologey .

Polyworks. (2018). Polyworks 2018 'modeler essential'. pp274. InnovMetric Software.

Puskar, R. J. (1983). The Opposition Effect in Optical Scattering from Rough Surfaces. *PhD thesis*. The Ohio State University. Retrieved October 15, 2022, from https://etd.ohiolink.edu/apexprod/rws_olink/r/1501/10?p10_etd_subid=136381&clear=10

Raghavendra, N. V., & Krishnamurthy, L. (2013). *Engineering metrology and measurements.* Oxford University Press.

Raja , V., & Fernandes, K. J. (2008). *Reverse engineering: an industrial perspective (Ch 1).* Springer-Verlag London Limited.

Renishaw. (2003). Cyclone - the complete scanning system for reverse manufacturing. *1003 A4 Part No. H-2000-3332-01-A*. Renishaw plc.

Rodger, G., Flack , D., & McCarthy, M. (2007). A review of industrial capabilities to measure free-form surfaces. National Physical Laboratory.

Rodger, Gordon; Flack, David ; McCarthy, Michael. (2007). *A review of industrial capabilities to measure free-form surfaces.* National Physical Laboratory.

Satyanarayana, A., Krishna, M., Chandrakanth, A., & Pradyumna, R. (2018). Influence of LASER CMM Process Parameters on Dimensional Inspection of Standard Spheres. *Materials Today: Proceedings*, 5 3965–3970.

Savio, E., De Chiffre, L., & Schmitt, R. (2007). Metrology of freeform shaped parts. *CIRP annals, Vol.56 (2)*, p.810-835.

Stojadinovic, S. M., Majstorovic, V. D., Durakbasa, N. M., & Sibalija, T. V. (2016). Towards an intelligent approach for CMM inspection planning of prismatic parts. *Measurement* , 92 326–339.

Taylor Hobson . (2011). *Exploring Surface Texture: A fundamental guide to the measurement of surface finish* (7th edition ed.). Leicester: Taylor Hobson Limited.

Taylor Hobson. (2015). Form Talysurf PGI Bearings Product specification. Leicaster: Taylor Hobson.

Thompson, W. B., Owen, C. J., De St Germain, J. H., & Stark, S. R. (1999). Feature-based_reverse_engineering_of_mechanical_parts. *IEEE transactions on robotics and automation*, 15-1.

Tsakiri, M., Ioannidis, C., & Carty, A. (2002). *Laser scanning issues for the geometrical recording of a complex statue*. Retrieved from Semantic Scholar: Laser scanning issues for the geometrical recording of a complex statue', Online available at: < https://www.semanticscholar.org/paper/LASER-SCANNING-ISSUES-FOR-THE-GEOMETRICAL-RECORDING-Tsakiri-Ioannidis/15dfedfc305f5e610a99713359d820e2146ff340#related-p

Van Gestel, N., Cuypers, S., Bleys, P., & Kruth, J.-P. (2009). A performance evaluation test for laser line scanners on CMMs. . *Optics and Lasers in Engineering* , 47:336–342.

Voisina, S., Pagea, D., Koschana, A., & Abidia, M. (2006, April). Reconstructing 3D CAD Models for Simulation Using Imaging-Based Reverse Engineering. *SPIE Modeling and Simulation for Military Applications, Vol. 6228*, 4-62,.

Vukasinovic , N., Mozina, J., & Duhovnik, J. (2012). Correlation between incident angle, measurement distance, object colour and the number of acquired points at CNC Laser Scanning. *Mechanical Engineering*, 58 1, 23-28.

Weckenmann, A., Estler, T., Peggs, G., & McMurtry, D. (2004). Probing Systems in Dimensional Metrology. *CIRP annals, Vol.53 (2)*, p.657-684.

Zhang, Y. (2003). Research into the engineering application of reverse engineering technology. *Journal of Materials Processing Technology, 139*, 472–475.

Zhang, Y., Zhou, Z., & Tang, K. (2018). Sweep scan path planning for five-axis inspection of free-form surfaces. *Robotics and Computer–Integrated Manufacturing* , 49 335–348.

Appendix A

A-1. Data used in Table Fig. 5.10 applied to hemispherical virtual data used in Fig 5.10.

Probe compensation method	Probe diam. (mm)	No. of virtual scan points (Millions)	Best fit diam. error (mm)	STD Of best fit residuals (mm)
Probe compensation in the probe approach direction (maintaining X, Y coordinates)	2	1	0.009	0.002
	4	1	0.033	0.003
	6	1	0.062	0.005
	2	2	0.008	0.001
	4	2	0.029	0.002
	6	2	0.061	0.005
	2	3	0.008	0.001
	4	3	0.029	0.002
	6	3	0.061	0.005
	2	4	0.008	0.001
	4	4	0.029	0.002
	6	4	0.061	0.005
Probe compensation in the direction of surface normal	2	1	0.015	0.005
	4	1	0.01	0.004
	6	1	0.005	0.001
	2	2	0.008	0.002
	4	2	0.003	0.001
	6	2	0.002	0.001
	2	3	0.005	0.002
	4	3	0.002	0.001
	6	3	0.001	0.001
	2	4	0.003	0.001
	4	4	0.002	0.001
	6	4	0.001	0.001

A-2. Data used in Fig 6. 5..

	Scan type	Probe diam. (mm)	No. of scan points (Millions)	Best fit sphere diam. (mm)	Best fit diam. error (mm)	STD Of best fit residuals (mm)
Probe compensation in the probe approach direction (maintaining X, Y coordinates)	Raw scan CPD	2	3.8	149.984	0.048	0.190
		4	3.8	150.020	0.012	0.204
		6	3.8	150.063	0.031	0.316
	Meshed in real time	2	4.0	150.050	0.018	0.005
		4	4.0	150.078	0.046	0.008
		6	4.0	150.117	0.085	0.010
Probe compensation in the direction of surface normal	Raw scan CPD	2	3.8	150.056	0.024	0.136
		4	3.8	150.067	0.035	0.431
		6	3.8	150.055	0.023	0.463
	Meshed in real time	2	4.0	150.034	0.002	0.004
		4	4.0	150.033	0.001	0.004
		6	4.0	150.035	0.003	0.004

A-.3. Bezier curve error X' 0.0mm, 'Z' 0.0 mm alignment error, up to 0.07mm scan error

X' 0.0mm, 'Z' 0.0 mm alignment error, up to 0.07mm scan error					
2mm probe		4mm probe		6mm probe	
Probe cent to surface dist.	Correction Error	Probe cent to surface dist.	Correction Error	Probe cent to surface dist.	Correction Error
0.947	0.001	1.943	0.003	2.944	0.004
0.941	0.001	1.940	0.001	2.941	0.002
0.939	0.001	1.940	0.002	2.939	0.001
0.945	0.009	1.942	0.003	2.940	0.000
0.945	0.002	1.940	0.000	2.942	0.004
0.937	0.001	1.938	0.001	2.941	0.005
0.942	0.006	1.936	0.000	2.937	0.000
0.941	0.003	1.937	0.000	2.937	0.000
0.939	0.001	1.936	0.000	2.940	0.004
0.939	0.005	1.940	0.004	2.941	0.001
0.938	0.002	1.937	0.002	2.937	0.003
0.935	0.000	1.934	0.001	2.935	0.001
0.933	0.000	1.938	0.001	2.935	0.002
0.936	0.002	1.936	0.004	2.933	0.002
0.933	0.001	1.932	0.001	2.932	0.000
0.936	0.005	1.933	0.000	2.933	0.001
0.934	0.000	1.935	0.003	2.932	0.001
0.934	0.003	1.931	0.000	2.932	0.002
0.935	0.003	1.936	0.002	2.932	0.001
0.934	0.001	1.932	0.000	2.934	0.002
0.936	0.004	1.934	0.003	2.933	0.000
0.935	0.004	1.932	0.001	2.932	0.001
0.932	0.002	1.932	0.001	2.931	0.000
0.933	0.000	1.934	0.003	2.932	0.001
0.935	0.003	1.935	0.001	2.932	0.002
0.933	0.003	1.933	0.000	2.932	0.001
0.937	0.006	1.935	0.003	2.933	0.000
0.935	0.002	1.933	0.001	2.933	0.001
0.935	0.001	1.936	0.001	2.934	0.001
0.934	0.001	1.934	0.000	2.936	0.001
0.941	0.007	1.935	0.000	2.935	0.001
0.937	0.001	1.935	0.001	2.937	0.002
0.938	0.000	1.937	0.001	2.936	0.001
0.940	0.005	1.937	0.001	2.936	0.001
0.939	0.001	1.938	0.001	2.937	0.000
0.941	0.005	1.937	0.001	2.939	0.002
0.937	0.000	1.937	0.000	2.939	0.003
0.941	0.003	1.941	0.002	2.939	0.001

0.938	0.001	1.942	0.002	2.940	0.001
0.942	0.001	1.940	0.001	2.939	0.001
0.941	0.001	1.939	0.000	2.939	0.000
0.943	0.004	1.943	0.004	2.944	0.003
0.945	0.005	1.941	0.000	2.940	0.000
0.941	0.002	1.941	0.001	2.940	0.000
0.943	0.002	1.940	0.000	2.942	0.002
0.943	0.001	1.941	0.001	2.943	0.003
0.943	0.002	1.942	0.003	2.942	0.001
0.944	0.001	1.941	0.000	2.941	0.001
0.943	0.001	1.942	0.000	2.943	0.001
0.942	0.001	1.941	0.000	2.943	0.001
0.942	0.001	1.944	0.004	2.942	0.000
0.942	0.001	1.941	0.000	2.942	0.001
0.942	0.000	1.943	0.003	2.941	0.001
0.943	0.002	1.943	0.003	2.941	0.000
0.941	0.000	1.942	0.002	2.941	0.001
0.944	0.004	1.942	0.003	2.940	0.001
0.942	0.002	1.941	0.001	2.940	0.001
0.943	0.005	1.939	0.000	2.939	0.000
0.940	0.002	1.941	0.000	2.940	0.000
0.941	0.001	1.940	0.000	2.940	0.001
0.942	0.003	1.938	0.001	2.943	0.002
0.940	0.003	1.941	0.003	2.939	0.001
0.941	0.002	1.938	0.001	2.937	0.000
0.937	0.001	1.939	0.003	2.936	0.000
0.937	0.001	1.938	0.000	2.935	0.000
0.938	0.000	1.937	0.001	2.937	0.003
0.936	0.001	1.937	0.004	2.936	0.002
0.935	0.001	1.935	0.001	2.935	0.001
0.936	0.000	1.935	0.002	2.935	0.001
0.935	0.000	1.935	0.000	2.934	0.001
0.937	0.005	1.934	0.000	2.935	0.002
0.936	0.004	1.933	0.001	2.933	0.001
0.934	0.000	1.934	0.000	2.932	0.001
0.933	0.002	1.933	0.000	2.933	0.000
0.933	0.002	1.933	0.000	2.932	0.000
0.936	0.006	1.931	0.000	2.932	0.001
0.933	0.001	1.934	0.001	2.932	0.001
0.931	0.001	1.933	0.001	2.931	0.001
0.939	0.001	1.935	0.003	2.932	0.001
0.931	0.001	1.935	0.001	2.933	0.000
0.933	0.001	1.934	0.001	2.931	0.000
0.936	0.003	1.933	0.002	2.933	0.001
0.938	0.004	1.934	0.002	2.933	0.002
0.933	0.003	1.934	0.000	2.933	0.001

0.938	0.005	1.932	0.001	2.933	0.000
0.935	0.001	1.936	0.003	2.934	0.001
0.934	0.000	1.935	0.003	2.934	0.000
0.936	0.003	1.936	0.001	2.937	0.004
0.940	0.001	1.937	0.001	2.935	0.001
0.938	0.005	1.939	0.004	2.938	0.001
0.944	0.002	1.936	0.001	2.936	0.001
0.939	0.000	1.937	0.001	2.937	0.001
0.937	0.002	1.938	0.000	2.938	0.003
0.936	0.000	1.941	0.002	2.939	0.001
0.939	0.000	1.942	0.006	2.938	0.001
0.940	0.002	1.938	0.001	2.940	0.001
0.945	0.008	1.940	0.000	2.939	0.000
0.943	0.000	1.943	0.000	2.941	0.002
0.948	0.006	1.941	0.001	2.942	0.003
Min	0.0001	Min	0.0000	Min	0.0001
Max	0.0092	Max	0.0060	Max	0.0048
Mean	0.0022	Mean	0.0014	Mean	0.0012
STD	0.0020	STD	0.0013	STD	0.0010

A-4. Bezier curve error ‘X' 0.1mm, 'Z' 0.1 mm alignment error, no scan error

‘X' 0.1mm, 'Z' 0.1 mm alignment error, no scan error					
2mm probe		4mm probe		6mm probe	
Probe cent to surface dist.	Correction Error	Probe cent to surface dist.	Correction Error	Probe cent to surface dist.	Correction Error
0.9636	0.0002	1.9636	0.0002	2.9635	0.0002
0.9612	0.0002	1.9610	0.0000	2.9609	0.0001
0.9587	0.0004	1.9583	0.0002	2.9583	0.0002
0.9556	0.0001	1.9556	0.0002	2.9555	0.0001
0.9528	0.0001	1.9528	0.0002	2.9527	0.0001
0.9501	0.0004	1.9499	0.0001	2.9498	0.0001
0.9470	0.0002	1.9469	0.0000	2.9469	0.0002
0.9445	0.0009	1.9438	0.0001	2.9439	0.0002
0.9407	0.0001	1.9407	0.0001	2.9406	0.0000
0.9375	0.0002	1.9376	0.0003	2.9374	0.0001
0.9342	0.0000	1.9342	0.0002	2.9343	0.0001
0.9308	0.0001	1.9309	0.0001	2.9308	0.0001
0.9281	0.0008	1.9277	0.0002	2.9275	0.0001
0.9242	0.0001	1.9241	0.0002	2.9241	0.0001
0.9207	0.0000	1.9207	0.0000	2.9207	0.0001

0.9173	0.0002	1.9173	0.0001	2.9172	0.0001
0.9140	0.0002	1.9140	0.0001	2.9139	0.0001
0.9106	0.0001	1.9105	0.0001	2.9106	0.0001
0.9072	0.0002	1.9072	0.0001	2.9072	0.0002
0.9039	0.0000	1.9039	0.0001	2.9040	0.0001
0.9007	0.0001	1.9007	0.0001	2.9007	0.0001
0.8978	0.0001	1.8976	0.0001	2.8976	0.0001
0.8949	0.0002	1.8948	0.0002	2.8946	0.0001
0.8918	0.0001	1.8918	0.0000	2.8917	0.0001
0.8892	0.0003	1.8891	0.0003	2.8890	0.0001
0.8866	0.0001	1.8866	0.0002	2.8864	0.0001
0.8841	0.0001	1.8841	0.0002	2.8840	0.0001
0.8820	0.0002	1.8818	0.0002	2.8817	0.0001
0.8797	0.0002	1.8796	0.0000	2.8796	0.0001
0.8781	0.0006	1.8777	0.0002	2.8776	0.0000
0.8759	0.0002	1.8759	0.0002	2.8758	0.0001
0.8742	0.0001	1.8742	0.0001	2.8744	0.0004
0.8727	0.0001	1.8726	0.0001	2.8726	0.0001
0.8712	0.0001	1.8713	0.0001	2.8713	0.0001
0.8701	0.0002	1.8701	0.0001	2.8700	0.0001
0.8693	0.0005	1.8689	0.0000	2.8689	0.0001
0.8679	0.0000	1.8679	0.0001	2.8681	0.0002
0.8670	0.0001	1.8671	0.0001	2.8670	0.0001
0.8663	0.0000	1.8663	0.0000	2.8663	0.0001
0.8656	0.0000	1.8656	0.0000	2.8656	0.0001
0.8651	0.0001	1.8651	0.0002	2.8650	0.0000
0.8648	0.0003	1.8646	0.0001	2.8646	0.0001
0.8641	0.0000	1.8641	0.0000	2.8642	0.0001
0.8637	0.0001	1.8638	0.0001	2.8638	0.0001
0.8636	0.0002	1.8634	0.0000	2.8635	0.0001
0.8632	0.0000	1.8632	0.0001	2.8632	0.0000
0.8631	0.0001	1.8630	0.0001	2.8631	0.0001
0.8630	0.0001	1.8629	0.0001	2.8629	0.0001
0.8629	0.0001	1.8630	0.0002	2.8629	0.0001
0.8629	0.0002	1.8628	0.0000	2.8629	0.0001
0.8629	0.0001	1.8630	0.0002	2.8629	0.0000
0.8630	0.0002	1.8629	0.0001	2.8629	0.0001
0.8631	0.0001	1.8631	0.0001	2.8630	0.0001
0.8633	0.0001	1.8632	0.0001	2.8632	0.0001
0.8634	0.0001	1.8635	0.0001	2.8635	0.0001
0.8638	0.0001	1.8637	0.0001	2.8638	0.0001
0.8643	0.0003	1.8641	0.0001	2.8641	0.0000
0.8647	0.0003	1.8645	0.0001	2.8645	0.0000
0.8650	0.0001	1.8650	0.0001	2.8650	0.0001
0.8655	0.0000	1.8657	0.0002	2.8656	0.0001
0.8664	0.0002	1.8663	0.0001	2.8662	0.0001

0.8669	0.0000	1.8670	0.0001	2.8669	0.0001
0.8681	0.0004	1.8678	0.0000	2.8678	0.0000
0.8689	0.0001	1.8688	0.0001	2.8688	0.0001
0.8702	0.0004	1.8699	0.0001	2.8699	0.0000
0.8711	0.0001	1.8711	0.0001	2.8711	0.0001
0.8725	0.0001	1.8724	0.0000	2.8725	0.0001
0.8740	0.0001	1.8740	0.0002	2.8739	0.0001
0.8756	0.0001	1.8755	0.0000	2.8755	0.0001
0.8774	0.0001	1.8773	0.0001	2.8773	0.0000
0.8794	0.0003	1.8792	0.0001	2.8792	0.0001
0.8814	0.0002	1.8814	0.0000	2.8813	0.0001
0.8841	0.0004	1.8836	0.0001	2.8836	0.0000
0.8860	0.0001	1.8866	0.0009	2.8859	0.0001
0.8885	0.0001	1.8885	0.0001	2.8885	0.0002
0.8913	0.0000	1.8912	0.0001	2.8912	0.0001
0.8941	0.0001	1.8941	0.0001	2.8940	0.0002
0.8970	0.0001	1.8970	0.0001	2.8970	0.0002
0.9003	0.0004	1.9004	0.0006	2.9001	0.0001
0.9034	0.0002	1.9032	0.0002	2.9033	0.0000
0.9066	0.0002	1.9065	0.0001	2.9065	0.0002
0.9104	0.0007	1.9099	0.0000	2.9098	0.0002
0.9137	0.0004	1.9133	0.0002	2.9132	0.0002
0.9167	0.0002	1.9166	0.0002	2.9165	0.0002
0.9200	0.0002	1.9200	0.0000	2.9200	0.0001
0.9235	0.0001	1.9234	0.0001	2.9234	0.0001
0.9271	0.0004	1.9270	0.0004	2.9268	0.0001
0.9305	0.0005	1.9302	0.0001	2.9303	0.0004
0.9339	0.0006	1.9335	0.0001	2.9335	0.0001
0.9369	0.0001	1.9369	0.0001	2.9369	0.0002
0.9401	0.0001	1.9401	0.0002	2.9400	0.0001
0.9433	0.0001	1.9432	0.0001	2.9432	0.0002
0.9466	0.0003	1.9464	0.0001	2.9463	0.0000
0.9493	0.0002	1.9497	0.0005	2.9493	0.0001
0.9525	0.0003	1.9523	0.0001	2.9523	0.0001
0.9555	0.0004	1.9551	0.0001	2.9551	0.0001
0.9578	0.0001	1.9578	0.0001	2.9578	0.0001
0.9605	0.0001	1.9605	0.0001	2.9605	0.0002
0.9631	0.0001	1.9632	0.0002	2.9630	0.0001
Min	0.0000	Min	0.0000	Min	0.0000
Max	0.0009	Max	0.0009	Max	0.0004
Mean	0.0002	Mean	0.0001	Mean	0.0001
STD	0.0002	STD	0.0001	STD	0.0001

A-5. Bezier curve error ‘X' 0.1mm, 'Z' 0.1 mm alignment error, to 0.07 scan error

‘X' 0.1mm, 'Z' 0.1 mm alignment error, to 0.07 scan error					
2mm probe		4mm probe		6mm probe	
Probe cent to surface dist.	Correction Error	Probe cent to surface dist.	Correction Error	Probe cent to surface dist.	Correction Error
0.905	0.001	1.904	0.002	2.905	0.000
0.906	0.003	1.901	0.000	2.901	0.000
0.903	0.005	1.898	0.002	2.900	0.001
0.895	0.003	1.896	0.002	2.895	0.002
0.892	0.001	1.892	0.001	2.892	0.001
0.893	0.003	1.888	0.002	2.889	0.002
0.885	0.002	1.886	0.002	2.887	0.006
0.883	0.005	1.883	0.004	2.881	0.001
0.881	0.002	1.881	0.005	2.877	0.000
0.876	0.001	1.872	0.001	2.874	0.003
0.875	0.004	1.871	0.001	2.869	0.000
0.865	0.001	1.867	0.004	2.867	0.003
0.865	0.002	1.864	0.002	2.864	0.004
0.862	0.007	1.857	0.000	2.858	0.000
0.854	0.001	1.855	0.002	2.853	0.000
0.852	0.002	1.854	0.005	2.851	0.001
0.846	0.001	1.847	0.003	2.845	0.001
0.845	0.003	1.844	0.003	2.843	0.000
0.841	0.003	1.840	0.000	2.838	0.000
0.837	0.003	1.836	0.001	2.835	0.000
0.835	0.000	1.834	0.002	2.836	0.003
0.830	0.002	1.832	0.001	2.832	0.000
0.827	0.000	1.826	0.001	2.826	0.000
0.825	0.001	1.827	0.001	2.824	0.001
0.823	0.000	1.822	0.003	2.821	0.001
0.820	0.002	1.819	0.002	2.819	0.000
0.818	0.003	1.817	0.001	2.815	0.000
0.818	0.004	1.815	0.002	2.816	0.001
0.812	0.000	1.816	0.001	2.814	0.000
0.815	0.005	1.813	0.003	2.812	0.000
0.811	0.002	1.811	0.001	2.810	0.001
0.810	0.000	1.810	0.000	2.810	0.001
0.813	0.002	1.808	0.001	2.809	0.000
0.812	0.006	1.806	0.000	2.807	0.001
0.806	0.001	1.807	0.002	2.806	0.001
0.807	0.002	1.809	0.001	2.806	0.001
0.809	0.002	1.806	0.002	2.807	0.000
0.810	0.001	1.804	0.000	2.806	0.000

0.808	0.002	1.807	0.003	2.806	0.003
0.806	0.004	1.808	0.004	2.805	0.001
0.806	0.002	1.805	0.000	2.806	0.000
0.814	0.007	1.804	0.000	2.804	0.001
0.807	0.000	1.805	0.001	2.806	0.003
0.805	0.002	1.805	0.001	2.804	0.001
0.807	0.002	1.805	0.001	2.804	0.001
0.806	0.003	1.804	0.000	2.804	0.001
0.806	0.005	1.805	0.000	2.804	0.001
0.804	0.000	1.804	0.000	2.805	0.000
0.804	0.001	1.806	0.001	2.803	0.000
0.806	0.002	1.805	0.002	2.804	0.001
0.808	0.000	1.805	0.000	2.805	0.001
0.807	0.001	1.806	0.002	2.805	0.002
0.804	0.001	1.805	0.002	2.806	0.002
0.809	0.004	1.804	0.000	2.806	0.001
0.806	0.004	1.804	0.000	2.805	0.002
0.810	0.001	1.804	0.000	2.805	0.000
0.808	0.001	1.805	0.002	2.804	0.000
0.807	0.005	1.806	0.001	2.807	0.004
0.804	0.002	1.803	0.000	2.806	0.002
0.805	0.002	1.807	0.002	2.807	0.001
0.804	0.000	1.806	0.002	2.806	0.003
0.806	0.000	1.806	0.003	2.807	0.002
0.806	0.001	1.807	0.002	2.807	0.002
0.809	0.005	1.808	0.003	2.806	0.000
0.811	0.002	1.808	0.002	2.807	0.000
0.809	0.001	1.806	0.000	2.808	0.001
0.808	0.001	1.808	0.002	2.807	0.000
0.813	0.004	1.809	0.002	2.811	0.002
0.812	0.002	1.810	0.001	2.812	0.004
0.814	0.003	1.811	0.001	2.812	0.000
0.816	0.001	1.814	0.002	2.812	0.001
0.815	0.001	1.814	0.000	2.816	0.003
0.822	0.000	1.817	0.001	2.816	0.001
0.821	0.003	1.818	0.000	2.819	0.000
0.825	0.006	1.822	0.002	2.823	0.002
0.829	0.003	1.823	0.001	2.824	0.001
0.827	0.003	1.826	0.001	2.827	0.001
0.830	0.002	1.828	0.001	2.828	0.000
0.833	0.003	1.831	0.000	2.831	0.001
0.838	0.001	1.841	0.006	2.838	0.004
0.844	0.001	1.840	0.001	2.839	0.002
0.842	0.002	1.843	0.001	2.841	0.000
0.850	0.005	1.847	0.003	2.848	0.002
0.851	0.003	1.850	0.002	2.850	0.001

0.855	0.001	1.854	0.001	2.853	0.001
0.860	0.002	1.858	0.001	2.857	0.002
0.862	0.003	1.862	0.000	2.860	0.001
0.868	0.004	1.865	0.002	2.863	0.000
0.868	0.000	1.870	0.004	2.868	0.000
0.876	0.002	1.871	0.001	2.874	0.000
0.884	0.002	1.875	0.001	2.879	0.000
0.883	0.005	1.879	0.000	2.881	0.003
0.888	0.001	1.883	0.001	2.886	0.004
0.891	0.004	1.889	0.002	2.888	0.003
0.894	0.002	1.893	0.001	2.891	0.001
0.900	0.002	1.898	0.004	2.895	0.002
0.903	0.007	1.901	0.002	2.897	0.000
0.904	0.002	1.901	0.002	2.901	0.002
0.906	0.003	1.905	0.003	2.906	0.001
Min	0.0001	Min	0.0001	Min	0.0001
Max	0.0072	Max	0.0062	Max	0.0060
Mean	0.0024	Mean	0.0015	Mean	0.0012
STD	0.0017	STD	0.0012	STD	0.0011

Appendix B

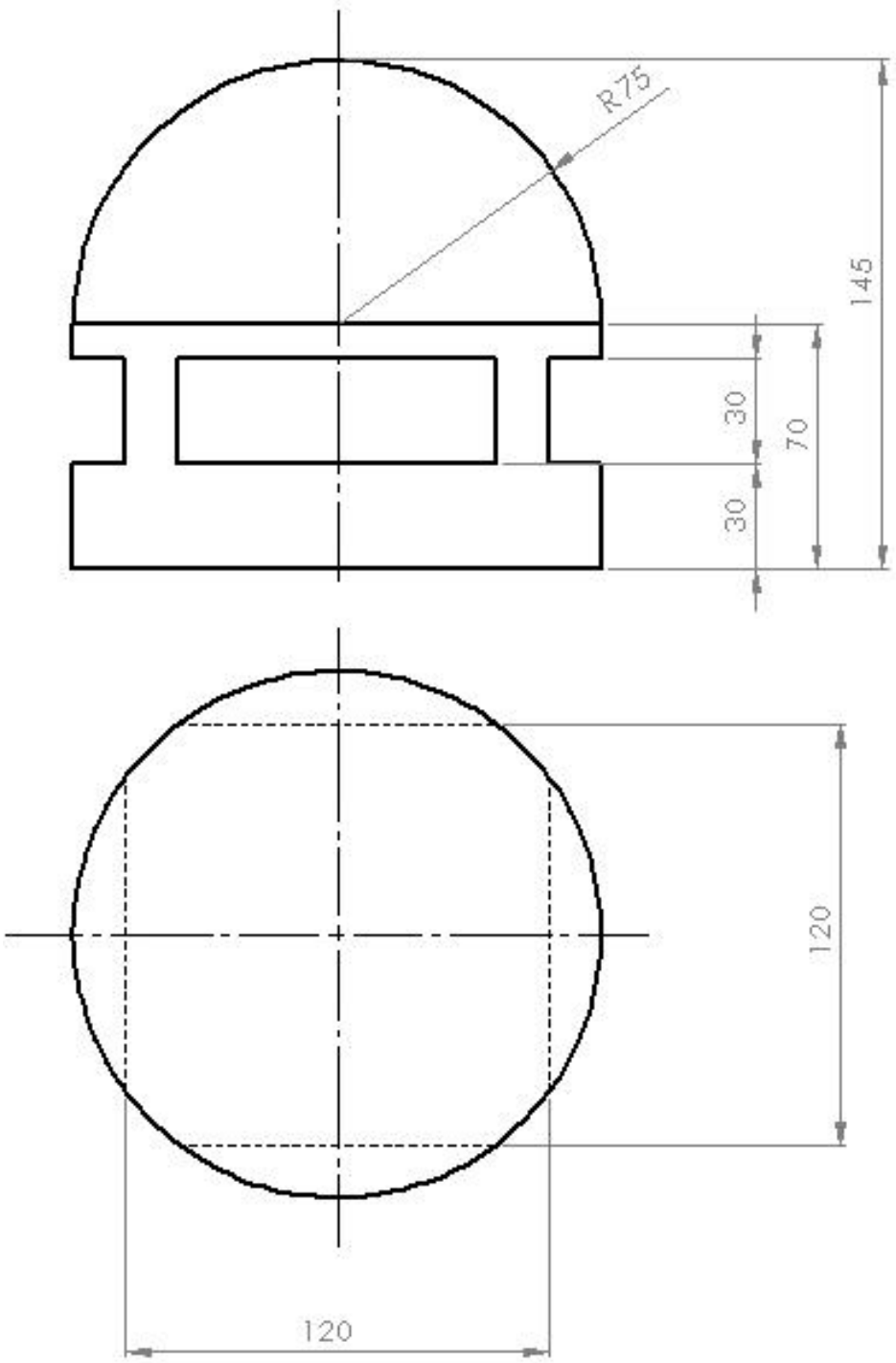

Fig B1. Detail drawing of hemispherical form. Dimensions shown are as designed but as machined dimensions are detailed in the main report.